PRODUCTION OF HOMOGENEOUS PARTICLES BY CONTROLLED NEUTRALIZATION OF ELECTROSPRAYS

Antonio Jesús Carrasco Muñoz

UNIVERSITAT ROVIRA i VIRGILI

Production of Homogeneous Particles by Controlled Neutralization of Electrosprays

Antonio Jesús Carrasco Muñoz

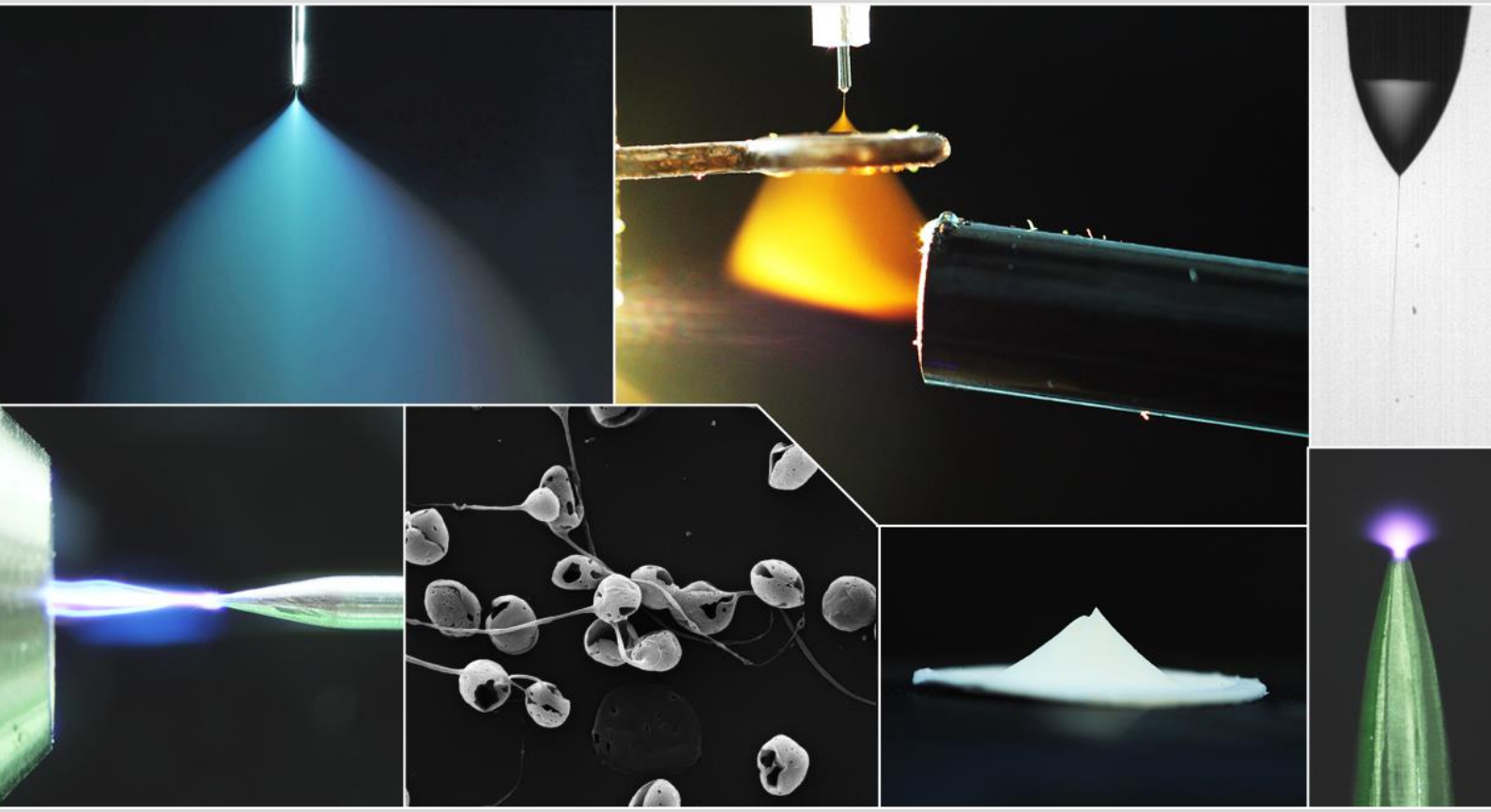

DOCTORAL THESIS
2021

Antonio Jesús Carrasco Muñoz

Production of Homogeneous Particles by Controlled Neutralization of Electrosprays

DOCTORAL THESIS

Department of Chemical Engineering

UNIVERSITAT ROVIRA i VIRGILI

Tarragona, Spain

2021

Production of Homogeneous Particles by Controlled Neutralization of Electrosprays

DOCTORAL THESIS

Supervised by

Dr. Joan Rosell Llompart

Department of Chemical Engineering

UNIVERSITAT ROVIRA i VIRGILI

Tarragona, Spain

2021

UNIVERSITAT
ROVIRA i VIRGILI

Escola Tècnica Superior d'Enginyeria Química
Departament d'Enginyeria Química
Avinguda dels Països Catalans, 26
43007 Tarragona (Spain)
Tel. +34 977 55 96 03
http://www.etseq.urv.es/deq/

In Tarragona, November 23, 2021.

I STATE that the present study, entitled "Production of Homogeneous Particles by Controlled Neutralization of Electrosprays", presented by Mr. Antonio Jesús Carrasco Muñoz for the award of the degree of Doctor, has been carried out under my supervision at the Department of Chemical Engineering of this university.

Signed by the doctoral thesis supervisor:

Joan Rosell Llompart

Acknowledgements

The completion of this thesis could not have been possible without the expertise, ideas, feedback, and great support of my supervisor Prof. Joan Rosell-Llompart and Prof. Jordi Grifoll-Taverna.

My warmest thanks to all the DEW group members, office colleagues and friends Dr. Nikolas Sochorakis, Dr. Eszter Bodnár, Elena Barbero, Dr. Laura Escorihuela, Dr. Ievgenii Liashenko, Reyda Akdemir, Dr. Carlos García, Dr. Benjamí Martorell, Dr. Llorenç Terrades, Dr. Gulsen Betul Aktas, Adam Ridouane, Paula Martínez, Deepak Parajuli, Ignasi G. Flores, Cristina Aguilar, Carlos G. Flores.

Thank you Núria Juanpere, Prof. Álex Fragoso, Ernest Arce with whom this trip have been more pleasant.

Thank you Prof. Luewton Agostinho, Prof. Klaus Glanzer, Prof. John Stark, Prof. Ismail Ahmed for inviting me to learn about and enjoy Science in a different environment, their labs.

I owe a big thank to Prof. Raúl Rica Alarcón for the great support over the years.

Special thanks to all the people who along the way believed in me.

This project has received funding from the Spanish Government through grants PGC2018-099687-B-I00 (MCI/AEI/FEDER, UE) and DPI2015-68969-P (MINECO/FEDER, UE), and from the Catalan Government through grant 2017SGR1516 (AGAUR).

Thank you Elena Rica Alarcón for accompanying me on this journey, without you it would not have been possible.

To my beloved parents

Contents

Summary

This thesis is focused on the efficient reduction of charge of electrospray droplets to produce homogeneously sized polymer particles by electrospraying a polymer solution. In the electrospraying process, a steady micro-jet is emitted, from the tip of the so-called Taylor cone, breaking up into highly charged tiny droplets. When using a polymer-containing solution, it results in narrowly dispersed particle sizes, from micrometer to nanometer scale, depending on liquid properties and operating conditions.

Therefore, electrospray is gaining research interest in different fields such as pharmaceutics. Among its advantages over other liquid atomization methods includes its ability to produce much smaller particles (in the few-microns and nano-metric size ranges) with size homogeneity and high energy efficiency.

But one problem is that the high charge induced on the droplets by this technique may distort the size uniformity. This occurs if the droplet undergoes a Coulombic instability. Just before that, while the volatile solvent is being evaporated, thus reducing its diameter, the droplet is maintaining its charge. Then, the so-called Rayleigh limit is reached when the repulsive Coulomb forces overcome the surface tension and the droplet explodes. After that, the created polymer particle loses its shape and size.

An electrospray-neutralization setup has been developed in which the droplet charge was reduced significantly, preventing Coulombic instabilities, and being able to generate homogeneous polymer particles in a controlled atmosphere conditions, obtain-

ing the desired particle morphology, and preventing filamentous particles.

To achieve an appropriate particle charge reduction, it was necessary to produce an opposite polarity ion current which must be comparable to the electrospray current, usually from tens to hundreds of nano-amperes. For this reason, we have developed and optimized a unipolar ion source based on corona discharge. This home-made tool was strategically attached to the system, allowing the electrospray droplets to be effectively discharged before they explode.

Another interesting feature of this system is that we can easily collect those particles by properly incorporating an extraction system. Due to the fact that, after the particle charge has been reduced sufficiently, they do not follow (at least with the same strength) the electric field anymore, they could be extracted by the gas velocity field, obtaining a high collection efficiency.

To check the robustness of our system, different polymer solutions with different electrical conductivities have been used, producing PS, PVP, chitosan particles.

Another possible advantage of reducing the droplet charge is that, since the throughput of a single emitter is too low from an industrial point of view, a barrier needs to be overcome: scaling-up the process. But in a multiple-emitter electrospray, the space charge might a problem in terms of developing a miniaturized system. Then, managing the space charge by controlling the charge reduction might be a key point in order to scale-up the process.

List of publications and conferences

Publications

- **Carrasco-Munoz, A.**, Barbero-Colmenar, E., Bodnár, E., Grifoll, J., Rosell-Llompart, J. (2021). Monodisperse droplets and particles by efficient neutralization of electrosprays. *Journal of Aerosol Science*, 105909. https://doi.org/10.1016/j.jaerosci.2021.105909
- **Carrasco-Munoz, A.**, Grifoll, J., Rosell-Llompart, J. (2021). Unipolar corona ion source for electrospray droplet discharging. (To be submitted)

Conferences

- **A. Carrasco-Munoz**, E. Barbero-Colmenar, E. Bodnár, J. Grifoll, J. Rosell-Llompart (2021). Discharging electrosprays with unipolar ions for producing globular nano- and micro-particles. In *European Aerosol Conference 2021 (EAC-2021)*, ONLINE. Oral presentation.
- **A. Carrasco-Munoz**, E. Barbero-Colmenar, E. Bodnár, J. Grifoll, J. Rosell-Llompart (2021). Discharging electrosprays with unipolar ions for producing globular nano- and micro-particles. In *European Workshop on Electrohydrodynamic Atomization and Electrospinning 2021*, Naples, Italy and ONLINE. Invited speaker.
- **A. Carrasco-Munoz**, E. Barbero-Colmenar, E. Bodnár, J. Grifoll, J. Rosell-Llompart (2020). Controlled discharging of electrosprays to produce homogeneous particles. [Poster, ID797] In *European Aerosol Conference 2020 (EAC-2020)*, Aachen, Germany and ONLINE.

- E. Barbero-Colmenar, **A. Carrasco-Munoz**, E. Bodnár, J. Grifoll, J. Rosell-Llompart (2020). Electrospray-based production of curcumin-loaded polyvinylpyrrolidone (PVP) microparticles. [Oral, ID876] In *European Aerosol Conference 2020 (EAC-2020)*, Aachen, Germany and ONLINE.

- E. Barbero-Colmenar, E. Bodnár, W. Latif, **A. Carrasco-Munoz**, J. Grifoll, J. Rosell-Llompart (2020). Globular monodisperse polymeric particles by electrospray. [Poster, ID883] In *European Aerosol Conference 2020 (EAC-2020)*, Aachen, Germany and ONLINE.

- **A. Carrasco-Munoz**, E. Barbero-Colmenar, E. Bodnár, J. Grifoll, J. Rosell-Llompart (2020). Production of homogeneous particles by controlled neutralization of electrosprays. In *European Workshop on Electro-hydrodynamic Atomization 2020*, Tarragona, Spain.

- E. Barbero-Colmenar, **A. Carrasco-Munoz**, E. Bodnár, J. Grifoll, J. Rosell-Llompart (2019). Curcumin-loaded PVP particles produced by electrospray. [Poster] In *NanoBio&Med2019 International Conference*, Barcelona, Spain.

- Sochorakis, N., **A. Carrasco-Munoz**, E. Barbero-Colmenar, E. Bodnár, J. Grifoll, J. Rosell-Llompart (2019). Charge Reduced Electrospray Plumes for the Production of Nanoparticles, *European Aerosol Conference 2019 (EAC-2019)*, Gothenburg, Sweden.

- Sochorakis, N., J. Grifoll, E. Bodnár, **A. Carrasco-Munoz**, E. Barbero-Colmenar, J. Rosell-Llompart (2019). Electrosprays for the production of nanoparticles, *Symposium of the European Electrohydrodynamic Atomization Group*, Málaga, Spain.

- **A. Carrasco-Munoz**, E. Barbero-Colmenar, E. Bodnár, J. Grifoll, J. Rosell-Llompart (2018). Production of Homogeneous Particles by Controlled Neutralization of Electrosprays. [Poster 7MS.1]. In *(10th International Aerosol Conference 2018 (IAC-2018)*, Saint Louis, Missouri, United States.

- **A. Carrasco-Munoz**, E. Barbero-Colmenar, E. Bodnár, J. Grifoll, J. Rosell-Llompart (2018). Uniformly Sized Droplets by Controlled Neutralization of

Electrosprays. [Poster FP-01] In *6th Iberian Meeting on Aerosol Science and Technology (RICTA-2018)*, Bilbao, Spain.

- **A. Carrasco-Munoz**, E. Barbero-Colmenar, E. Bodnár, J. Grifoll, J. Rosell-Llompart (2018). Homogeneous droplets by controlled neutralization of electrosprays. [Oral WM1-02] In *Aerosol Technology 2018 (AT-2018)*, Bilbao, Spain. Oral presentation.

AT: Aerosol Technology

EAC: European Aerosol Conference

IAC: International Aerosol Conference

RICTA: Iberian Meeting on Aerosol Science and Technology

List of Figures

List of Tables

Nomenclature

Physics Constants

ε_0	Vacuum permittivity	$8.8541878128(13) \cdot 10^{-12} F/m$ (or $A^2 \cdot s^4 \cdot kg^{-1} \cdot m^{-3}$)

Symbols

γ	Surface tension coefficient
μ	Viscosity coefficient
ρ	Density
ε_r	Relative permittivity
d_d	Droplet diameter
d_R	Critical droplet diameter
E	Electric field
I	Electrical current
K	Conductivity
Q	Flow rate
q	Electric charge
q_R	Rayleigh limit charge
r_j	Jet radius

R_S Safety resistor

V Voltage

Acronyms

DAQ Data Acquisition system

EHDA Electrohydrodynamic Atomization

ES Electrospray

HF HEPA filter

HV High Voltage

HVPS High Voltage Power Supply

— A scientist in his laboratory is not a mere technician: he is also a child confronting natural phenomena that impress him as though they were fairy tales.

Marie Curie

1

Introduction and Aims

1.1 Particle Engineering Encapsulation

The concept of nanotechnology was firstly introduced by Richard Feynman, physicist and Nobel Prize laureate, on December 29, 1959, during the American Physical Society's annual meeting (Feynman, 1960) in a lecture entitled "There's Plenty of Room at the Bottom". He discussed about the problem of manipulating and controlling things on a small scale, challenging the audience with questions like how to write the entire 24 volumes of the Encyclopaedia Britannica on the head of a pin. He also discussed the question of how to read it, and even further, how to make copies of it.

In recent years, Nanotechnology has become a strong branch in the never-ending story of Science, and more specifically, Particle Engineering plays an important role given that not only nanoparticles ($< 100\ nm$), but also submicroparticles ($< 1\ \mu m$), and small microparticles (1-10 μm) (Nature, 2019) are receiving increasing interest in diverse technological and scientific applications (Anderson et al., 2016; Bayda et al., 2020). Therefore, there exists a significant need for the development of efficient delivery methods and carriers.

Particle size monodispersity, as well as 'shape monodispersity', are critical in some applications of polymer-based micro- and nanoparticles. In nutritional and medical applications, the overall objective is to enhance the targeted and prolonged pharmacological effect, thus obtaining an efficient drug delivery. Then, particle size matters since these particles will be delivered to the body through different delivery routes, and for some administrations not only very specific sizes are required (i.e. inhalable route size 1-3 μm is desirable) but also very small sizes (intravenous delivery)

(Kipp, 2004; Bisht et al., 2010; Emami et al., 2018; Calzoni et al., 2019). Moreover, particulate delivery systems protect the pharmaceutical compound from degradation immediately after preparation, while storing, and during transportation, and, even further, providing certain benefits which reduce side effects such as improved bioavailability, biocompatibility, and, absorbability (Elsabahy and Wooley, 2012; Cejková et al., 2013; Webster et al., 2013; Wicki et al., 2015; Montané et al., 2020; Dima et al., 2020; Cun et al., 2021). In summary, these particles are used as vehicles for drug delivery (Xie et al., 2006b; Xu et al., 2009), where the release profile of an encapsulated active pharmaceutical ingredient (API) is strongly influenced by the particle size.

Promising developments also concern agricultural industry in applications like fertilizers, pesticides, herbicides, sensors and quality stimulants, among others, where there is a need for continuous innovation due to the growing global challenges of food security and climate change (Parisi et al., 2015; Paramo et al., 2020; Sharma et al., 2021; Dhiman et al., 2021). Encapsulation of nanoparticles protects the active content and can affect diffusion, interaction and activity. Furthermore, Particle Engineering has also become important in the cosmetic (Katz et al., 2015; Bilal and Iqbal, 2020; Fytianos et al., 2020), food (Sridhar et al., 2021), animal feed (Hill and Li, 2017; Peters et al., 2016), chemical (Qu et al., 2013; Ibrahim et al., 2016), electronics (Tan et al., 2019), and other industries, seeking to alter particles' characteristics to allow businesses to deliver better products and services.

The industrial production of particles by liquid-to-particle conversion provides a simple, low cost, and chemically versatile manufacturing route over broad ranges of particle sizes and morphologies (Okuyama and Lenggoro, 2003). Indeed, different widely used Particle Engineering technologies have implemented diverse and complex designs to develop particle delivery systems, mainly for biological purposes Wan et al. (2013); Giorgiutti-Dauphiné and Pauchard (2018); Pardeshi et al. (2021), such as spray drying (Masters, 1991), emulsion solvent evaporation method (Park and Kim, 2004; Sheorey et al., 1991), spray freeze drying (Schiffter et al., 2010; Sebastiao et al., 2019; Adali et al., 2020), complex coacervation (Rutz et al., 2017; Brito de Souza et al., 2020), and many more (Pawar et al., 2018).

In addition, some authors have developed numerous conventional methods for producing microspheres from a polymer-containing solution: Berkland et al. (2001) combined an acoustic excitation method with a non-solvent carrier stream to produce poly(d,l-lactide-co-glycolide) PLG microspheres. They precisely controlled the droplet size distribution for a wide diameter range, from ∼5 to >500 μm. But for spheres as small as ∼1–2 μm in diameter the size distribution was broader. They also showed results in encapsulation and in vitro release of a model drug compound, rhodamine B. Artiga et al. (2020) used an inkjet-based technology to encapusulate 14 nm diameter gold nanoparticles (AuNPs) in a chitosan hydrogel, genereting 30 μm diameter polymeric particles, where they obtained a high throughput, though. They demonstrated biocompatible cell-adhesion properties and resist degradation over a large range of pH, being relevant for a variety of potential health applications. Xu et al. (2009) used a microfluidic flow-focusing device to fabricate monodisperse biodegradable drug-loaded microparticles, engineered with defined sizes, ranging from 10 μm to 50 μm, and being nearly monodisperse (polydispersity index = 3.9 %).

More specifically, Spray Drying (Masters, 1991), one of the most commonly used techniques, has successfully been developed for the generation of droplet sizes of the order of tens and hundreds of microns, where a wide dispersion of droplet sizes can be tolerated. This technique has been implemented for the industrial production of dried foods, pharmaceuticals, and fertilizers (Wang and Langrish, 2009; Vehring et al., 2020; Boel et al., 2020), among others.

But, yet, it has been difficult to extend such approaches to the droplet size range below about one micrometer (Sosnik and Seremeta, 2015; Salama, 2020; Malamatari et al., 2020; Jafari et al., 2021). Making homogeneous micrometer and nanometer droplets by liquid fragmentation with high energy efficiency is inherently difficult, as the conversion of mechanical energy to surface energy must be controlled at nanometric scales (Rosell-Llompart and Gañán-Calvo, 2008).

1.2 Electrospray Technique

1.2.1 Introduction

Electrohydrodynamic atomization (EHDA), also known as *electrospray*, is gaining research interest in different fields such as pharmaceutics. Among its advantages over other liquid atomization methods includes its ability to produce much smaller particles (in the few-microns and nano-metric size ranges) with size homogeneity (Bodnár et al., 2018; Smeets et al., 2018) and high energy efficiency (Rosell-Llompart et al., 2018; Gañán-Calvo et al., 2018).

Early fundamental studies on instabilities of electrified liquids where conducted by Rayleigh (1878, 1882). Later, Zeleny (1917) described for the first time long jets of electrified glycerin, becoming a pioneer in the electrospray technique. Key contributions were made by Taylor (1964), who analyzed the electro-hydro-static equilibrium of conical menisci. From that moment, the electrospray was reborn and nowadays is commonly used in many fields, existing many reviews about it, for a wide range of applications.

In the electrospraying process, the liquid to be atomized is electrified in order to establish a high non-uniform and axisymmetric electric field at the vicinity of the liquid meniscus. This field pulls the liquid in the direction of minimum potential, thus causing the liquid-gas interface to adopt a conical shape. Then, when the electric stresses overcome the surface tension, from the tip of such Taylor cone meniscus (Taylor, 1964) a steady micro-jet is emitted, which breaks up into highly charged tiny droplets (Fig. 1.1). The so-called cone-jet mode (Rosell-Llompart et al., 2018) is sustained by continuously feeding liquid to the Taylor cone, typically through a capillary tube. Downstream, the high electrical charge on the droplets produces the Coulomb repulsion between each other forming the characteristic spray plume. Notably, the jet breakup often happens by the Rayleigh mechanism, which periodically releases droplets in repeatable sizes (Hartman et al., 2000), resulting in narrowly dispersed droplet sizes, from micrometer to nanometer scale, depending on liquid properties and operating conditions (Rosell-Llompart and Fernández de la Mora, 1994; Chen et al., 1995). Indeed, at the minimum flow rate (Q_{min}) not

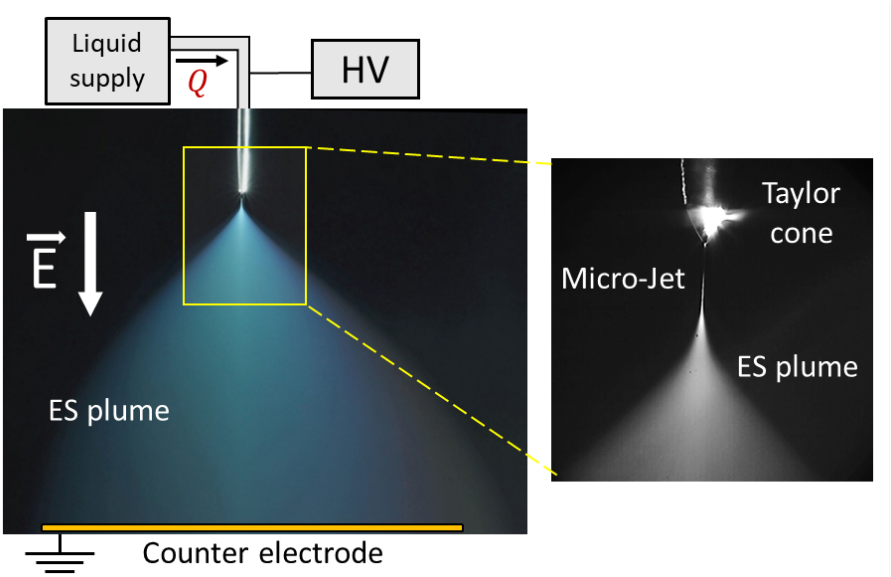

Figure 1.1. Electrospray main operation elements. Left: Conventional ES setup. Right: Droplet emission region.

only the smallest possible jet is developed, thus the smallest droplets are produced, but also the jet breakup is more regular, favouring the size monodispersity (Rosell-Llompart and Fernández de la Mora, 1994; Gañán-Calvo et al., 2013; Scheideler and Chen, 2014).

Some other features, that make the electrospray technique as unique, are related to the electrical charge carried by the droplets, which are unfeasible in other atomization techniques. For example, the aggregation is prevented since the charged droplets repel each other and therefore the size distribution is not distorted. The trajectory of the droplets (i.e. the shape of the electrospray plume) can be modified, if necessary, by tuning the electric field. This is possible to a certain extent since the space charge plays an important role. A clear example is shown in Sochorakis et al. (2019), where the authors used an additional electrode to conveniently direct several electrospray plumes in a linear array preventing lateral tilting.

Another advantage over other atomization systems when using a solution that contains solutes such as polymers or colloidal particles is that, since the micro-jet is roughly a couple of orders of magnitude smaller than the nozzle, clogging in the capillary tube may be easily prevented. Typically, the jet diameter is a few micrometers while the nozzle diameter is usually tens to few hundreds of micrometers.

In other atomization methods, like spray drying, it is common the use of gas streams to produce droplets, making the process more energetically expensive, whereas in electrospray the electrical force is predominant over inertia and no other energy sources are needed.

Other important applicable feature is that, since electrospray is based on laminar micro-flows, different liquids can be coaxially combined forming coaxial jets in order to produce structured multi-phase droplets, which can be used to make core-shell particles (Loscertales and Gañán-Calvo, 2002; Loscertales et al., 2004; Gómez-Mascaraque et al., 2019; Smeets et al., 2019).

Unfortunately, a noticeable issue is the low throughput that can be a problem for some applications in terms of productivity, where attempts for higher production evolves nozzle designs (Morad et al., 2016). Then, there is a need for scaling up the process by increasing the number of emitters to increase the throughput (Bocanegra et al., 2005; Deng et al., 2006; Deng and Gomez, 2007; Almería et al., 2011; Yang et al., 2012; Lojewski et al., 2013; Olvera-Trejo and Velásquez-García, 2016; Sochorakis, 2018; Sochorakis et al., 2019).

In sum, electrospray (ES) is a feasible technique for nebulising liquids to produce charged micro- and nano-sized droplets, with near size monodispersity, being an unrivalled method compared to other liquid atomization methodologies, which produce larger droplets, and/or wider dispersion of droplet sizes.

1.2.2 Electrospray operation and scaling laws

The simplest electrospray setup may be formed by few elements (Fig. 1.1). First element is a metallic capillary tube by which the conductive liquid is pumped to a nozzle. In order to obtain a fine control of the steady liquid flow rate of the order of nl/min to μl/min, the feeding is usually carried out by pressurizing the line or by means of a liquid pump. Another important element is a high voltage power supply (HVPS), which is connected to the capillary tube, providing electrical potential to the liquid meniscus.

To establish the electrostatic field that pulls the liquid meniscus from the nozzle,

an Earth-grounded counter electrode is usually placed at a given distance. Since the droplets are driven towards the counter electrode, the distance depends on the application requirements (space flexibility, liquid evaporation rate, particle drying, deposition spot area, etc.).

Beyond the conventional setup, another not mandatory element, but widely used for spray stability, is the *extractor ring electrode*. This additional element is symmetrically placed near the electrospray capillary tube. In down or up configuration, the voltage difference between both the extractor ring and the liquid meniscus establishes the electric field necessary to generate the electrospray. An advantage of the ring down configuration is that, downstream the extractor ring, the distance adjustment with a counter electrode allows more flexibility due to the Taylor cone is *screened* from external electrodes.

The parametric space defined by both the voltage (V) provided to the ES liquid and the liquid flow rate (Q), at which the system operates stable, was studied by Cloupeau and Prunet-Foch (1989), where they discovered the existence of a *stability island* defined by the minimum and maximum parameter values with respect to the configuration of the electrodes in the system. Outside the stability island boundaries, a variety of electrohydrodynamic (EHD) modes develop, where the most commonly used are:

— **Periodic EHD modes:** Electro-dripping[1], Spindle[2], Intermittent cone-jet[3].
— **Steady EHD modes:** Cone-jet[4], Multi-jet[5].
— **Cone-jet sub-modes:** Varicose jet breakup[6], Whipping jet[7].

Furthermore, the stability of the electrospray is also governed by the liquid mechanical and electrical properties. Consequently, a decrease of the volumetric flow rate (Q) will be imposed by an increase on the electrical conductivity (K). Likewise, an

[1]Cloupeau and Prunet-Foch (1990); Verdoold et al. (2014); Hijano et al. (2015)
[2]Sample and Bollini (1972); Cloupeau and Prunet-Foch (1990); Grace and Marijnissen (1994); Jaworek and Krupa (1999)
[3]Smith (1986); Juraschek and Röllgen (1998); Marginean et al. (2004); Bober and Chen (2011)
[4]Cloupeau and Prunet-Foch (1990); Hijano et al. (2015); Rosell-Llompart et al. (2018)
[5]Cloupeau and Prunet-Foch (1990); Grace and Marijnissen (1994); Juraschek and Röllgen (1998)
[6]Huebner and Chu (1971); Grace and Marijnissen (1994); López-Herrera et al. (2005)
[7]Huebner and Chu (1971); Ku and Kim (2002); Barrero and Loscertales (2007); Eggers and Villermaux (2008)

increase of the surface tension (γ) will impose an increase on the voltage (V) needed to sustain the stable cone-jet mode.

Different authors have developed physical models to predict the scaling laws that govern the electrospray process. Fernández de la Mora and Loscertales (1994) proposed, based on experimental work, theoretical considerations, and dimensional analysis, that for given liquid properties and operation conditions, the jet radius (r_j), as well as the electrical current (I) could be predicted (for a liquid with high electrical conductivity (K)) by the following scaling laws:

$$r_j \approx \left(\frac{Q\varepsilon_0\varepsilon_r}{K}\right)^{1/3} \tag{1.1}$$

$$I = f(\varepsilon_r)\left(\frac{\gamma K Q}{\varepsilon_r}\right)^{1/2} \tag{1.2}$$

where ε_r is the relative permittivity of the liquid, ε_0 is the electrical permittivity of vacuum (8.854 pF/m), γ is the surface tension, and f is an empirical function.

Independently, Gañán-Calvo et al. (1997) proposed the following scaling laws:

$$r_j = Q^{1/2}\left(\frac{\rho\varepsilon_0}{\pi^4\gamma K}\right)^{1/6} \tag{1.3}$$

$$I = 4.25\left(\frac{\gamma Q K}{ln\left(\sqrt{Q/Q_0}\right)}\right)^{1/2} \tag{1.4}$$

where is defined as $Q_0 = \gamma\varepsilon_0/K\rho$, being ρ the liquid density. They considered that the droplet diameter can be deduced as $d_d \sim 2.3r_j$, convenient for practical purposes.

Due to the increasing interest on the electrospray technique, there exist further efforts for revising the scaling laws for much wider liquid properties ranges (Chen and Pui, 1997; Hartman et al., 1999; Gañán-Calvo, 1999, 2004; Ku and Kim, 2002; Gamero-Castaño and Hruby, 2002; Smith et al., 2006; Basak et al., 2007; Higuera, 2009; Gañán-Calvo and Montanero, 2009; Maißer et al., 2013; Gañán-Calvo et al., 2013; Xia et al., 2019).

Even though polymer solution electrospray (Faramarzi et al., 2016; Smeets et al.,

2017; Bodnár et al., 2018) is a widely used technique, unfortunately, despite a well-established theoretical framework exists for pure solvents electrosprays, the complexity of the mechanisms involved requires an improvement of the understanding on this area.

1.2.3 Applications of electrospray

Interest in the electrospray route for producing small droplets and particles has been rekindled in different areas (Yurteri et al., 2010; Bock et al., 2012). In addition, due to features like high droplet charge number, dispersion of droplets by electrical repulsion, etc, there exists a wide range of applications where electrospray is used.

Yamashita and Fenn (1984) settled down the electrospray technique as a novel ion source. They succeeded in the production in vacuo of a wide variety of cluster ions for examination by various spectroscopic techniques. In 2002, Professor John Fenn was awarded a share of the Nobel Prize in Chemistry (Fenn, 2003) for his contributions specifically related to the development of *electrospray ionization* (Fenn et al., 1989, 1996). Nowadays, *Electrospray ionization mass spectrometry* (ESI-MS) is a commonly used technique for large molecules and routine liquid chromatography-tandem mass spectrometry.

The fact that droplet trajectories are controlled by the electrical field makes *electrospray deposition* (ESD) very suitable for making thin coatings and particulate films on a counter electrode for different applications (Hoyer et al., 1996; Hogan et al., 2007; Hogan and Biswas, 2008; Jaworek, 2007a; Rietveld et al., 2006; Khan et al., 2012; Gulfam et al., 2012; Bodnár and Rosell-Llompart, 2013; Arumugham-Achari et al., 2013; Altmann et al., 2014; Tang and Gomez, 2017; Jaworek et al., 2018). In energy production, storage and conversion devices, ESD has been used to improve the performance of materials, such as solar cells, photo-electrochemical cells, rechargeable batteries, and capacitors Tang et al. (2016); Kelder et al. (2018); Castillo et al. (2018). Recently, ESD has been used for applications using (O)LEDSs for lightning devices, and quantum dots to achieve luminescent properties (Koekoekx et al., 2020), or in biomolecule deposition (Morozov, 2010; Librán et al., 2017;

Kavadiya and Biswas, 2018).

Due to the unique feature which is the generation of sized monodisperse droplets, electrospray is widely used on *particle synthesis* (Fantini et al., 2006; Jaworek and Sobczyk, 2008; Almería et al., 2010; Bock et al., 2012; Pawar et al., 2018). As mentioned above, with great interest on the pharmaceutical and nutraceutical industries, solid biodegradable micro- and nanoparticles made out of polymer are widely used in therapeutics for remedial treatment of diseases (drug delivery, biomedical imaging, implant coating, tissue engineering, sensing...) (Yurteri et al., 2010; Chen and Pui, 2010; Bock et al., 2012; Nguyen et al., 2016; Mai et al., 2017; Nikolaou and Krasia-Christoforou, 2018; Boda et al., 2018; Sverdlov Arzi and Sosnik, 2018; Steipel et al., 2019; Wang et al., 2019; Ali et al., 2021; Rostamabadi et al., 2021), due to enhanced solubility of a payload of drug in order to improve drug stability and bioavailability. Furthermore, depending on their size, the particles can be targeted to different body organs with controlled drug release

Another application with increasing interest is related to the field of satellite propulsion, where *electrospray thrusters* are a type of electrostatic propulsion. Nowadays, the miniaturisation of satellites, as well as the increasing number of commercial launches, are highlighting the need for electric propulsion, which makes the technique of electrospray useful as it can work in the thrust range of a few micro-Newtons (Gamero-Castaño and Hruby, 2001). Recent developments use ionic liquids as a propellant, providing efficient propulsion capabilities to micro and nano satellites (1–100 kg) when very precise positioning is required for space missions (Gassend et al., 2009; Dandavino et al., 2014; Lemmer, 2017). Depending on the emission regime from the Taylor cone, there are two types of electrospray thrusters that expands the possibilities: colloid thrusters rely on droplet emission, and field emission electric propulsion (FEEP) thrusters rely on ion emission. Microfabricated arrays have been developed by some authors to obtain increase thrust (Lemmer, 2017; Dandavino et al., 2014; Gassend et al., 2009; Alexander et al., 2006; Stark et al., 2005; Alexander et al., 2006; Gassend et al., 2009; Dandavino et al., 2014; Lemmer, 2017).

Some other fields where electrospray has a significant influence must be mentioned: As a source of droplets or particles for calibration of aerosol instruments (Hogrefe

et al., 2004; Steiner et al., 2017) or sizing of different types of colloids (oxides, metals, and polymers) (Lenggoro et al., 2002), in *food technology*, where food encapsulation and packaging are enhanced the food properties and conservation (Gomez-Estaca et al., 2012; Khan et al., 2012; Gomez-Estaca et al., 2012; Echegoyen et al., 2017; Librán et al., 2017; Gómez-Mascaraque et al., 2019; Tsai and Ting, 2019; Yilmaz et al., 2019; Niu et al., 2020; Wang et al., 2020; Torres-Giner et al., 2020), or the increasing interest in *cosmetics* (Mehta et al., 2017; Bae et al., 2019).

The effect of glow corona discharge present during electrospraying for given conditions has been used for decontamination of liquids or in material processing (Jaworek et al., 2019).

Other approaches for the production of nanomaterials are, for example, *emulsion electrospray* (Wang et al., 2013; Jaworek, 2008; Wang et al., 2013; Ho Lee et al., 2021), and ES combined with its electrohydrodynamic twin technique, *electrospinning* (Zong et al., 2018; Dai et al., 2018).

1.2.4 Droplet charge as a problem

Even though the electrical charge carried by the electrospray droplets is usually an advantage, unfortunately, from the point of view of using electrospray to produce particles, the net electrical charge carried by the droplets leads to several issues. First, when making non-conductive particles collected as a particulate film on a substrate under the spray, the buildup of static charge on the film causes the progressive expansion of the electrospray plume (Bodnár and Rosell-Llompart, 2013). Meanwhile, hypothetically, micro-discharges in the film could develop, damaging the particles (although, to our knowledge, the existence of micro-discharges inside electrospray films has not been directly observed) (Uecker et al., 2010). Second, when multiplexing electrosprays, the electrostatic repulsion between different sprays limits the scalability of the process (Bocanegra et al., 2005; Deng et al., 2006; Almería et al., 2011; Sochorakis et al., 2019). Thirdly, the charged droplets attain fast speeds in the high electrical field (of order m/s) and can reach the collection electrode as incompletely dried particles, thus forming a continuous film instead of a particu-

late film. This situation is favored with low volatility solvents (e.g. DMF), larger droplets (several micron in diameter, commonly encountered), and multiplexed systems, where the spray cannot be allowed to expand much (Sochorakis et al., 2019).

Coulombic instabilities of the droplets

A fourth issue caused by the high electrical charge on the droplets is the occurrence of the so-called *Coulombic instabilities* (CIs), which trigger during droplet evaporation when the destabilizing electrical stress on the droplet's surface (where the net charge resides) grows to the point at which it exceeds the stabilizing capillary tension stress, which grows slower (Gomez and Tang, 1994; Davis and Bridges, 1994; Saville, 1997; Duft et al., 2003).

Theoretically, the Coulombic instability will occur, for a spherical charged droplet of an inviscid perfectly conducting fluid, when it reaches a *critical droplet diameter* (Rayleigh, 1882):

$$d_R = \left(\frac{q^2}{8\pi^2 \varepsilon_0 \gamma} \right)^{1/3}, \tag{1.5}$$

where q is the droplet charge, γ is the surface tension coefficient of the liquid, and ε_0 is the electrical permittivity of vacuum (8.854 pF/m). Some authors use the *Rayleigh limit charge* expression related to the electrical charge necessary for a droplet with diameter d to undergo droplet fission (Fernández de la Mora, 2007):

$$q_R = \sqrt{8\pi^2 \varepsilon_0 \gamma d^3} \tag{1.6}$$

Coulombic instabilities are particularly detrimental for liquid-to-particle conversion, as they lead to non-spheroidal (elongated or filamentous) particle shapes or mixed fragment sizes (Li et al., 2007; Almería et al., 2010; Bodnár et al., 2018). Fig. 1.2 shows an example of polystyrene particles, produced in our laboratory, carrying filaments due to Coulombic instability events during drying. CIs can sometimes be prevented by the early formation of a solid shell on the evaporating droplet (Bock et al., 2012; Almería and Gomez, 2014; Bodnár et al., 2018). In the case of polymeric solutes, this strategy works only within a narrow range of solute concentrations

(Fantini et al., 2006; Meng et al., 2009), while sometimes only working in one region of the spray (due to even slight differences in droplet size and charge) (Bodnár, 2016). Another way an early shell may form is by uptake of a non-solvent vapor, e.g., at ambient relative humidity (Bodnár et al., 2018).

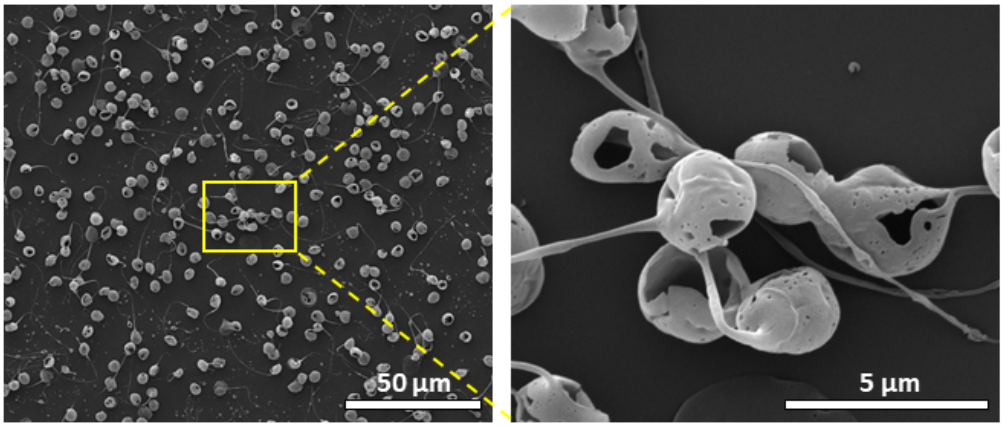

Figure 1.2. SEM images of polystyrene particles carrying filaments developed due to Coulomb instabilities.

1.2.5 Charge reduction of electrospray droplets

Reducing the droplet charge may be a steeping-stone on the way to prevent the Coulomb instabilities, as well as other charge related issues like those mentioned above. Few authors have discussed about the usefulness of discharging electrosprays, probably due to the fact that the charge itself constitutes an advantage for their applications. Indeed, controlled discharging (total or partial) of electrosprays may be necessary for different practical purposes. For instance, in the case of particle production, reducing significantly the electrical mobility of the droplets may lead to obtain free aerosols, and consequently to easily transport the particles to be collected, minimizing the particle losses (provoked, without discharging, by space charge), and with the advantage of the possibility of controlled manipulation of the transported particles (not possible in general electrospray applications) (Yurkstas and Meisenzehl, 1964; Noakes et al., 1989; Cloupeau, 1994). For example:

— Tuning the drying path when the solvent evaporation rate is low to help the particles to properly dry.

— Heating the neutralized particles along a tubular oven to make them solid (not

hollow) and, moreover, reducing their size.

In addition, it is well-known that the throughput of a single emitter is too low from an industrial point of view, thus a barrier needs to be overcome: *scaling-up* the process. But in a multiple-emitter electrospray (Sochorakis et al., 2019), the space charge might be a problem in terms of developing miniaturized systems. Then, managing the space charge by reducing the droplet charge in a controlled manner may be a key point in order to scale-up the process.

Therefore, we believe that the discharge of electrospray droplets can be a tool for manipulating the transported electrosprayed droplets/particles.

Aerosol charging/discharging. Brief review

The transport of aerosol particles is influenced by the net electrostatic charge they carry (Liu et al., 1985; Pähtz et al., 2010), both in natural environments as in artificial systems, generated in industrial production or in the laboratory (Forsyth et al., 1998; Hinds, 1999). The electrical charge may be desirable or undesirable. As an example of desirable, the net electrical charge on aerosol particles is famously used for characterizing the size distribution of ultrafine aerosol particles, by determination of their electrical mobility (Cheng et al., 1981; Flagan, 2011). Net electrical charge is also important in the electrical sensing/detection of particles constitutes an important method for aerosol measurement (such as in mobility spectrometers (Russell et al., 1995), diffusion charging-based sensors (Burtscher, 1992), electrical low pressure impactor (ELPI) (Keskinen et al., 1992)). Advantages of electrical sensing over optical sensing is cost, the possibility to miniaturize, and to collect with high time resolution ($<$ 1s); see Dhaniyala et al. (2011). Electrodynamic levitation of particles is another important example of the importance of charge (Wuerker et al., 1959; Davis, 1997; Achtzehn et al., 2005; Conangla et al., 2020). Electrical charge is also exploited in particles sampling (Flagan and Seinfeld, 1988) and in electrostatic precipitators and other devices designed to remove particles from gas/air streams [electrostatic air cleaning] (Cheng et al., 1981; Mizuno, 2000; Jaworek et al., 2007, 2006). In this case, active charging of the aerosol particles is necessary to achieve as high a charge state as possible, so field charging by corona discharges is common

(Flagan, 2011).

On the other hand, the electrical charge may also be undesirable, thus existing a need for reducing the charge, for example, to reduce electrostatic losses in aerosol measuring equipment, or to establish a reference low charge state in aerosol differential mobility analyzers. Then, when undesired, the aerosol particles can be neutralized. In unipolar clouds, such as aerosols created artificially, the neutralization of the cloud needs the droplets to be presented with a bipolar or unipolar stream of ions (of opposite polarity for the latter). This is for example the case of the electrospray technique (Rosell-Llompart et al., 2018).

First attempts to reduce aerosol charge involved the use of radioactive sources (Cooper and Reist, 1973; Fan et al., 2003; Ji et al., 2004), bipolar corona discharge (Zamorani and Ottobrini, 1978; Adachi et al., 1983, 1993; Romay et al., 1994; Stommel and Riebel, 2004), photoionization by UV-light (Burtscher et al., 1982; Matter et al., 1995) and by soft X-ray radiation sources. Also aerosol neutralization by post-DBD (dielectric barrier discharge) has been suggested (Mathon et al., 2017).

In the particular case of *electrosprays*, some authors have tried to neutralize them by similar techniques (Yurteri et al., 2010), such as radioactive sources (Lewis et al., 1994; Chen et al., 1995; Kaufman et al., 1996; Lenggoro et al., 2000; Frey et al., 2005; You et al., 2014), with the disadvantage that in many laboratories the use of radioactive materials is forbidden, or a proper licensing is difficult to obtain. Others are oppositely charged electrosprays (Borra et al., 1999; Camelot et al., 1999; Morozov, 2011; Fu et al., 2012; Mou et al., 2013; Tang et al., 2016, 2017; Fernandez de la Mora and Barrios-Collado, 2017; Fernandez de la Mora, 2018), soft X-rays (Modesto-Lopez et al., 2011; Liu and Chen, 2014) or sub-kHz AC electrospray (Dau et al., 2020).

The corona discharge approach was attempted in producing inhalation aerosols for drug delivery (Noakes et al., 1989; Zimlich et al., 2002; Davies et al., 2005), pharmaceutical particles (Tang and Gomez, 1994; Ijsebaert et al., 2001; Zimlich et al., 2002; Davies et al., 2005; Xie et al., 2006b,a; Ciach, 2006, 2007; Xie and Wang, 2007; Almería and Gomez, 2014), and ceramic powders (Rulison and Flagan, 1994; Tang et al., 2017). One advantage of this method over others is the higher concentra-

tion of ions generated. An interesting design for production of particles which uses corona discharge is the so-called "Delft Aerosol Generator" (DAG), firstly introduced by Meesters et al. (1992), where the corona discharge needle is naked, facing the electrospray nozzle. Other authors used a device similar to the DAG (Hartman et al., 1995; Xie et al., 2006b), and Cloupeau (1994), being first in isolating corona needle using counter electrodes for ES and corona discharge, dedicated a critical study section to the DAG device. In this case, they do not report information about droplets reaching the corona needle affecting the corona discharge process, or, otherwise, amount of ions reaching the Taylor cone, affecting the electrospray stability. Other authors isolated the corona by a cylindrical mesh (Ebeling et al., 2000; Lu and Koropchak, 2004). Interestingly, corona ions have also been used to charge-reduce droplets and analyte ions in electrospray ionization mass spectrometry (ESI-MS) (Fenn, 2003), an analytical technique by which solutes (importantly, proteins and large biological entities) can be transformed into gas-phase ions and be weighed by standard mass spectrometers (Ebeling et al., 2001, 2000; Bornschein and Ruotolo, 2015; Campuzano and Schnier, 2013). However, the aim in these studies is ion analysis; therefore, the optimal configurations and chemical compositions of those studies do not apply to the goal of producing particles.

In none of the mentioned works where the electrospray is combined with corona ions to make particles could we find data on the droplet discharging efficiency, the particle morphology changes, or their dependence on the independent variables of the problem (electrode geometrical parameters, corona conditions, electrospray conditions, etc.). Nor have the ion losses and droplet losses to the electrodes been investigated typically, despite their importance. All these important questions must be answered to improve and optimize electrospray-corona systems. Some authors have published numerical methods to simulate the mechanisms concerning the electrospray neutralization (Higuera, 2016; Khalifehei and Higuera, 2020), and, in addition, such data should be useful for informing numerical simulations on these systems. One recent exception is Mustika et al. (2021), focused on producing low-charge airborne nanoparticles by electrospraying dilute nanoparticle suspensions, and having unsuitable particle losses for our purpose.

1.2.6 Corona discharge

A well-known method to generate unipolar ions is the *corona discharge* (Townsend, 1915; Goldman et al., 1985; Chang et al., 1992; Adamiak and Atten, 2004), an atmospheric-pressure plasma. It consists of a stream of ions generated at a high-field ionization region by electrical breakdown of the surrounding gas around the active sharp electrode. The emission begins when the electric field near the electrode surface reaches a certain threshold, E_0. Theoretically, the threshold (E_0) at the tip of a hyperbolic point can be written in the form of the Peek's law:

$$E_0 = 3.1 \times 10^4 \delta \left(1 + \frac{0.308}{\sqrt{0.5\delta r}}\right) \tag{1.7}$$

where $\delta = PT_0/P_0T$, and r is the electrode radius in cm, T_0 the standard temperature, T the actual temperature, P_0 the standard pressure and P the actual pressure of gas.

In the low field drift region, which connects the ionization region with the low potential counter electrode, ions or electrons, when positive or negative polarity, respectively (Loeb, 1948), are drifted reacting with neutral gas molecules. The space charge field will determine the ion density distribution and the I-V characteristics (Townsend, 1915; Lama and Gallo, 1974; Giubbilini, 1988), which, for a point-to-plane configuration, follows the so-called Townsend's law:

$$\frac{I_C}{V_C} = \mathcal{C}\,(V_C - V_0) \tag{1.8}$$

where I_C is the corona current emitted at the needle tip, V_C is the corona voltage provided to the needle, and $\mathcal{C}$ is a constant that depends on the system configuration.

— We are just an advanced breed of monkeys on a minor planet of a very average star. But we can understand the Universe. That makes us something very special.

Stephen Hawking

2

Unipolar Corona Ion Source for Electrospray Droplet Discharging

2.1 Introduction

The generation of highly charged droplets by the *electrospray* technique (Rosell-Llompart et al., 2018) may lead to several issues, thus reducing their charge is needed. One example is when polymer solution electrosprays are used to produce homogeneous particles and the net electrical charge carried by the droplets may trigger occurrence of the so-called the *Coulombic instabilities* (Bodnár et al., 2018), thus distorting the particle size distribution and morphology.

In our study, focused on electrospray neutralization for the production of globular particles, one of the important design decisions was whether the needle should be exposed or hidden behind an orifice (Cloupeau, 1994). In prior works, the corona needle has been hidden by different ways (Frey et al., 2005; Nagato et al., 2006; Viikov et al., 2009), but none of them have studied the effect of the orifice size on the extracted current. If the corona needle is exposed to the spray, then the field lines pervading the zones of the spray will be focused on the needle, so the droplets will/may have a strong tendency to accumulate on the needle if they are not neutralized. Whereas if the needle is hidden behind an orifice, the ion current extracted can be in principle be regulated or reduced to the level needed to achieve the discharging of the spray. Another advantage of hiding the needle is that the system becomes more controllable. This is due to the fact that both corona needle and electrospray (or any other external system) are thus electrostatically isolated from each other, with the possibility of controlling each electrostatic field independently, which is very important in order to tune the extracted corona current to properly study the effects of the ions on the electrospray droplets. In case of polymer solu-

tion electrosprays, the final particle shape, size, or any other characteristic, may be affected by the amount of ions that collide with the particles, reducing the charge, before they are being dried.

Our objective was the development and characterization of an ion generating device suitable for the neutralization of electrosprays in the 10-100 nA range. Although electrosprays have currents in a broader range, typically between about 10 nA (for large particles) and about 500 nA (for small droplets from highly conductive liquids). However, we focus on the 10-100 nA range where electrospray currents typically lie when used for producing small microparticles and submicrometer particles from polymeric solutions (Bodnár, 2016; Bodnár et al., 2018; Carrasco-Munoz et al., 2021). In this study we determine the configurations leading to stable production of ions in this current range, and we characterize the distribution of the extracted ions (ion profiles) and the sensitivity of the extracted current and ion profiles to key geometrical parameters. Our hypothesis is that it is possible to neutralize (or severely discharge) an electrospray plume by a corona ion plume having similar current in a coaxial configuration.

2.2 Methodology

2.2.1 Corona ion source design

A purpose-made unipolar ion source was built. It consisted of a corona discharge needle (15 μm tip radius, 32º total angle), made by sharpening a tungsten rod (Alfa Aesar, 1.5 mm diameter), axi-symmetrically anchored inside a modified tee connector (IDEX P-714 Low-Pressure Tee Assembly, Natural PEEK) which acts as the housing. The anchoring was made by a PEEK nut and an PTFE ferrule flangeless fitting (parts of the IDEX P-714). A head electrode (Fig. 2.1a), mechanized from a brass rod (RS, 12 mm diameter), was used as an Earth-grounded counter electrode, and had an orifice through which the ions were extracted. The voltage difference between the corona needle and the head electrode establishes the electric field to sustain the corona discharge. Fig. 2.1b shows a photography of the device where the housing is capped with the head electrode. The applied electric potential at the corona needle was provided by a HVPS (Ultravolt HVRACK-4-250-0032), and continuously monitored by means of a HV probe (Testec, TT-HVP-40, $10^9\Omega$). The current at the head electrode was measured by a picoammeter (Keithley 6485). Synthetic air was fed to the corona discharge region at a low flow rate Q_C (13.3 ml/min, corresponding to a plug-flow gas speed of 71 mm/s). The corona discharge needle, centered and tight inside the device. The Earth-grounded head electrode, through a nanoammeter, measured the non-extracted current from the ions that did not exit the device through the orifice. Therefore, the voltage difference between the corona needle and the head electrode orifice, at a given distance d (Fig. 2.1a), established the electric field needed to sustain the corona discharge. The polarity used for the corona discharge was *negative* because it is highly localized at atmospheric pressure conditions: air at 1 atm.

Since the head electrode orifice allows the ions to pass through it, both diameter and thickness are important parameters that are studied. For this purpose, different head electrodes were mechanized with different orifice sizes for both diameter, a, and thickness, t, shown in Table 2.1. The edge of each orifice was hand polished trying to make it both rounded and smooth enough to prevent sparks.

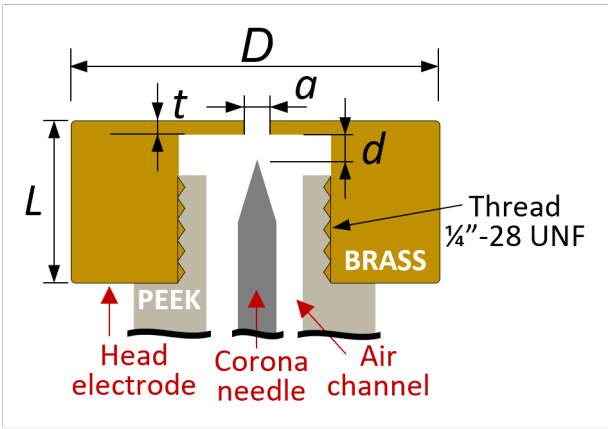

(a) Configuration inside the head electrode

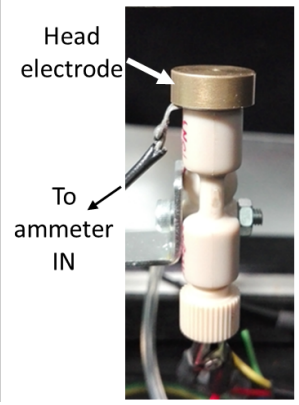

(b) Ion source

Figure 2.1. Elements of the ion source device. (a) Sketch of the head electrode, including the interior of the ion source with the corona discharge needle and the PEEK thread where the head electrode is screwed. The zone between the needle tip (high voltage) and the orifice (low voltage) is the ionization zone. (b) Picture of the device used as an ion source.

Table 2.1. Head electrodes orifices dimensions, where a is the diameter and t is the thickness. Coloured cells match with each other in one parameter. In all cases, D was 12 mm (Fig. 2.1a).

Head #	1	2	3	4	5
$\boldsymbol{a}$ $[mm]$	1.0	1.5	2.0	1.5	1.5
$\boldsymbol{t}$ $[mm]$	0.4	0.4	0.4	0.6	2.0

Synthetic air was fed to the corona discharge region in order to control the ambient composition surrounding the corona needle tip, allowing the renewal of air as well at low flow rate Q_C (typically 13.3 ml/min, corresponding to plug-flow gas speed of 71 mm/s). We have tried nitrogen as the feeding gas, but the corona did not work as stable as when using synthetic air, so we finally decided to use the latter. Since the chamber is not pressurized, the corona works at atmospheric pressure (1 atm).

To determine the distance of the needle tip to the head orifice d (Fig. 2.1a), we used a dial indicator mounted on an optical microscope. In this way, by focusing on each element the relative positions between the needle tip and the orifice outer edge were measured, and then we obtained d after subtracting the orifice thickness t.

Last but not least, we checked the centering of the negative corona discharge emission (near the needle tip) relative to the head electrode orifice to guarantee that the radial coordinate of the electric field, within the ionization zone (region between the needle

tip and the orifice), is homogeneously distributed, and therefore the ion flux is axi-symmetric. For this reason, to check the emission point centering, a camera with a zoom lens attached was used for visualization purposes (Fig. 2.2).

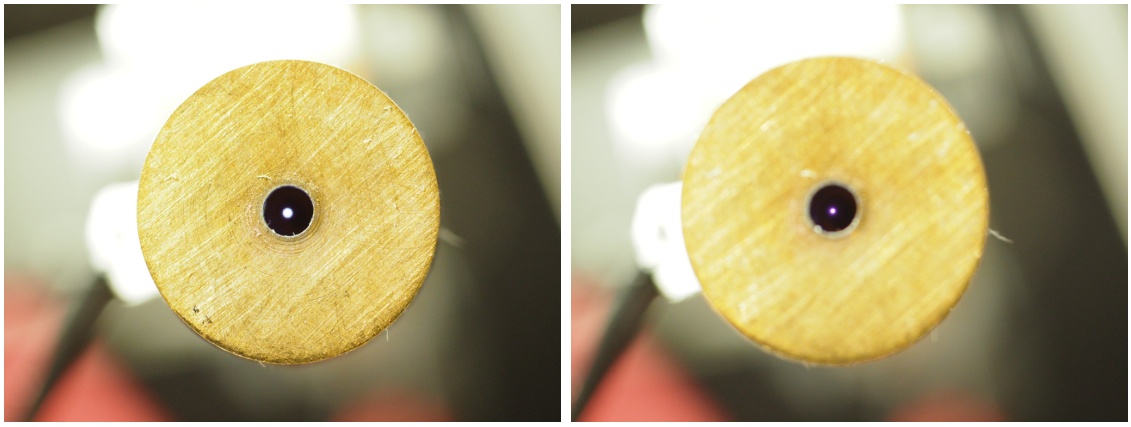

(a) Focused on the head electrode orifice **(b)** Focused on the corona needle tip

Figure 2.2. The light coming from the negative corona discharge emission point allows us to ensure a centered position of the needle tip.

2.2.2 Extracted current characterization

The characterization of the unipolar ion source device is important to understand how intense is the ion current, after the ions exit the device through the orifice, as a function of an *external* electric field. Thus, we obtain information about the ion current reaching a zone of interest that may be useful for some applications. In our case, we are interested in ion flows that allow us to discharge an electrospray plume by exposing it to the unipolar ion source. Therefore, the ion current must be of the order of the electrospray current.

A. Extracted ion current characterization with a plate electrode

To characterize the unipolar ion source, we measured the *extracted ion current* (I_{Ext}) on a brass plate from those ions that were generated by a corona discharge, afterward passed through the head electrode orifice, and finally, by following the electric field lines, driven towards a counter electrode.

The counter electrode was a flat brass plate (100 × 100 × 1 mm) mounted in front of

the ion source, as shown in Fig. 2.3, at a distance H. In order to efficiently attract the ions, the area of the plate electrode was chosen large enough compared to the narrow ion plume expected, and so the ion plume does expand significantly, thus preventing ion losses. The purpose was to establish an adjustable external electric field between the plate electrode and the head electrode, which will attract the ions passing through the orifice to the plate. The extracted ion current (I_{Ext}) is directly measured by a battery powered nanoammeter, connected inline with the HVPS. The characterization was performed inside a closed chamber.

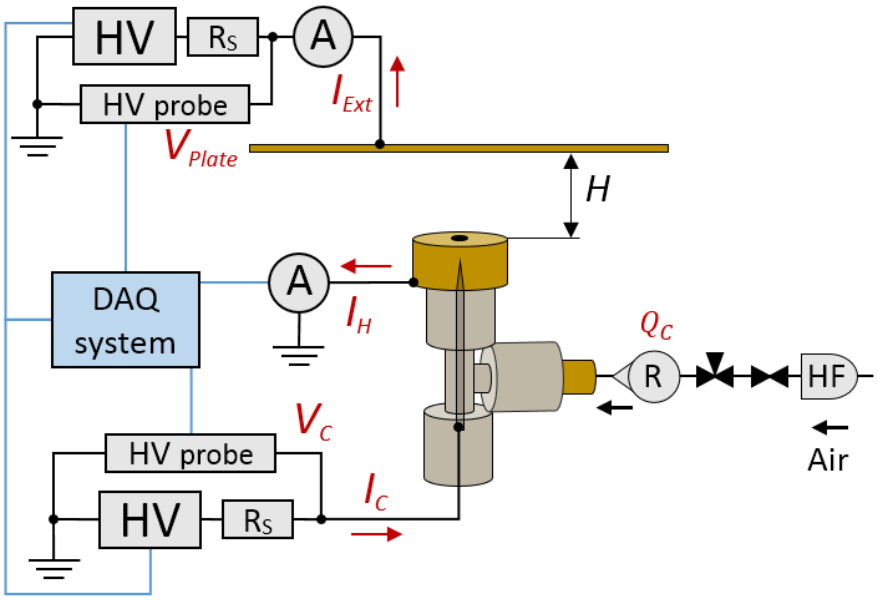

Figure 2.3. Setup used for characterizing the extracted ion current through the ion orifice towards a plate electrode. System schematic comprising unipolar ion source, and ion current measurement electrode. Acronyms: DAQ = Data acquisition; HV = high voltage; HVPS = HV power supply; A = ammeter; HF = HEPA filter; R = rotameter; R_S = safety resistor (250 MΩ).

The current measured at the plate electrode was recorded by hand, since the nanoammeter was connected inline, thus floating at high voltage. On the other hand, the output voltages from the picoammeter of the head electrode, the HV probes, and the two HVPS remote monitoring were recorded by a data acquisition system (National Instruments PCI-6221 DAQ card).

B. Extracted ion current characterization with a covered ring electrode

In applications like electrospray neutralization, the electric field, which depends on the electrodes' voltages and geometries, presumably governs the trajectories of both ions and droplets. In order to characterize the unipolar ion source in a situation closer to an electrospray-neutralization system, an additional configuration was used. As will be shown in the following two chapters, the electrospray will be created from an electrified needle facing a ring counter electrode. Therefore, the counter electrode was replaced by a ring (Fig. 2.4), at a distance H, and connected to high voltage in order to attract the ions. To ensure the trapping of any central ions, the ring was covered with a metal disc (12.7 mm diameter) (Fig. 2.4b). These

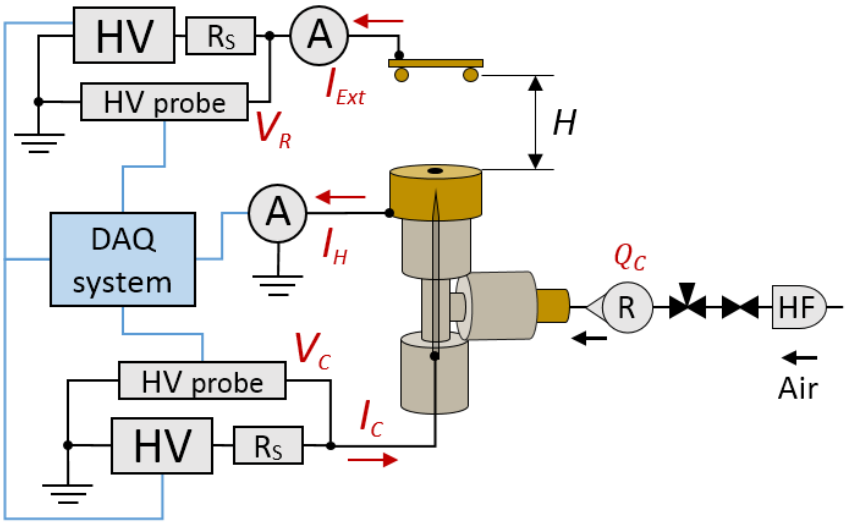

(a) Sketch of the corona device-to-ring setup

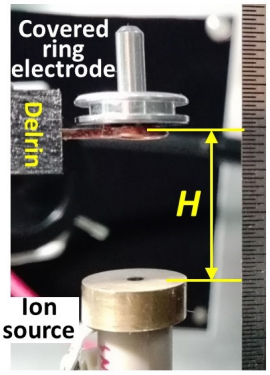

(b) Photography of the extracted ion current path

Figure 2.4. Setup used for characterizing the extracted ion current through the ion orifice towards a covered ring electrode. (a) System schematic comprising unipolar ion source, and ion current measurement electrode. (b) Photography of the ion source and the covered ring electrode. Acronyms: DAQ = Data acquisition; HV = high voltage; HVPS = HV power supply; A = ammeter; HF = HEPA filter; R = rotameter; R_S = safety resistor (250 MΩ).

geometry changes allowed us to determine I_{Ext} without elimination of the essential elements. Compared to the previous configuration, the electric field is changed, and one objective was to check whether there exists any ion losses through, for instance, the ring electrode support (black Delrin® piece at the upper-left side in Fig. 2.4b), because the intention of the device is to be attached to the electrospray system.

2.2.3 Ion current profile determination

We also investigated how the ion flux is spatially distributed. In other words, how the ion plume expandes along its journey, and how intense the ion current flux is throughout a cross section, at a given distance. Regarding our goal of exposing an electrospray plume to the ion source, understanding the ion plume is key to comprehend, in advance, whether the ions could reach all zones of the spray.

To determine the ion current profile, we measured a small fraction of the total extracted ion current (I_{Ext}) as a function of the position in an orthogonal plane and, for this purpose, the setup was slightly changed (Fig. 2.5). The flat brass plate (100 × 100 × 1 mm) was again used as an electrode to measure the extracted ion current (I_{Ext}) but, in this case, it was Earth-grounded through a nanoammeter. In addition, an orifice (1 mm diameter) was drilled in its center to measure a small fraction of the total current I_{Pin}, on a 1 mm diameter pin electrode. This electrode

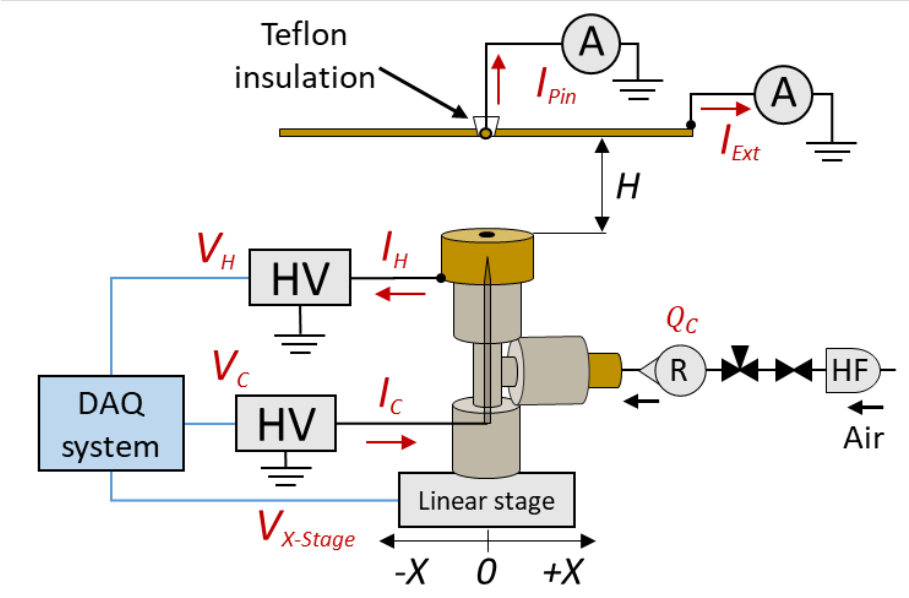

Figure 2.5. Sketch of the setup made for determine the flux profile of the extracted ion current, exiting the ion orifice toward the counter electrodes. A fraction of the extracted ion current is measured at a pin electrode while the ion source can be moved in the X direction.

was Earth-grounded through the Keithley 6485 picoammeter and electrically isolated from the plate electrode by a teflon piece, was inserted through the plate orifice. To reduce the signal noise, the backside of the pin was isolated by a BNC connector.

For easier visualization, a photo of the system is shown in Fig. 2.6.

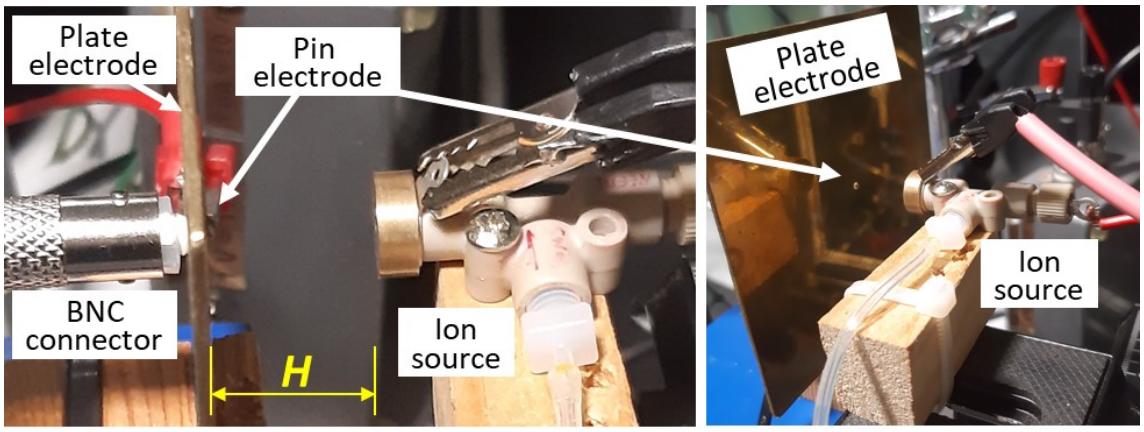

Figure 2.6. Photos of the setup used for the determination of the ion current profiles. Left: Photo taken perpendicular to the ion source axis showing the insertion of the pin electrode through the plate. Right: Photo taken at an angle where the large plate-to-pin area ratio can be appreciated

Another change in the setup, compared to the previous design, is about the electrodes where the electrical potential is now applied. Since the current to be measured at the pin electrode I_{Pin} was expected to be very small, below 10 nA, we used a picoammeter, which can not be floating at high voltage. Therefore, to adjust the *external* electric field between the ion source and the plate and the pin electrodes, these were Earth-grounded (through ammeters), and the head electrode was set at a high negative voltage. Consequently, we needed to adjust (increase) the voltage at the corona discharge needle to a value that we could sustain a corona discharge.

Finally, to scan the ion flux profile we needed to control the horizontal position X of the ion source relative to the pin electrode, and, for that purpose, the ion source was mounted, perpendicular to the plate, on a linear stage. The linear stage was mechanically coupled by a simple gear assembly to a linear potentiometer (Vishay 5 kΩ) that, connected, to a voltage reference (10 V) as input, allowed us to monitor the output voltage V_X as a function of the horizontal position. The calibration curve is shown in Fig. 2.7.

Furthermore, the pin-plate electrode assemblage was mounted on a lab jack, which allowed setting its height so that the pin electrode and the corona device orifice were positioned at the same height.

In this setup, both plate and pin currents, as well as the potentiometer output

voltage V_X were recorded by the data acquisition system, as the other signals. The safety resistor were removed.

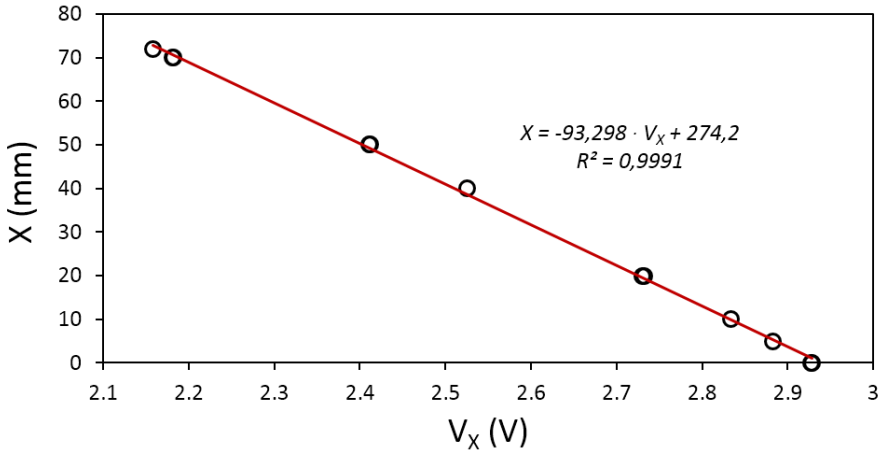

Figure 2.7. Calibration of the positioning system. The line is a linear fit from a linear regression analysis

2.3 Results on corona discharge in point-to-plate configuration

2.3.1 I-V characteristic of corona discharge in point-to-plane configuration

We have first used several corona discharge needles *naked* (head electrode removed) in front of a disc electrode (37.5 mm diameter) to characterize the corona current as a function of the voltage, and thus obtaining the I-V characteristic curve for this point-to-plane configuration and different needle tip radius (Table 2.2).

Table 2.2. Tungsten needles used in the corona discharge characterization experiment, where r is the tip radius, α is the angle near the tip, and H is the needle tip-to-disc distance. In all cases, they were made from a 1.5 mm diameter tungsten rod.

Needle #	n_1	n_2	n_3
$\boldsymbol{r}$ $[\mu m]$	30	15	440
α [°]	22	32	28
$\boldsymbol{H}$ $[mm]$	4.50	5.80	5.80

In addition, in order to study the effect of the surrounding gas, the system was enclosed inside a chamber at atmospheric pressure (Fig. 2.8). The gases used were synthetic air and nitrogen. The corona needle was connected to high voltage and the disc electrode was grounded through an nanoammeter.

Furthermore, we tried to study the effect of the corona discharge polarity, but in the case of *positive* polarity it was not possible to maintain a stable corona discharge with any needle in either gas. In fact, sparks and glow channels were created, making the process unsuitable to be used to neutralize electrosprays. Two examples of the development of glow channels at a given positive voltage are shown in Fig. 2.9. Then, due to the more successful control of the corona discharge in *negative* polarity, we chose this as the preferential one, since using it with electrosprays, the latter would conveniently work at positive polarity. Indeed, electrosprays are more commonly operated at positive polarity.

To obtain the I-V characteristic curves, the chamber was previously filled with the

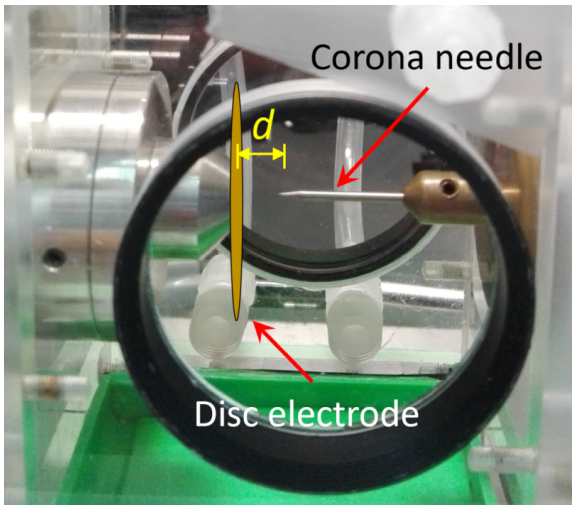

Figure 2.8. Chamber used to obtain the corona discharge I-V characteristic curves in a point-to-plane configuration, with a controlled gas ambient. Synthetic air and nitrogen were used. The disc electrode diameter was 37.5 mm, and in this case has been digitally added due to unavailability of a proper photo.

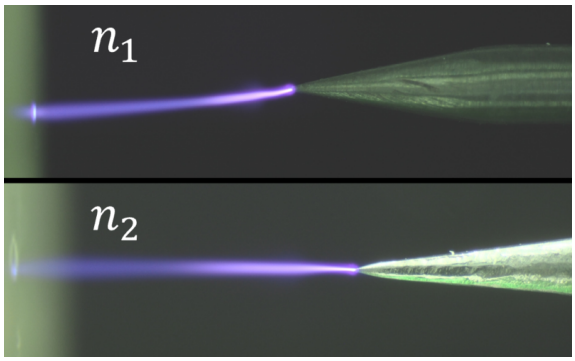

Figure 2.9. Snapshots of glow channels created with positive corona discharge for needles n_1 and n_2. Exposure time = 500 ms.

appropriate gas (synthetic air or nitrogen), at a flow rate of ∼1.3 l/min for 5 minutes. The gauge pressure was measured inside the chamber by a digital manometer, and was constant during all the experiments. During each run, the gas flow rate was lowered to ∼0.4 l/min. Then, operating in current regulation, both current and voltage were recorded.

Fig. 2.10 shows the I-V characteristic curves, of negative corona discharge, for the tungsten needles shown in Table 2.2. The data was digitally filtered by a moving average filter. When synthetic air was used (n_i^{Air}), the highest corona current (I_C), at a given voltage (V_C), was obtained for n_2^{Air}, the needle with the smallest tip radius (15 μm). For the needle with slightly bigger tip radius, n_1 (30 μm), the current was

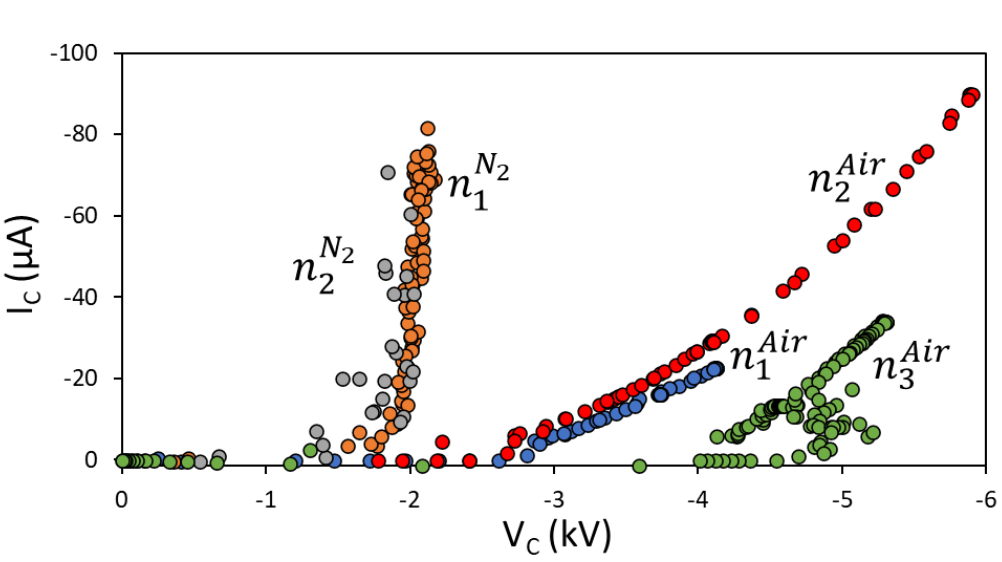

Figure 2.10. Corona discharge I-V characteristic curves for 3 different corona needles n_i^{gas} in two different gases (synthetic air and nitrogen).

a little lower, even though the distance to the plate (H) was slightly smaller for n_1 than for n_2 ($H_1 < H_2$). In the case of n_3^{Air}, corresponding to a much larger needle tip radius (440 μm), the current was significantly lower than the others, and even further, the current was not stable until ∼20 μA.

The branches corresponding to nitrogen shown in Fig. 2.10 appeared at much lower voltages. Notice that there is no branch for $n_3^{N_2}$ because in this case the corona discharge was unstable. Even though the corona current, with nitrogen, was significantly higher than when using synthetic air, the system was quite unstable and fluctuations were present along the runs, making the process much more unstable than in the other case. Moreover, although the data shown is filtered and the fluctuations are not visible, it is clear, when comparing with the previous data n_i^{Air}, that when using synthetic air the corona current was more stable (>20 μA for $n_3^{N_2}$).

Figure 2.11 shows, according to Townsend's law (Eq. 1.8), the evolution of I_C/V_C vs. V_C. From the linear extrapolation (at low I_C/V_C in n_2^{air} for the comparison) we found that the corona onset voltage $V_{C,0}$ was -2.37 kV for n_1^{air} and -2.06 kV for n_2^{air}. In the case of n_3^{air} the corona onset occurred at a higher voltage, $V_{C,0}$ = -3.98 kV, and, in accordance with Peek's law (Eq. 1.7), this is due to the fact that a larger needle tip radius needs a higher voltage $V_{C,0}$ to accumulate enough charge at its surface to reach the critical electric field E_0 that initiates the ion emission.

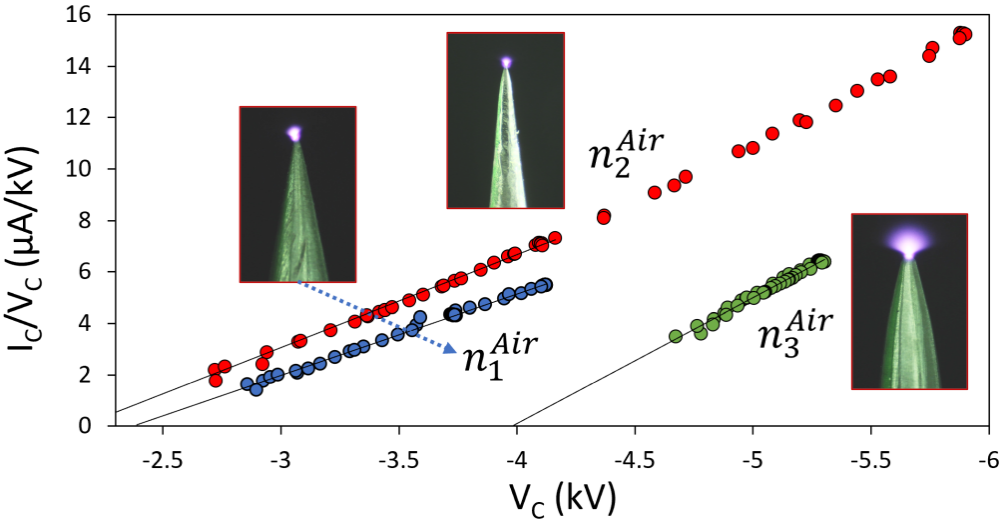

Figure 2.11. I_C/V_C vs. V_C for each corona discharge needle in synthetic air, n_i^{air}. Insets: Photos of the ion emission at the tip of each needle. Linear regressions for each of the branches: n_1^{air}: I_C/V_C = -3.27V_C - 6.76, n_2^{air}: I_C/V_C = -3.16V_C - 7.51, n_3^{air}: I_C/V_C = -4.89V_C - 19.46.

Therefore, n_3 is the least efficient needle.

From these experiments, we concluded that, due to the need of operating with a stable corona discharge for long periods of time, the best option for our purpose is to use, in our system, the corona needle #2 (15 μm radius) with synthetic air and negative polarity.

2.4 Results on corona discharge in point-to-orifice configuration

The current fraction exiting the corona device through an orifice must be small because corona currents (a few μA) far exceed electrospray currents (tens of nA). Furthermore, the capture of ions by the droplets depends critically on the droplets' and ions' trajectories, thus on the electrical field, which depends on the electrodes' voltages and geometries. The corona head acts as the counter electrode to the corona needle, thus collecting most of the ions emitted from the corona, and allowing only a small fraction of the corona current to pass through its orifice and become available to interact with other systems, for instance, electrospray droplets.

Therefore, taking into account the physics involved, in the following sections we have studied the behavior of the ion source device with the aim of obtaining relevant information such as reproducibility, stability of the extracted ion current (I_{Ext}), as well as its sensitivity to an external electric field.

2.4.1 Stability of the corona discharge within the ion source

The stability of the corona discharge within the ion source device is a determining factor because our goal is to extract, from the initial corona current (I_C), a stable low fraction, of about 2 or 3 orders of magnitude lower than I_C. To neutralize different electrosprays, which work at a very low and stable current of tens of nanoamperes, they will be exposed to this small amount of ions. In addition, the ability to work steady for long periods of time would make this technology industrially applicable.

The corona discharge current (I_C) and voltage (V_C) were recorded for one hour at the following working conditions: head electrode #4 (Table 2.1), needle #2 (Table 2.2), d = 1.30 mm, H = 13.0 mm, V_{Plate} = 300 V, $Q_C(air)$ = 0.4 l/min (setup in Fig. 2.3, pg. 26). Figure 2.12 shows the recorded data over time. The corona current (red line) and the head electrode current (grey line) were very similar and considerably stable for one hour, with average values of $I_C \sim$ -15.33 μA and $I_H \sim$ -15.13 μA. The latter is slightly lower than the former, consistent with the emission

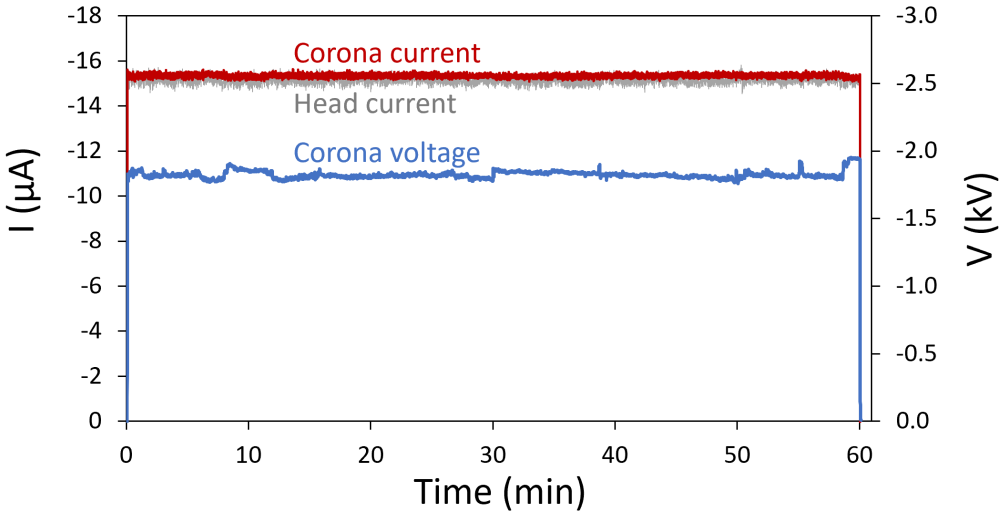

Figure 2.12. Stability test of the corona discharge within the unipolar ion source device, where both corona current, I_C (red line), and head electrode current, I_H (grey line), were stable over time, while the corona voltage, V_C (blue line), being in average steady, fluctuated appreciably. Conditions: head electrode #4, d = 1.30 mm, H = 13.0 mm, V_{Plate} = 300 V, Q_C = 0.4 l/min.

of ions through the head electrode orifice. The corona voltage (blue line) was $V_C \sim$ -1.82 kV on average and, even though this signal fluctuated slightly, the high voltage power supply, working in current regulation, could maintain a steady corona current.

2.4.2 Effect of the gas flow rate through the orifice

We also established that the gas flow rate, at low values, does not affect the corona discharge process within the device. This is true for values below a flow rate of ∼60 ml/min. Indeed, even in experiments were the feeding gas flow rate was Q_C = 0 ml/min, the behavior of the corona discharge was similar to those experiments where gas was used.

This is an useful result because our objective is to expose the ion flux to an electrospray plume to discharge the droplets, as well as being able to extract the neutralized aerosol within a controlled flow field. Being able to maintain a gentle gas flow rate through the corona device to renew the surrounding the corona discharge environment, prevents any significant distortion of the flow for outside the ion source device.

The main conclusion is that the system can be fed at a low range of flow rates while

running a stable corona discharge.

2.4.3 I-V characteristics of the ion source device

We next characterized the corona discharge within the ion source device, in the point-to-orifice configuration with the setup in Fig. 2.3, pg. 26. Head electrode #4 (Table 2.1) and corona needle #2 (tip radius $r = 15$ μm, Table 2.2), where used with a needle tip-to-orifice distance $d = 1.30$ mm (Fig. 2.1a). For d smaller than $\sim$1 mm the corona discharge was difficult to initiate due to the occurrence of electrical sparks. The head electrode faced the plate electrode at a distance $H = 13.0$ mm, and at $V_{Plate} = 300$ V. Then, similarly to previous subsection, the voltage was scanned, and both the corona current and the voltage were recorded. Synthetic air was used at a flow rate of $Q_C = 0.4$ l/min.

Two independent runs using the same needle at the same above working conditions were performed in order to test the system's reproducibility. Figure 2.13a shows the I-V characteristic curves for the comparison of these two runs n_2 and $n_2^{'}$. In Fig. 2.13b, data is presented in the form of the Townsend's law (Eq. 1.8) as I_C/V_C vs. V_C, and the linear regressions are included and extrapolated to zero ordinate to obtain the corona onset voltage ($V_{C,0}$). The slightly difference between branches for n_2 and $n_2^{'}$ and their corona onset voltage, shows that the corona's response is quite reproducible. A possible reason for this difference is that these runs corresponded to two different days, between different experiments in which the head electrode was switched, thus the geometry could have changed slightly.

Another observation to take into account was that the corona discharge produced sparks above the upper part of the branches shown, making the process unstable. On the other hand, below the lower part of these branches, the corona discharge was not stable either since it needs to reach the onset voltage to be sustained. Therefore, this results in a few tens of microamperes range where the corona discharge can work steadily.

In Fig. 2.10, the branch corresponding to n_2^{Air} has been included in the graph to compare the corona discharge behavior in the ion source device against the case in

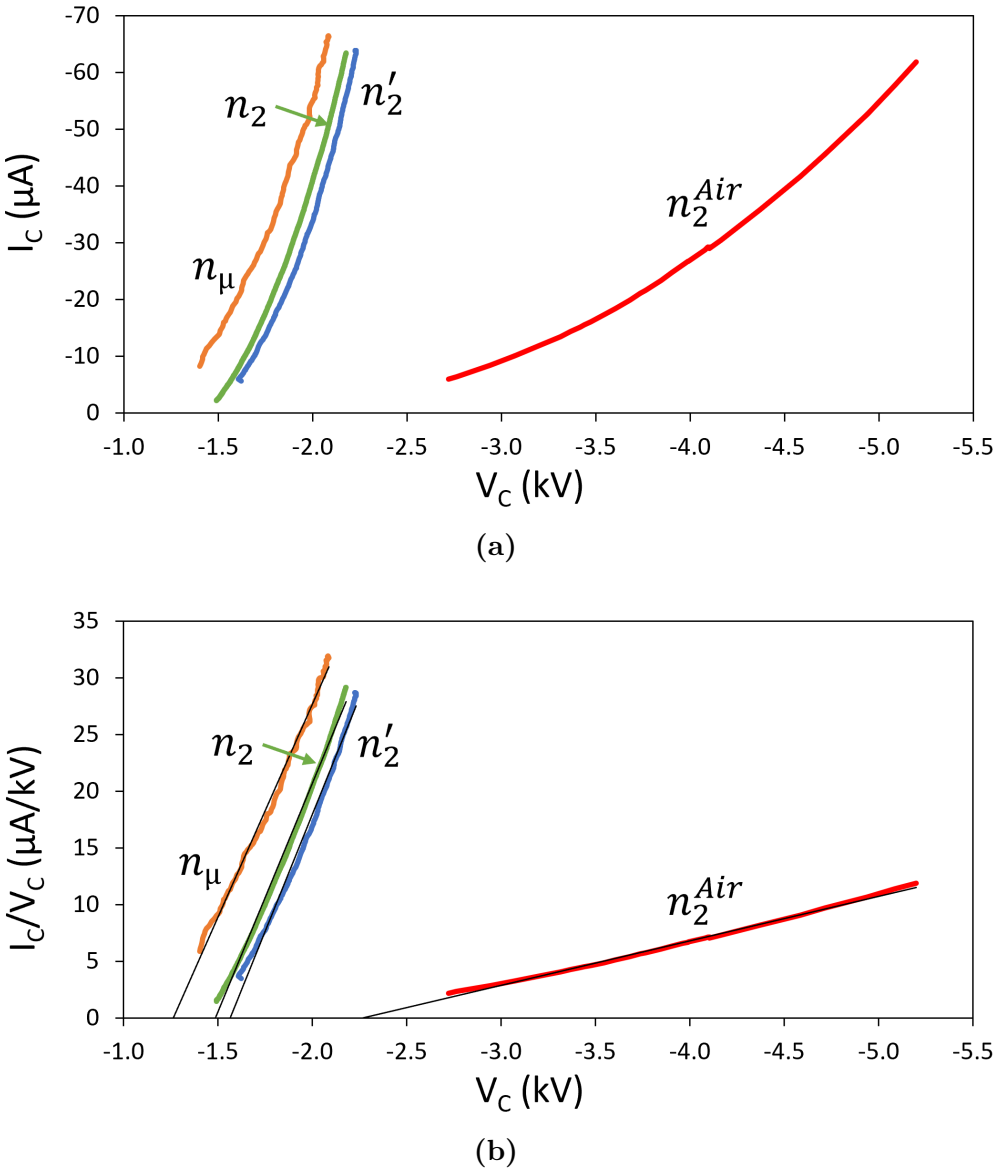

Figure 2.13. Comparison of different corona discharge characteristic curves in a point-to-orifice configuration. To check the reproducibility, both n_2 and n_2' correspond to the same tapered tungsten needle at same working conditions, but different days. Curve for n_2^{Air} (presented in previous subsection) has been added for comparison, as well as curve for n_μ which corresponds to a commercial tungsten micro-needle. (a) Corona discharge I-V characteristic curves. (b) I/V vs. V in the form of Townsend's law (Eq. 1.8)

which the corona discharge was naked (point-to-plane configuration). (Upper data values have been subtracted for better visualization.) Since in n_2^{Air} the distance of the needle tip to the counter electrode (plate) was significantly greater ($d = 5.80$ mm) than in the case of the ion source, where the distance to the orifice was ∼1.30 mm, the current of the former was much lower with a higher onset voltage.

In addition, commercial tungsten micro-needles (1-μm tip radius, typically used for micro-dissection) have also been tested at the same above working conditions (head electrode #4, $d = 1.30$ mm, $H = 13.0$ mm, $Q_C = 0.4$ l/min), with the expectation of generating much higher corona current. Nonetheless, although more current, and a much lower onset voltage were obtained (branch n_μ in Fig. 2.13), these needles melted very quickly ($\sim$30 minutes), compromising the stability of the process.

2.5 Results on the extracted ion current

2.5.1 Extracted current stability

Usually, artificial charged aerosols are generated at steady conditions. This is, in fact, necessary when fluctuations may distort the process. A clear example is the electrospray, where changes in current (due to changes in flow rate, conductivity, etc) will disrupt the uniformly sized distribution of the droplets. Hence, it is important to maintain the ion source at stable conditions if trying to neutralize electrosprays.

During the experiment of the previous subsection, the extracted current (I_{Ext}) was also measured at the plate electrode, which was connected to high voltage at V_{Plate} = 300 V to attract the ions (setup in Fig. 2.3, pg. 26). The extracted current (I_{Ext}) was measured as discrete values at the plate electrode by a nanoammeter which was floating at the high voltage V_{Plate}. The working conditions were the same as before: head electrode #4 (Table 2.1), needle #2 (Table 2.2), d = 1.30 mm, H = 13.0 mm, Q_C = 0.4 l/min. Fig. 2.14 shows, as a function of time, the stable current generated by the corona discharge, I_C (same left axis than in Fig. 2.12), and the extracted current (I_{Ext}) reaching the plate electrode (right axis), obtaining for the latter a mean value of I_{Ext} = -24.7 nA, with a standard deviation of 1.1 nA (excluding the first two points, belonging to the initial transient).

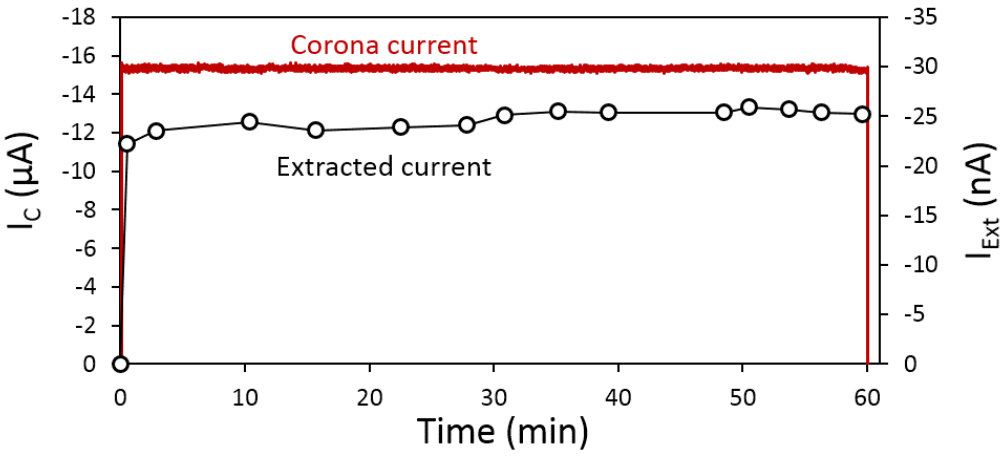

Figure 2.14. Long term stability of the extracted current. Circles connected with lines represent instantaneous values of the current collected on the plate electrode (I_{Ext}). Conditions: head electrode #4, d = 1.30 mm, H = 13.0 mm, V_{Plate} = 300 V, Q_C = 0.4 l/min

As conclusion, this system is able to provide a stable extracted ion current (I_{Ext}) for long periods of time. In this case, it was working stably for one hour, with a value of I_{Ext} = -24.7 ± 1.1 nA.

2.5.2 Sensitivity of the extracted current to the corona current

Another important question to answer is how sensitive the extracted ion current (I_{Ext}) is to the corona discharge current (I_C). This information is crucial to know the range of operation of I_{Ext} by tuning I_C, within a stable range. For this reason, the characterization of the extracted ion current (I_{Ext}) as a function of the corona discharge current (I_C) is presented in this subsection.

For different voltage values at the plate electrode, V_{Plate} (setup in Fig. 2.3, pg. 26) the corona current (I_C) was scanned, by current regulation, through the operation range from the onset voltage V_0 until the current at which the corona discharge got unstable. The working conditions were the same as before: head electrode #4 (Table 2.1), needle #2 (Table 2.2), d = 1.30 mm, H = 13.0 mm, Q_C = 0.4 l/min. The extracted current (I_{Ext}) was measured as discrete values at the plate electrode by a nanoammeter which was floating at the high voltage V_{Plate}.

Fig. 2.15a shows the extracted current (I_{Ext}) as a function of the corona current (I_C) for different voltages at the plate electrode (V_{Plate}). As expected, I_{Ext} increases when I_C increases. However, it appears to develop a plateau, although in fact has a power law dependence, as shown in Fig. 2.15b where the same data is plotted by the logarithmic values. In addition, the sensitivity of I_{Ext} to V_C is not very pronounced. Nonetheless, the dependence with V_{Plate} may allow, along with I_C, a fine adjustment/control of the extracted current (I_{Ext}), being, in this case, similar to the electrospray current.

To know how efficient is the ion extraction from the corona discharge within the device through the orifice, the *ion extraction efficiency* $\mathcal{F}$ is computed as the fraction of the total initial corona discharge current (I_C) which is measured at the plate (I_{Ext})

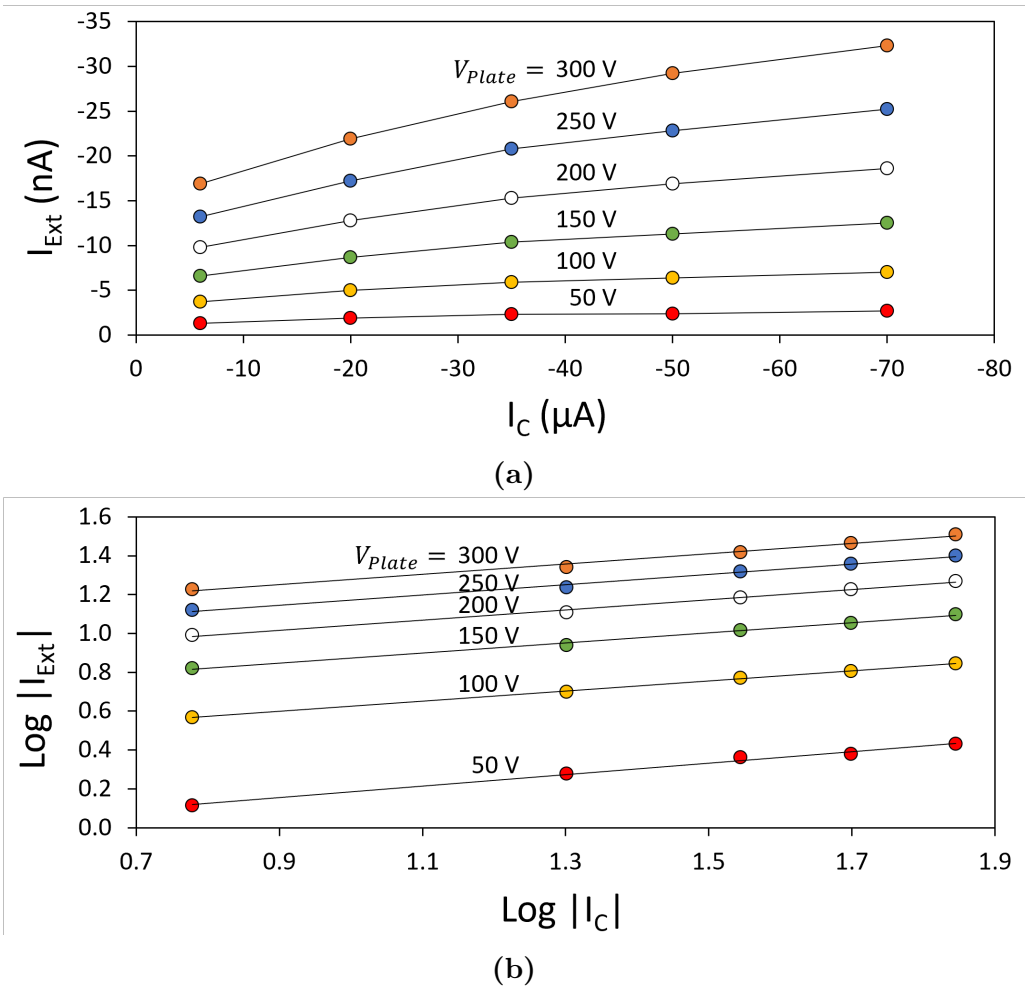

Figure 2.15. Sensitivity of the extracted current (I_{Ext}) to the corona current (I_C) for different voltage values (V_{Plate}) at the plate electrode. (a) Extracted current values as circles connected by lines vs. corona current. (b) Log-Log plot of extracted ion current I_{Ext} (< 0) including linear regressions.

as extracted ions, for a given plate voltage (V_{Plate}):

$$\mathcal{F}[\%] = \frac{I_{Ext}}{I_C} \times 100 \tag{2.1}$$

Fig. 2.16a shows the ion extraction efficiency, $\mathcal{F}$ as a function of the corona current (I_C) where each branch corresponds to a different V_{Plate}. In this case, $\mathcal{F}$ decreases when I_C increases, following a power law as shown in Fig. 2.16b. Notice that the $\mathcal{F}$ values are very small, indicating that probably these ions come from those field lines close to the axis.

As a conclusion, a fine adjustment of the extracted ion current (I_{Ext}) is possible, for a given external electric field, where the efficiency of the ion extraction is higher at

low corona current (I_C).

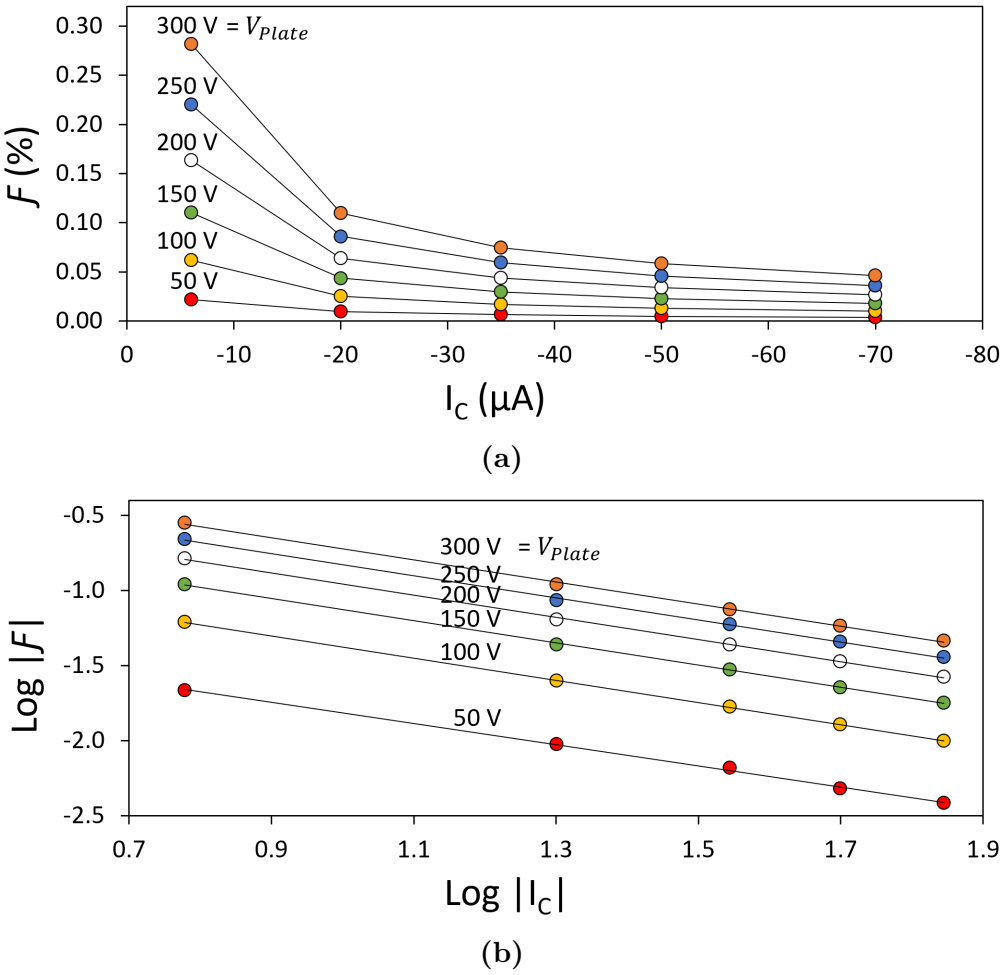

Figure 2.16. Ion extraction efficiency as a function of the corona discharge current (I_C) for different voltage values (V_{Plate}) at the plate electrode. (a) Ion extraction efficiency values as circles connected by lines vs. corona current. (b) Log-Log plot of the ion extraction efficiency $\mathcal{F}$ including linear regressions.

2.5.3 Sensitivity of the extracted current to the external electric field

The unipolar ion source may be used for applications where a continuous ion flux is needed. But those applications might operate with electric fields and therefore it is important to understand how sensitive the extracted ion current (I_{Ext}) is to an external electric field. For this reason, we present in this subsection the characterization of the extracted ion current (I_{Ext}) as a function of a constant external electric field.

The external electric field ($|\vec{E}_{Ext}| \sim V_R/H$) was established by providing a high voltage at the plate electrode (V_{Plate}), placed at a fixed distance H with the ion source head electrode (Earth-grounded). The working conditions were: head electrode #4 (Table 2.1), needle #2 (Table 2.2), $d = 1.30$ mm (Fig. 2.1a, pg. 24), $H = 13.0$ mm, $Q_C = 0.4$ l/min. The extracted current (I_{Ext}) collected at the plate electrode was measured by a nanoammeter floating at V_{Plate} versus discrete values of V_{Plate}. Although the corona voltage (V_C) was the constant parameter in each scan, we operated under voltage regulation, at different values of corona current (I_C) (Fig. 2.3, pg. 26).

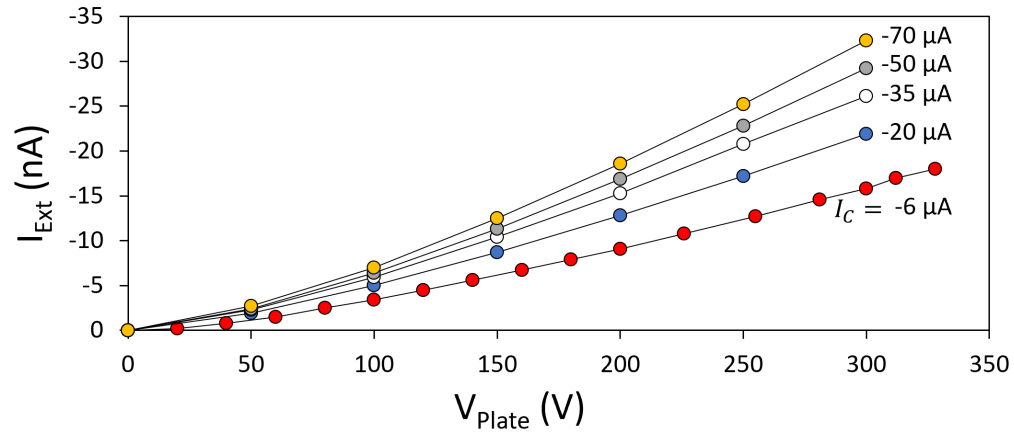

(a)

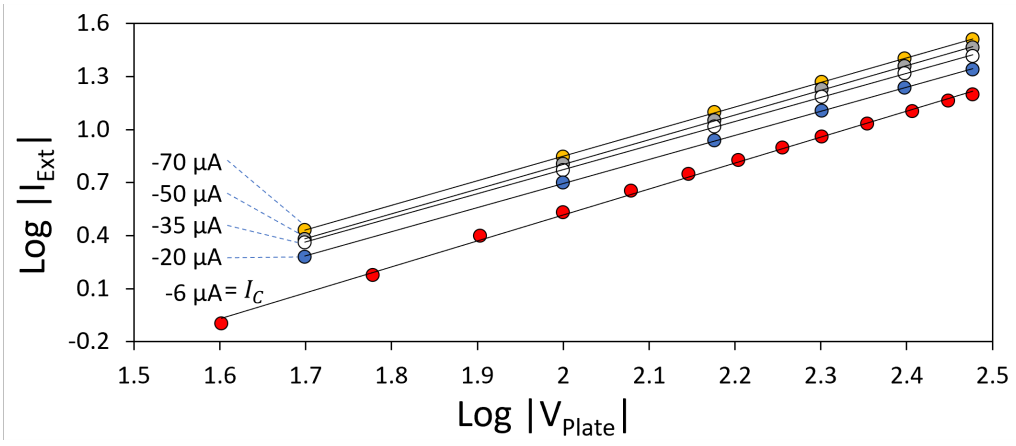

(b)

Figure 2.17. Sensitivity of the extracted current (I_{Ext}) to an external field ($|\vec{E}_{Ext}| \sim V_R/H$) for different the corona current (I_C) values. (a) Extracted current values as circles connected by lines vs. corona current. (b) Log-Log plot of extracted ion current I_{Ext} (< 0) including linear regressions. $H = 13.0$ mm.

Fig. 2.17a shows the extracted current (I_{Ext}) as a function of the plate electrode

voltage (V_{Plate}) where each branch corresponds to a given corona current value (I_C). I_{Ext} increases significantly by increasing V_{Plate}, for any I_C, following a power law, as shown in Fig. 2.17b. This is very interesting result because, while the corona discharge is strongly shielded from the external electrical field by the Earth-grounded head electrode, the amount of extracted ions is strongly dependent by this electrical field. This suggests that the external electric field strength attracts toward the plate the amount of ions that exit the ion source device, and that otherwise would fly-back towards the head electrode. I_{Ext} can be adjusted by tuning the external electric field to obtain a wider range than by scanning I_C (see previous subsection). Furthermore, both parameters I_C and the external electric field $|\vec{E}_{Ext}| \sim V_R/H$ could be used as control parameters to obtain a *fine/coarse* control of the extracted ion current.

As previously shown, the efficiency of the ion extraction (Eq. 2.1, pg. 42) from the corona discharge emission within the device through the orifice, $\mathcal{F}$, is computed, but, in this case, as a function of V_{Plate}, for a given value of I_C. Fig. 2.18a shows the ion extraction efficiency, $\mathcal{F}$ as a function of V_{Plate}, where each branch corresponds to a different I_C. Interestingly, in this case $\mathcal{F}$ increases when V_{Plate} increases, for any I_C, following a power law as can be seen in Fig. 2.18b.

As a conclusion, the unipolar ion source can provide an ion current which is stable and sensitive to external electrical field, being adjustable with a fine control. Consequently, this information brings the possibility of making controlled changes in the geometry, if needed. For instance, in the case of electrospray droplet discharge, this can be an advantageous feature, since we have obtained similar current that can be adjusted depending on the system requirements, for example, changes in electrospray solution conductivity which would work at a different electrospray current. Indeed, the electrospray creates its own electric field which would affect the ion extraction. Moreover, in the case of particle production by electrosprays, from a polymer solution for example, if changes in the system geometry were necessary, like, for example, due to the solvent evaporation rate is high and the Coulombic explosions may appear nearer to the emission point (Taylor cone), we might place the ion source closer to the electrospray system in order to introduce deeper the ions in the plume and prevent the explosions.

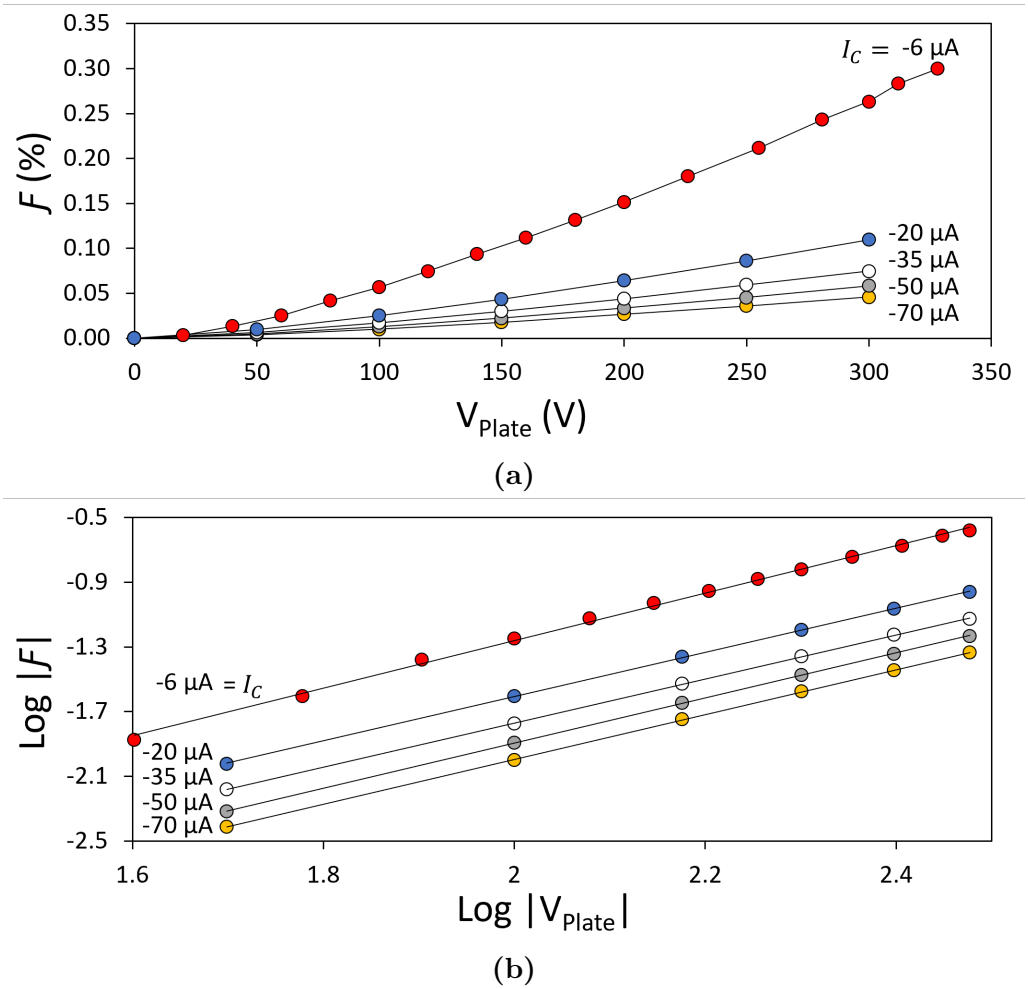

Figure 2.18. Ion extraction efficiency as a function of the plate electrode voltage (V_{Plate}) for different corona discharge current values (I_C). (a) Ion extraction efficiency values as circles connected by lines vs. plate electrode voltage. (b) Log-Log plot of the ion extraction efficiency $\mathcal{F}$ including linear regressions. $H = 13.0$ mm.

Finally, in the case that an application needed a much higher electric field, the head electrode may be connected to high voltage to obtain a better control of the required external electric field. In that case, the voltage *difference* between the head electrode and the corona discharge needle should be kept at a value that allows to sustain a stable corona discharge.

2.5.4 Characterization with covered ring electrode

In the case of discharge of electrospray droplets, the capture of ions by the droplets depends critically on the droplets' and ions' trajectories, thus on the electrical field,

which depends on the electrodes' voltages and geometries.

We studied how sensitive the ionic current passing through the head electrode orifice into the spray region (I_{Ext}) is to both the corona current (I_C) and the ring voltage (V_R), in an electrospray system (setup in Fig. 2.4). In these experiments, the electrospray capillary was removed. Also, to ensure the trapping of any central ions, the ring was covered with a metal disc (12.7 mm diameter). These geometry changes allowed us to determine I_{Ext} without elimination of the essential elements. The working conditions were: head electrode #3 (Table 2.1), needle #2 (Table 2.2), d = 2.50 mm, H = 17.0 mm, Q_C = 20 ml/min. Fig. 2.19 shows that I_{Ext} is (i) weakly dependent on the corona current, and (ii) can be regulated by means of the electrical field $\vec{E}_{Ext}$ in the region outside of the corona device through V_R, where $|\vec{E}_{Ext}| \sim V_R/H$.

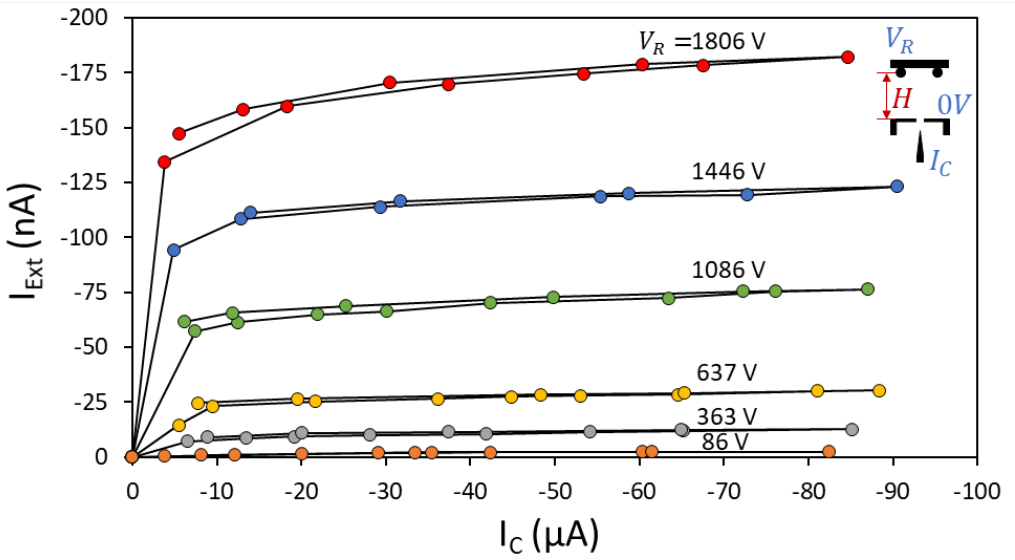

Figure 2.19. Plot of extracted ion current I_{Ext} (< 0) measured at the counter electrode (ring plus disk, as shown in the inset) versus the corona current I_C, at varying ring voltage V_R (values displayed). (H = 17.0 mm. Q_C = 20 ml/min.). Electrode diagram is included, showing the absence of electrospray capillary and the covering of the ring with a disc.

Then, from Fig. 2.19 we can conclude that the electrical field outside of the corona device (head electrode) strongly influences the ion current available to discharge droplets. Indeed, the current reached has been as high as -182 nA, therefore covering a wide range of ion currents that may cover the needs for neutralization of different electrosprays.

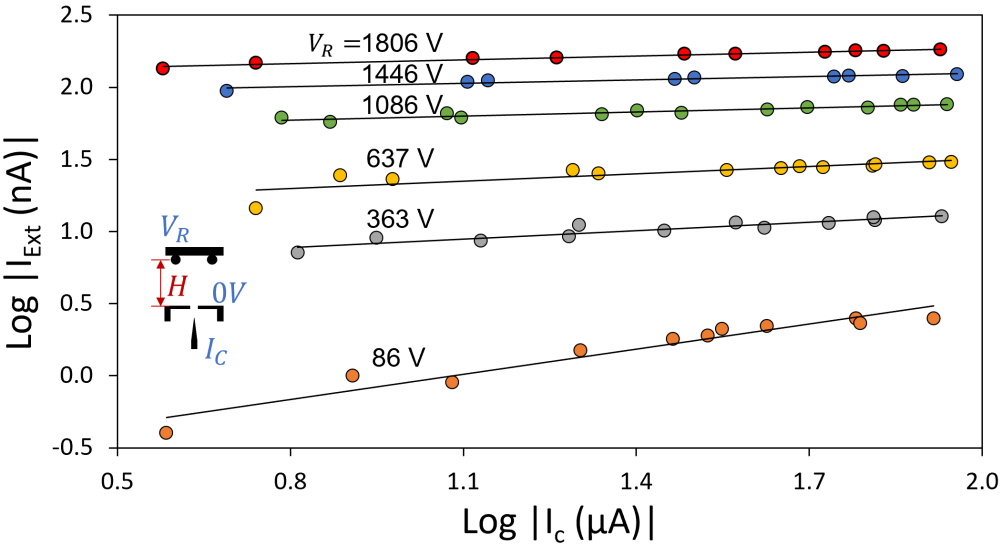

Figure 2.20. Log-Log plot of extracted ion current I_{Ext} (< 0) measured at the counter electrode (ring plus disk, as shown in the inset) versus the corona current I_C, at varying ring voltage V_R (values displayed). (H = 17.0 mm. Q_C = 20 ml/min.). Electrode diagram is included, showing the absence of electrospray capillary and the covering of the ring with a disc. Lines are power-law fits.

In Fig. 2.20, the data has been plotted in log-log scale to show that the behaviour of the extracted ion current as a function of the corona discharge current, follows a power-law in all cases.

The conclusion is that, in a configuration which is more similar to an electrospray setup, the extraction of ions is still weakly sensitive to corona current and strongly sensitive to the external electric field.

2.5.5 Effect of the orifice diameter

To study the effect of the orifice diameter, a (Fig. 2.1a), three head electrodes #1, 2, 3, previously presented in Table 2.1, and with the same orifice thickness of t = 0.4 mm were used. Their diameters (a_i) are included in Table 2.3, together with the corona needle tip-to-orifice distances (d_i) used. Due to the difficulty of adjusting d_i, there are small differences between the values, specially in the case of d_3, which is ∼0.8 % smaller. The other working conditions in these tests were: needle #2 (Table 2.2), H = 13.0 mm, I_C = -30 μA, Q_C = 20 ml/min (setup in Fig. 2.3).

Table 2.3. Parameters used in this study, where a_i is the head electrode orifice diameter, and d_i is the needle tip-to-orifice distance. In all cases: t = 0.4 mm, D = 12 mm (Fig. 2.1a).

Head #	1	2	3
a_i $[mm]$	1.0	1.5	2.0
d_i $[mm]$	1.31	1.30	1.21

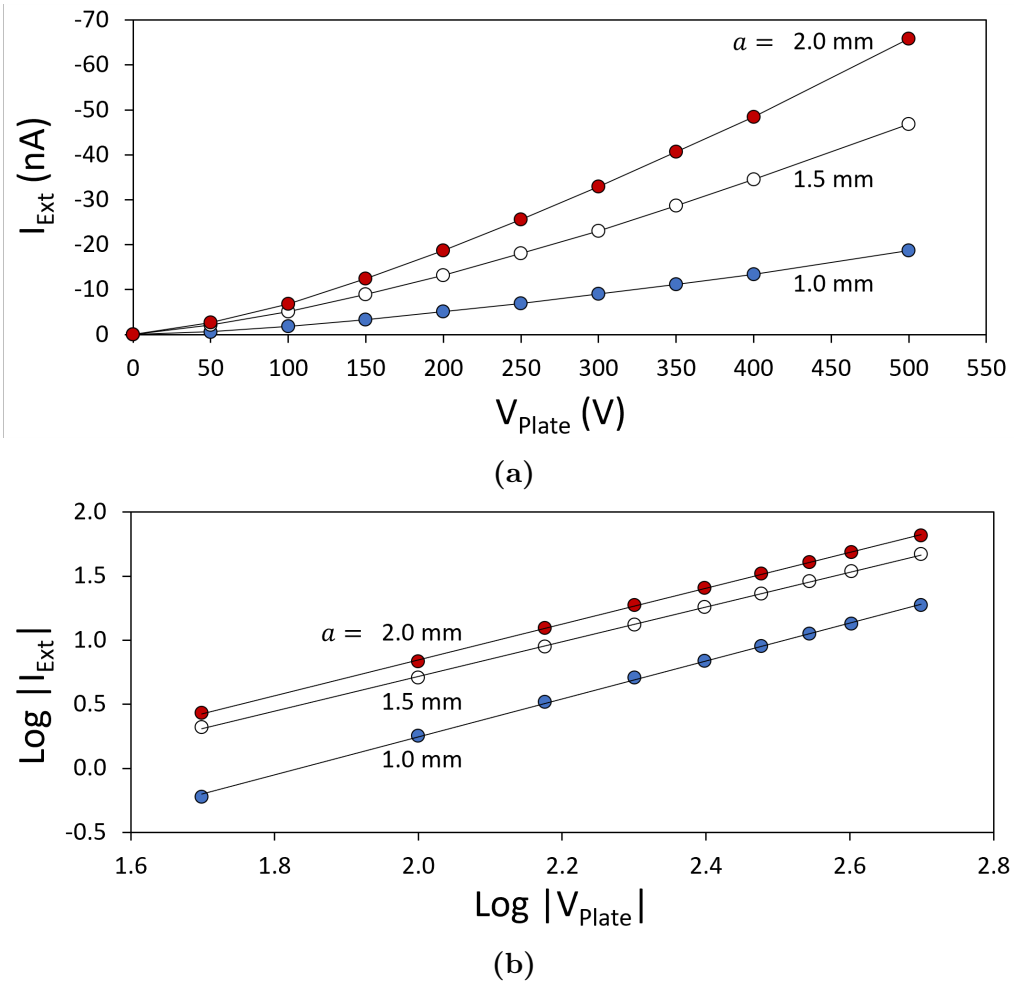

Figure 2.21. Comparison of different I/V characteristic curves for different orifice diameter values (a_i). (a) Extracted current values as circles connected by lines vs. plate voltage. (b) Log-Log plot of extracted ion current I_{Ext} (< 0) including linear regressions. I_C = -30 μA, t_i = 0.4 mm, H = 13.0 mm.

Fig. 2.21 shows, for different orifice diameters a_1, a_2, a_3, the extracted ion current (I_{Ext}) as a function of the plate electrode voltage (V_{Plate}), at a given corona discharge current of I_C = -30 μA. Apart from the aforementioned sensitivity of I_{Ext} to the external electric field and power law dependence (Fig. 2.21b), a clear tendency of increasing I_{Ext} versus orifice diameter, at any V_{Plate}, is observed. This is expected since the bigger the orifice diameter is, the more number of electric field lines would

be permitted to pass through it, allowing a bigger amount of ions to escape the ion source, even with space charge presence.

2.5.6 Effect of the orifice thickness

Another crucial parameter is the orifice thickness (t_i), where a preliminary expectation was that the thicker the orifice is, the smaller the amount of ions would pass through it, because as the thickness increases more electric field lines entering the orifice would be directed to the walls instead of continuing through the orifice. In addition, as shown in Fig. 2.22 in the situation **a**, an ion following the red electric field line would exit the device, reaching the target, whereas the same ion in the situation **b**, with a thicker orifice, even though it passes through the orifice, it would fly-back toward the head electrode. Another ion following the blue electric field line would pass through the orifice only in **a**, flying back toward the head electrode though, whereas in **b** it would directly impact the orifice wall.

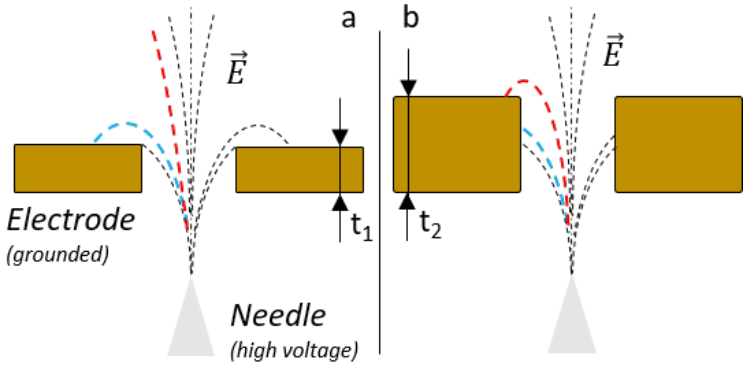

Figure 2.22. Sketch of the electric field lines for two different orifice thicknesses.

Similarly to previous subsection, three head electrodes previously presented in Table 2.1 have been used to study the effect of the orifice thickness. But in this case the head electrodes were #2, 4, 5 which have the same orifice diameter, a = 1.5 mm, Their thicknesses (t_i) are presented, together with the corona needle tip-to-orifice distances (d_i) in Table 2.4. There is a slight difference between the distances d_i, due to the difficulty of adjusting it. The working conditions were: needle #2 (Table 2.2), H = 13.0 mm, I_C = -30 μA, Q_C = 20 ml/min (setup in Fig. 2.3).

Table 2.4. Parameters used in this study, where t_i is the head electrode orifice thickness, and d_i is the needle tip-to-orifice distance. In all cases: a = 1.5 mm, D = 12 mm (Fig. 2.1a).

Head #	2	4	5
t_i $[mm]$	0.4	0.6	2.0
d_i $[mm]$	1.30	1.26	1.18

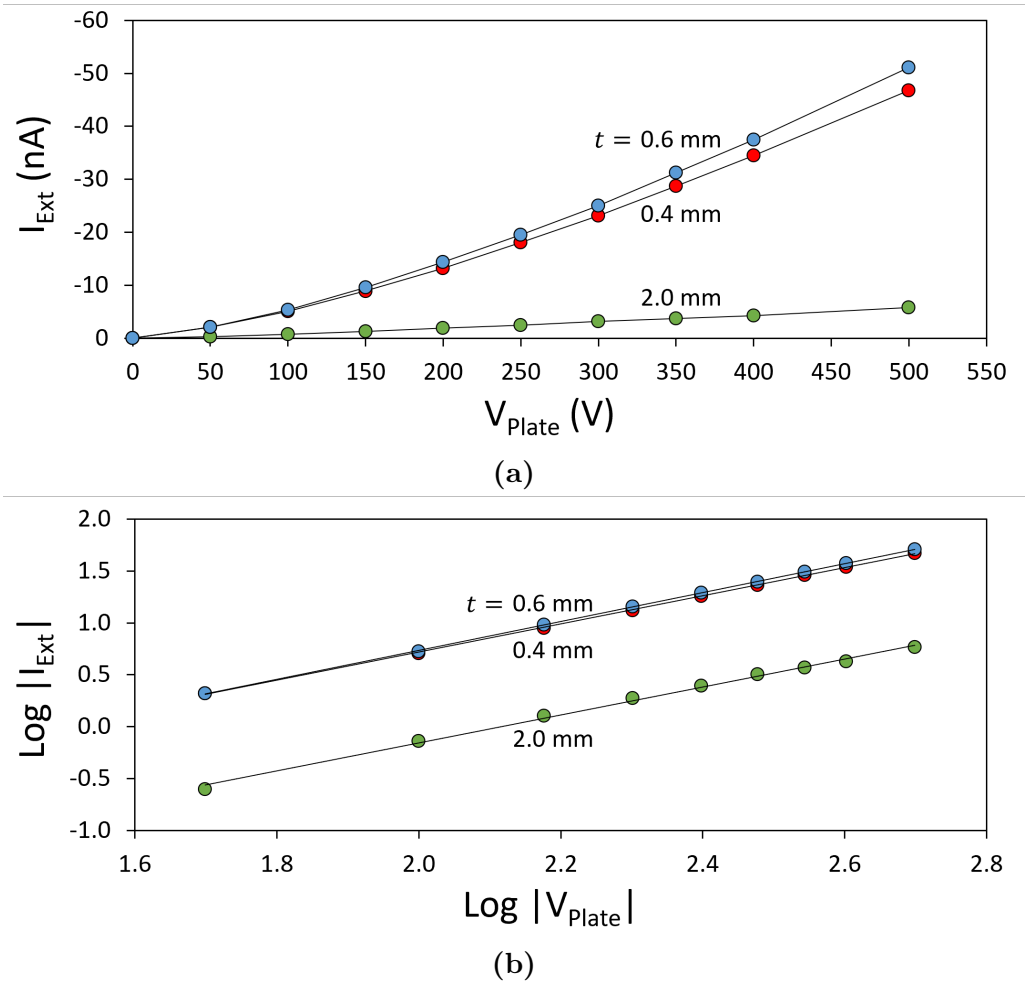

Figure 2.23. Comparison of the extracted ion current (I_{Ext}) as a function of the plate electrode voltage (V_{Plate}), for three different orifice thicknesses (t_i). (a) Extracted current values as circles connected by lines vs. plate voltage. (b) Log-Log plot of extracted ion current I_{Ext} (< 0) including linear regressions. I_C = -30 μA, a_i = 1.5 mm, H = 13.0 mm.

Fig. 2.23a shows the extracted ion current (I_{Ext}) as a function of the plate electrode voltage (V_{Plate}), at a given corona discharge current of I_C = -30 μA, and, this time, for different orifice thicknesses t_2, t_4, t_5 (Table 2.4). And, as before, plotted in logarithmic scale in Fig. 2.23b to show that the curves follow a power law. Comparing data from head electrode #5, which had the thickest orifice (t_5 = 2.0

mm), with the others (#2 and 4), the current is much smaller for the former probably due to the fact that a thicker orifice would affect directing the electric field lines to the orifice wall much more strongly than in the case of a thinner diameter, as mentioned earlier.

On the other hand, comparing data for head electrodes #2 and 4, whose thicknesses slightly differed ($t_2 = 0.4$ mm and $t_4 = 0.6$ mm), we would expect the current I_{Ext} using the thinner (#2) to be slightly higher than the other. But on the contrary, I_{Ext} was a little higher for the thinner (t_2), although the observed difference falls within the reproducibility due to both thickness values are quite similar compared to t_5. This could be due to several factors like, for example, the contribution of different experimental errors, or it could be the difference of the needle tip-to-orifice distances. In any case, it seems clear that head electrodes with thinner orifice walls can to extract a higher ion current than thicker orifices under the same conditions of operation. Although this conclusion suggests that, to obtain an efficient ion extraction, the head electrode orifice should be as thin as possible, sharp borders should be avoided to prevent sparks.

2.5.7 Extracted ion current profiles

In axisymmetric configurations, a consequence of the space charge is the spreading of the plume of ions in the radial coordinate as these ions travel in the direction of the axis, towards a counter electrode. Therefore, controlling the ion flux in the gap is crucial to control the process.

The profile of the extracted ion current (I_{Ext}) as a function of the distance provides information about the radial distribution of the ions, which is interesting when applications require to control the ions' distribution along a planar surface. In the case of electrosprays, for example, exposing an ion flux to an oppositely charged droplet plume might need the ion density to be high enough near the droplet emission to reach an efficient discharge before the droplets explode, but also not too high to prevent the destabilization of the process if the ions reach the Taylor cone.

To measure current profiles, setup was modified (Fig. 2.5, pg. 28). In this experi-

ments, the head electrode was placed at high voltage as explained in subsection in page 28. Since the positioning system was too large to keep the chamber closed, the experiments were performed in open chamber, at laboratory conditions of RH = 34.7 % and T = 19.4 °C. Other experimental conditions were: head electrode #3 (Table 2.1), needle #2 (Table 2.2), d = 2.65 mm.

To outline the ion current profile, the horizontal position of the ion source orifice relative to the pin electrode (X) was scanned, from right to left and vice versa, by using a linear stage, while the extracted current was measured both at the pin electrode (I_{Pin}) and at the plate electrode (I_{Ext}). But firstly the vertical position (Y) was set at its coordinate origin ($Y = 0$ mm) by determining the point at which I_{Pin} was maximized. Then, different profiles were measured as function of several parameters, such as the external electric field strength ($|\vec{E}_{Ext}| \sim \Delta V/H$) [by varying the voltage difference ($\Delta V = V_H$) between head and plate electrodes at a fixed distance (H)], the corona current (I_C), and the gas velocity at the orifice (v_{gas}) [computed as the gas flow rate (Q_C) divided by the orifice area (A): $v_{gas} = Q_C/A$].

A. Profiles for different external electric field ($|\vec{E}_{Ext}| \sim V_H/H$)

Fig. 2.24 shows several profiles of both I_{Pin} (upper graph) and its percentage distribution I_{Pin}/I_{Ext} (bottom graph) as function of different head electrode voltages (V_H), at the following fixed conditions: H = 10 mm, I_C = -6.57 μA, v_{gas} = 0 mm/s. The current I_{Pin} reaches a maximum when passing through the center, X = 0 mm, and the curves, decreasing smoothly, are symmetrical. Comparing the profiles for different V_H, we obtained the same result as above-mentioned where the total extracted ion current (I_{Ext}) increases as V_H is increased. But, even further, the fraction I_{Pin}/I_{Ext} increases near $X = 0$ mm is sensitive to V_H, suggesting that the ion distribution near the center does depend on the electric field strength, increasing homogeneously as V_H increases. Another interesting result is that the profile borders (tails), which depend on the spreading angle due to the electric field and the space charge, are comparable to the distance H, forming the ion plume a ∼45 degrees cone in all cases.

Consequently, this results indicate that the ion plume shape, as a ion density distri-

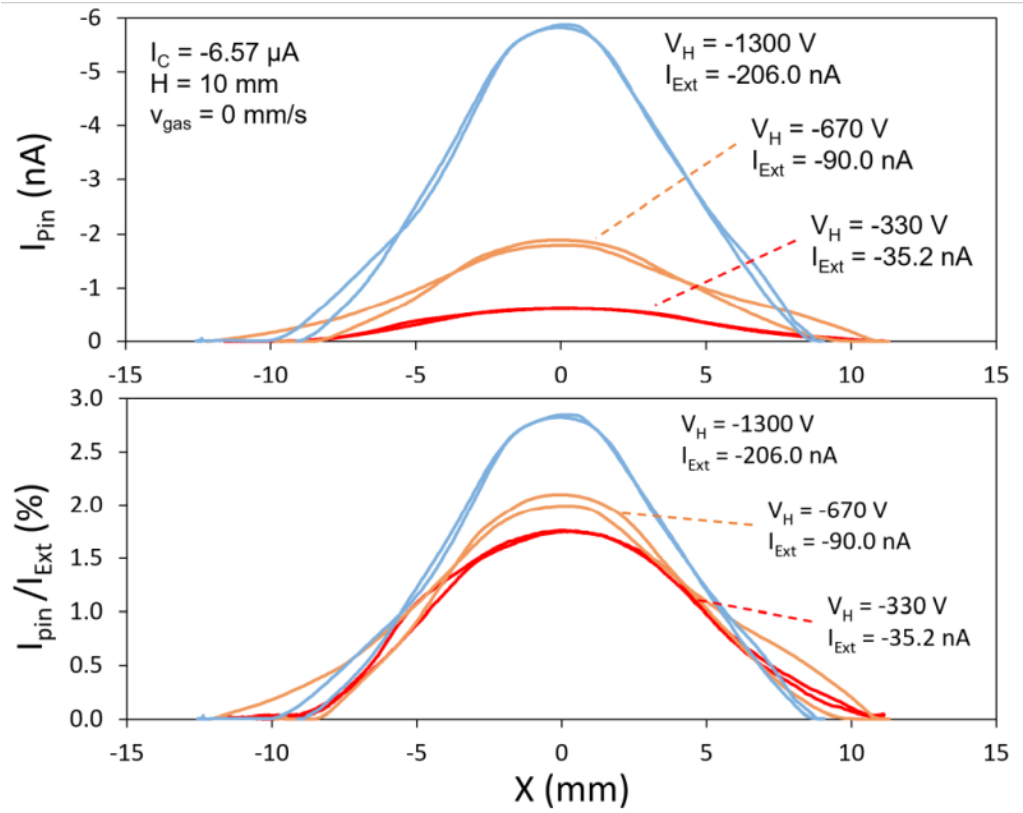

Figure 2.24. Extracted ion current profiles for different external electric field strength values by measuring a fraction of the total current (I_{Ext}) by a pin electrode (I_{Pin}) as a function of the X coordinate, scanned in two directions. Upper side: direct values. Bottom side: percentage distribution. H = 10 mm, I_C = -6.57 μA, v_{gas} = 0 mm/s.

bution, is symmetrical, with a maximum ion current (I_{Pin}) at its center whose ion density (I_{Pin}/I_{Ext}) surrounding the center depends on the external electrical field, being steeper at higher V_H.

B. Profiles at different gas velocity at the orifice (v_{gas})

It has already been mentioned that the gas flow rate (synthetic air), in our system, does not have a significant effect on the extracted ion current (subsection in pg. 36), at values below a flow rate of ∼60 ml/min. Now, to check whether the gas affects the ion plume distribution, several profiles have been measured, at different gas velocities at the orifice.

Shown in Fig. 2.25, the ion current profiles for three different gas velocities are essentially identical. The corona discharge was not stable at higher values. Therefore,

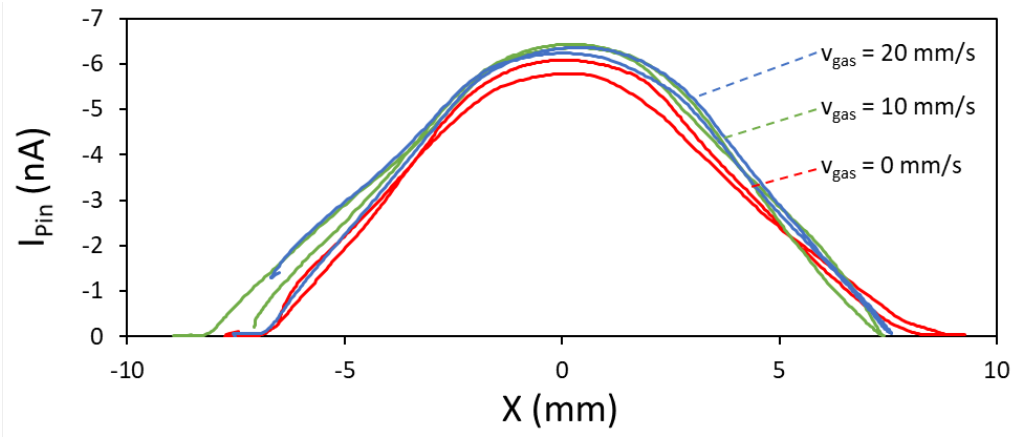

Figure 2.25. Extracted ion current profiles, at different gas velocities at the head electrode orifice. H = 10 mm, I_C = -6.57 μA, V_C = -3.86 kV, V_H = -1.30 kV, I_{Ext} = -240 nA

a conclusion is that the gas velocity at the orifice, for low gas flow rates, does not affect the distribution of ions at the counter plate electrode. In future experiments, gas flow rate will be set at low values to renew the environment near the corona needle tip.

C. Profiles at different distance (H)

In this case, two profiles were measured at different ion source orifice-to-plate electrode distance (H = 10, 20 mm) to be compared. Fig. 2.26 shows the ion current profiles, where, at the upper graph can be observed that for the one measured at a smaller distance (H = 10 mm), extracting a higher amount of ions (I_{Ext} = -240 nA), the ion density is more focused to the center, and, on the contrary, the profile at larger distance (H = 20 mm), which extracts less ions (I_{Ext} = -123 nA), is more widely distributed along the X axis.

On the other hand, in the bottom graph, where I_{Pin} and X have been scaled by dividing all values by their maximum, it can be observed that both scaled profiles are pretty identical. This means that actually the ion flux behaves similarly for either value of H, and consequently the ion density distribution, at each extent, is similar.

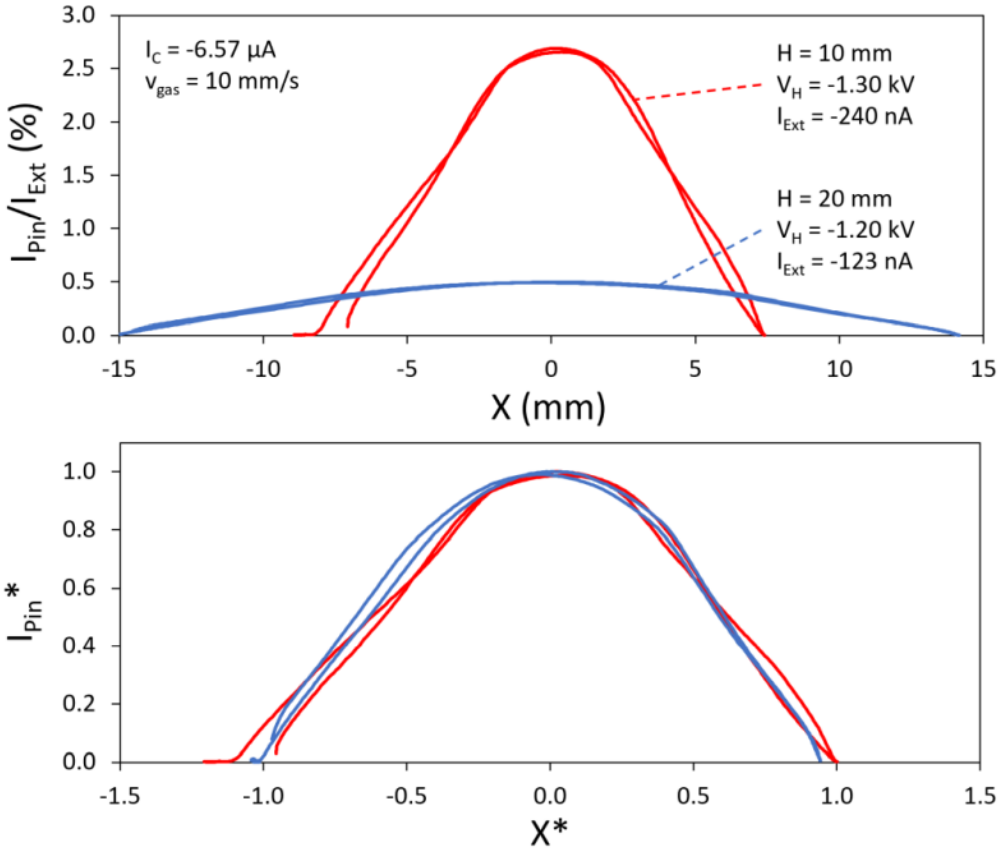

Figure 2.26. Extracted ion current profiles, at different distance with the counter electrodes (H). Upper side: direct values. Bottom side: scaled values. I_C = -6.57 μA, V_C = -3.86 kV, v_{gas} = 10 mm/s.

As a conclusion, the ion spreading for a symmetrical configuration did not change significantly, being an important result that provides insight before exposing the ions to an oppositely charged system.

2.6 Results on the evolution of the corona needle tip

After being exposed to DC corona discharge, the corona needle tip may be eroded from sputtering due to the bombardment of positive ions formed in the interelectrode region (Brodie, 1975). Therefore, the tip erosion may affect the long-term stability of the process if the needle tip is distorted, thus changing the radius and, consequently, the electric field which is responsible for sustaining the corona discharge.

Fig. 2.27 shows, from two different orientations, that the needle tip surface was affected by the exposition to corona discharge. Indeed, from bottom pictures is visible a fractal structure (cauliflower-like shape) developed at the tip, similar to those found by Nashimoto (1988), although they used air containing DMPS (dimethylpolysiloxane) vapor to grow amorphous silicon oxide structures and thin films on a tungsten wire cathode. In our case, elemental analysis (EDX) determined that the structure was formed by tungsten dioxide, WO_2.

To assess the evolution of the tip shape after being exposed to negative DC corona discharge, SEM pictures were taken over time, between some experiments. The pictures are shown in Fig. 2.28, sorted by time from left to right, in columns with two different orientations. Panel **a** corresponds to the same images as previously (upper images in Fig. 2.27). This was the first time we detected a relevant erosion at the needle tip. Thereupon, panel **b**, the needle was gently cleaned with a soft cloth to continue with the experiments. Since the structure was not solid, it could be easily removed. From that moment, we decided not to clean the needle tip to follow its evolution. After a total of ∼3 hours of corona discharge experiments, the needle tip was checked again by SEM and, as shown in panel **c**, although the structures grew again, the shape of the tip was not significantly distorted. Finally, SEM images in panel **d** corresponded to the status of the tungsten needle tip after a period of around 40-50 hours of being exposed to corona discharge, for different type of experiments, at an average corona current (I_C) of around -20 μA. Clearly, the needle tip shape has not changed considerably over time, demonstrating that the durability of the tungsten needle, at least with this shape, is crucial to develop

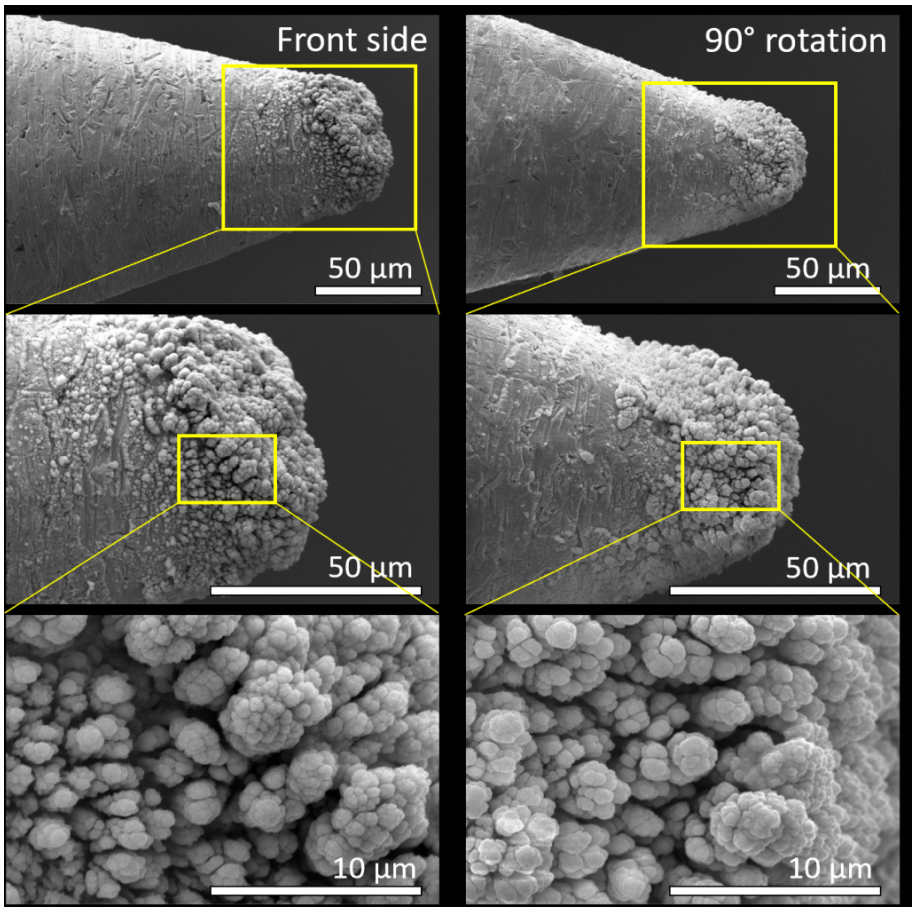

Figure 2.27. SEM pictures of the corona needle tip (#2), at different magnifications. A fractal structure (cauliflower-like shape) was grown after being exposed to corona discharge. Left column: needle tip front side. Right column: tip rotated 90º.

unipolar ion source devices ensuring long-term stability.

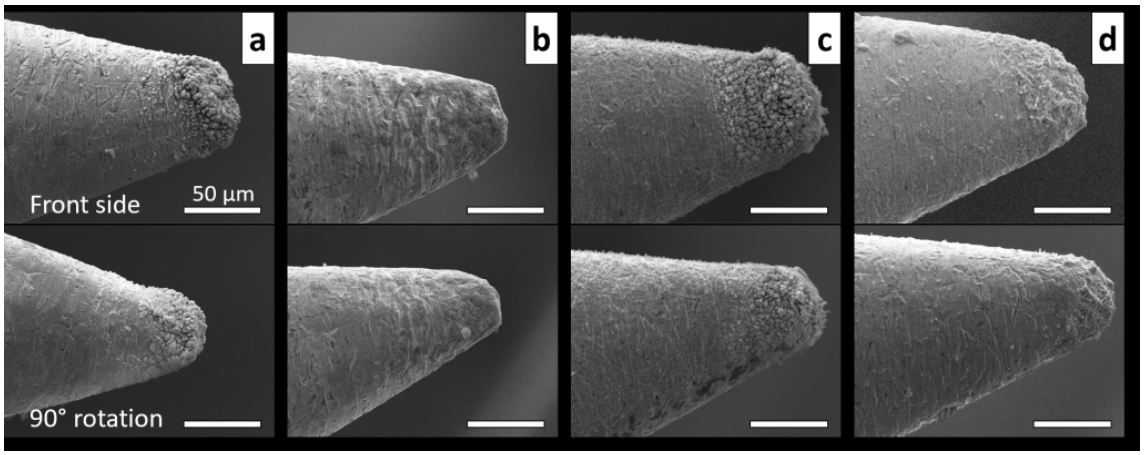

Figure 2.28. Corona needle tip evolution. SEM pictures of the tip corona needle tip (#2) after being exposed to corona discharge in different dates. Upper photos: needle tip front side. Bottom photos: tip rotated 90º. Scale bars: 50 μm.

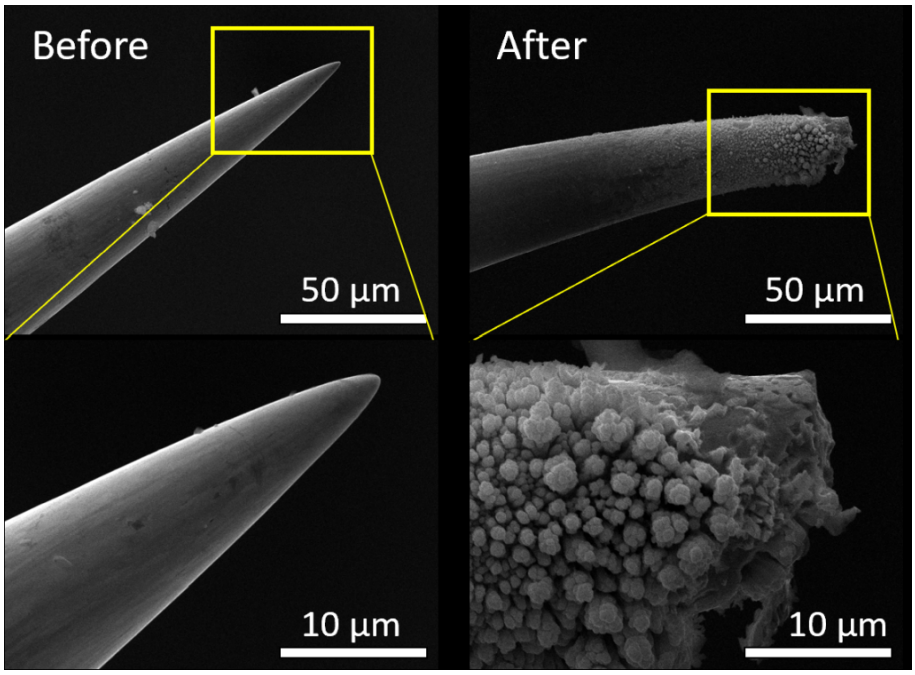

Figure 2.29. SEM pictures of the tip of a commercial tungsten micro-needle, at different magnifications, dramatically distorted after being exposed to corona discharge. The fractal structure (cauliflower-like shape) grew after being exposed to corona discharge. Left column: before corona discharge exposition. Right column: after corona discharge exposition.

On the contrary, as shown in Fig. 2.29, the aforementioned (early in page 37) 1-μm radius tungsten micro-needles were dramatically distorted by short exposition to corona discharge ($\sim$30 minutes). Then, they are not suitable for long-term processes due to the low durability.

As a conclusion, there exist a balance between the extracted current, and the stability of the needle tip shape, which, for the same material, strongly depends on the needle tip radius, and suggests to preferentially use larger tip radius values which, providing less extracted current, would preserve the stability of the process.

2.7 Conclusions

The main conclusions from this work are as follows:

Regarding the corona discharge characteristics in a point-to-plane configuration, we have observed that by comparing two different gas compositions for the DC corona discharge, synthetic air and nitrogen, we have found that with air the system works much more stably than in the case of nitrogen. Although when using nitrogen the extracted ion current was significantly higher in our system, due to the need of operating in stable conditions for long periods of time, the best option was to use air.

We have compared positive and negative corona discharge polarities, and only in the case of negative polarity we could produce a stable ion current for long periods of time, being the appropriate polarity for next experiments.

The corona needle tip radius was studied. Smaller radius generates more corona current at lower voltage, shifting the onset voltage to lower values.

Regarding the study of the extracted ion current through the ion source orifice:

It is possible to generate a stable ion flux which is adjustable with current similar to that of the typical electrospray current, by means of the presented unipolar ion source.

The extracted ion current was adjusted by tuning the corona discharge current, although the sensitivity is not high. Higher extraction efficiencies were obtained at low corona current values, probably due to a weaker space charge. Moreover, the extracted ion current was adjusted over a wide current range by tuning the external electric field. In this case, higher extraction efficiencies were obtained at a higher external electric field. This conclusion was also reached with a configuration in which a covered ring as the counter electrode was used, being this configuration more similar to an electrospray setup.

The orifice dimensions strongly affects the ion current extraction. The extracted ion

current was higher, as the orifice diameter was increased, and as the orifice thickness was decreased.

The extracted ion current is not affected by the flow rate of the corona discharge feeding gas (synthetic air) at low values (<60 ml/min). On the other hand, the corona discharge was unstable above ∼60 ml/min and below the corona onset voltage.

Extracted ion current profiles revealed that the ion distribution is typically symmetrical with the maximum at the axis, as expected. An increase of the external electric field increased the ion density near the axis, whereas the profile tails were less affected.

On the other hand, the gas velocity at the orifice did not affect the ion profile shape. Therefore, a low gas flow rate can be used to renew the gas environment near the corona needle tip.

Needle tip evolution: there exist a balance between the extracted current, and the stability of the needle tip shape, which, for the same material, strongly depends on the needle tip radius, suggesting to preferentially use larger tip radius values which, even though provide less extracted current, would preserve the stability of the process.

For the case of the 15-μm radius tungsten needle, the shape of the tip did not change considerably over time, demonstrating the high durability of this tungsten needle.

— *The good thing about science is that it's true whether or not you believe in it.*

Neil deGrasse Tyson

3

Neutralization of Electrospray Droplets

3.1 Introduction

Electrohydrodynamic atomization (EHDA), also known as *electrospray*, is a widely used technique for the atomization of liquids, mainly due to its unique feature of generating tiny droplets within a narrow size distribution (Rosell-Llompart et al., 2018).

By applying a high electrical potential (high voltage) to a conductive liquid in a capillary tube, of the order of a few kilovolts, a high electrostatic field is established. An intrinsic effect of this high voltage-based technique is that the electric field force governs the space surrounding the liquid meniscus over others, like capillary or gravitational force, pulling the liquid meniscus in the direction of the field, thus forming a cone shape called *Taylor cone*. When the electrical force overcomes the surface tension, a micro-jet develops. Downstream, the jet breaks up into highly electrically charged droplets, and, if the so-called *cone-jet mode* is established by continuously feeding liquid, the system is capable of working in a steady state, creating droplets in a mono-disperse size distribution that can be from tens of nanometers to a few micrometers, being the main characteristic of this technique.

As a consequence, the electric field lines drive the droplets towards a counter electrode, thus forming a characteristic spray shape, bringing different benefits, like, for instance, the ability to make depositions (Castillo et al., 2018; Kelder et al., 2018; Jaworek et al., 2018; Tang and Gomez, 2017; Arumugham-Achari et al., 2013; Bodnár and Rosell-Llompart, 2013; Jaworek, 2007a; Hogan et al., 2007; Hogan and Biswas, 2008). The electrostatic field distribution and therefore the droplets' trajectories will strongly depend on the counter electrodes added in the system. The

electric repulsion may not necessarily be a problem since it helps to prevent the agglomeration of the droplets. Also, the high droplet charge number is useful for some applications like Electrospray Ionization (ESI) (Fenn et al., 1989), where the droplets undergo Coulomb fissions by successively reaching the Rayleigh limit, and multi-charged ions are produced from macromolecules.

But the charge on the droplets may be a non-desired effect, becoming a problem for some applications. One example is when the electrospray droplets are used for calibration of sizer devices, where the droplet size may be distorted by the Coulomb instabilities. Another example is in colloidal thrusters where the droplets used to generate thrust must be discharged to prevent them to fly back to the satellite thus reducing thrust. Or in polymer solution electrosprays, where the narrow size distribution and morphology of dried particles is crucial in the areas of medical and pharmaceutical applications (Rostamabadi et al., 2021; Ali et al., 2021; Sverdlov Arzi and Sosnik, 2018; Boda et al., 2018; Nguyen et al., 2016; Bock et al., 2012; Yurteri et al., 2010), ceramics (Tang et al., 2016; Suhendi et al., 2013), and food encapsulation (Echegoyen et al., 2017).

We have studied the conditions to reduce the droplet charge that yield to the prevention of the Coulomb instabilities. We show that this configuration allows to easily discharge a charged aerosol generated by electrospray, and efficiently extract the discharged aerosol to a sampling device to be characterized.

We present a new approach for in-situ charge reduction of electrospray droplets, which allows the efficient transport (extraction) of the discharged aerosol. A unipolar ion source based on corona discharge generates a controllable ion flux of opposite polarity to the electrospray. The ions are introduced axially into the spray, while the Taylor cone is screened from the ions by an extractor ring electrode. Efficient and steady droplet discharge and extraction through an orthogonal aerosol-extraction tube was attained when the inlet of the tube was near the spray emission and the ring electrode, resulting in dramatic changes in droplets' trajectories.

3.2 Methodology

3.2.1 Materials

All the chemical reagents were used as purchased, without further purification. Ethylene glycol (EG) (reagent grade, CAS Number 107-21-1) was purchased from Sigma Aldrich. Sodium chloride (NaCl) (ACS grade, CAS Number 7647-14-5) was purchased from Scharlau. Synthetic dry air 99,998% purity was purchased from Carburos Metálicos, Spain (20.9% ±1% O_2 with 3 ppm molar of H_2O, 0.2 ppm molar of THC and 1 ppm molar of CO and CO_2, the rest being N_2).

3.2.2 Solution preparation and characterization

We have used two different liquid solution conductivities with a nonvolatile solvent (EG). A stock solution was first made by dissolving 21 mg of NaCl in 75 ml of ethylene glycol and stirring the solution overnight. This initial solution was then diluted under stirring to obtain 0.007% w/v and 0.0007% w/v solutions. The electrical conductivity was measured with a portable conductivity meter (CRISON 35) using a glass-body probe (CRISON 50 61). The solutions concentrations and properties are given in Table 3.1.

Table 3.1. Properties of the solutions.

Solution code	Solutes and concentrations	Solvent	Electrical conductivity, S/m	Solution density, g/cm^3
007EG	NaCl: 0.007% w/v	Ethylene glycol	9.6 $\times 10^{-4}$ (24.5°C)	1.116 (25.0°C)[1]
0007EG	NaCl: 0.0007% w/v	Ethylene glycol	1.13 $\times 10^{-4}$ (24.5°C)	1.116 (25.0°C)[1]

[1]Not available. Value shown is for the pure solvent.

3.2.3 Electrospray-corona apparatus and particle extraction system

The electrospray and corona subsystems were housed in a chamber for gas ambient control (Fig. 3.1). The chamber consisted of a fixed black Delrin® platform (to which the electrospray subsystem and corona ion source were mounted), a Delrin® base frame sitting on the platform, a black Delrin® wall for all the connections (electrical, gas, and liquid supplies, particle sampling and extraction, etc.) which is screwed to the base frame, and a removable glass urn made of three glass panels (175×130×1.8 mm) and a glass top (135×135×3 mm) (Fig. 3.2). The urn's edges sit on rubber seals, so the urn can be lifted easily. During electrospraying, the urn was in place (except where noted) and synthetic dry air was supplied to the chamber at 4.4 lpm. The air exited the chamber through the particle extraction tube and passed through the collection filter, as well as through a port exhausting to a remote fume hood. The chamber gas inflow was set to maintain about 5-10 Pa in the chamber, sensed by a Magnehelic differential pressure meter (cat. no. 2000-125Pa C). Meanwhile, the relative humidity in the chamber (RH) was monitored using a Vaisala HM34 meter probe inserted through the Delrin® lateral wall.

A. Electrospray subsystem

The electrospray capillary was made of 304 stainless-steel capillary tubing (Tubos Capilares, Spain; 160 μm ID, 400 μm OD), square cut to a 30 mm length, and polished on its exit end. It was centered inside a square-ended glass tube (1.16 mm ID, 2.00 mm OD) and its protrusion varied (∼0.5 mm in the particle generating experiments, and longer in the ethylene glycol experiments). When spraying polymer solutions, a gentle sheath flow of solvent-saturated gas (synthetic air) flowed through the glass tube, around the capillary, at a typical average speed of 70 mm/s, to prevent polymer precipitation at the Taylor cone (TC) meniscus caused by solvent evaporation. The use of such flow was first suggested by Larsen et al. (2004) but is not widely practiced, although we often find it necessary when making small particles by electrospray (Bodnár and Rosell-Llompart, 2013; Bodnár et al., 2018).

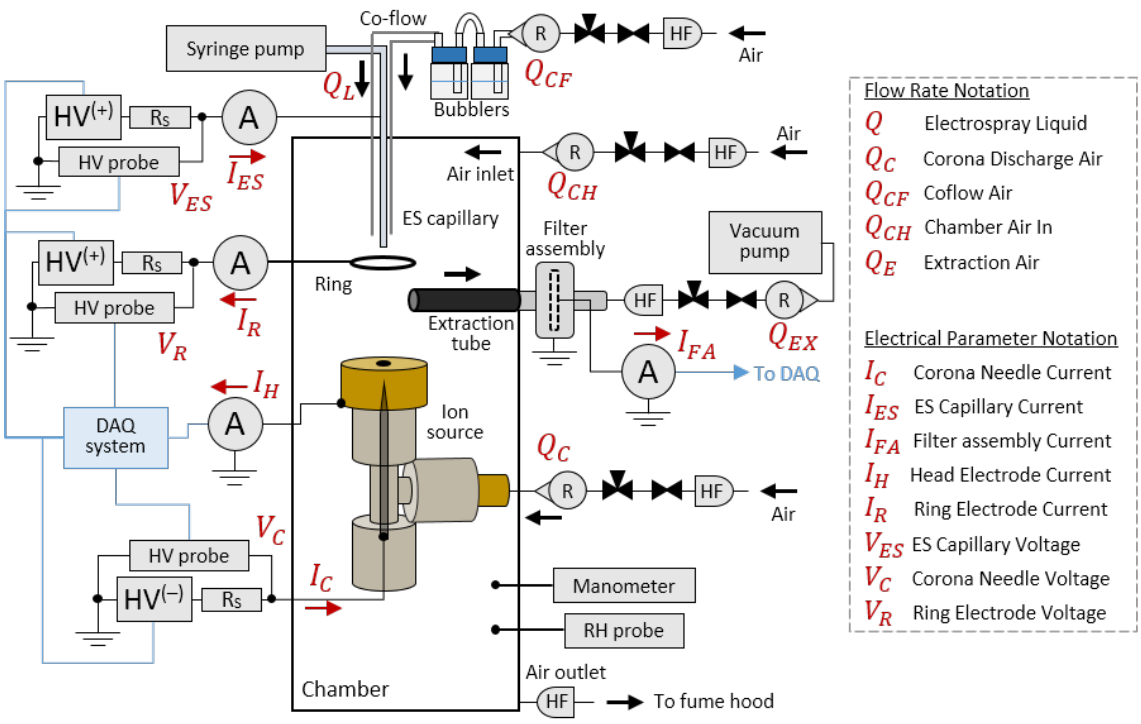

Figure 3.1. Setup used for generating ions and electrospray droplets. System schematic comprising electrospray with co-flow, unipolar ion source, sampling tube with filter assembly. Acronyms: DAQ = Data acquisition; HV = high voltage; HVPS = HV power supply; A = ammeter; HF = HEPA (High Efficiency Particulate Air) filter; R = rotameter; R_S = safety resistor (250 $M\Omega$).

The liquid solution was fed to the capillary by a syringe pump (Harvard Apparatus PHD 2000) from a glass syringe (Hamilton® syringe, 1000 series GASTIGHT®, 1 ml) connected to a 27-gauge × 1/2" hypodermic needle fitted to a PTFE capillary tubing (Teknokroma, 360 μm ID, 580 μm OD) into the electrospray capillary.

A ring electrode (5 mm ID, 1 mm thickness) was placed beneath the electrospray capillary in nozzle-to-ring down configuration (Figs. 3.1 & 3.3). This configuration is commonly used in electrospray practice to provide electrostatic shielding (Cloupeau, 1994; Jaworek, 2007b). The voltage difference between the capillary and the ring established the electric field that is needed to generate the electro-atomization. Here, the ring has the important additional benefit of shaping the electrical field to guide the ions to interject the droplets' trajectories.

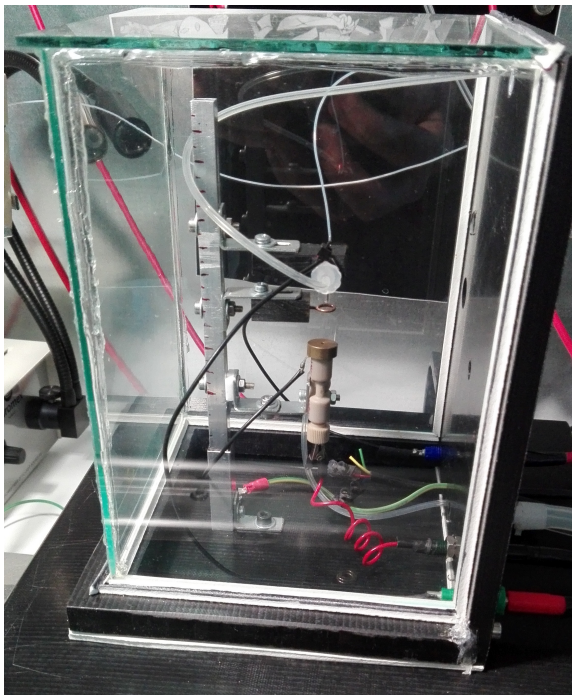

Figure 3.2. Electrospray neutralization apparatus. The glass walls are glued together forming an urn. This urn, which can be easily separated from the frame, is resting on rubber seals stuck to the frame. The frame can be moved horizontally to adjust the sampling tube position when inserted through the Delrin® lateral wall.

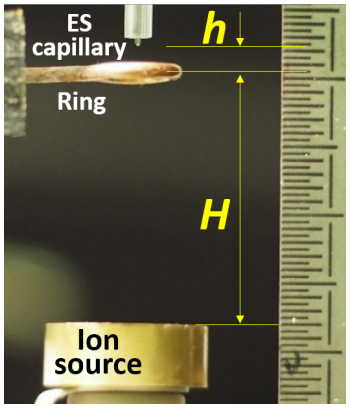

Figure 3.3. Photography of the discharge zone with height parameters, being h the distance between the electrospray nozzle and the extractor ring and H the distance between the extractor ring and the ion source head electrode.

B. Unipolar ion source

In conceiving the ion source, we hypothesized that attaining efficient discharging required injecting the ions coaxially with the spray. In addition, we hypothesized that the ion and spray currents must be alike (though not necessarily equal). Since

corona currents easily exceed electrospray currents by an order of magnitude or more, an orifice plate ("corona extractor") was placed in front of the corona needle. This limited the ionic current passing to the spray region. In the context of particle production by electrospray and corona discharging, an intermediate electrode was previously used also by Tang et al. (2017), and briefly by Cloupeau (1994). Therefore, as above presented in previous Chapter, the home-made unipolar ion source consisted of a corona discharge needle (tungsten Alfa Aesar, 1.5 mm diameter rod, sharpened to 15 μm tip radius, with 32^o total angle) housed inside a modified tee connector (IDEX P-714 Low-Pressure Tee Assembly, Natural PEEK), capped with an Earth-grounded "head electrode" which coaxially had an orifice for ion extraction into the spray region (Figs. 3.1 & 2.1a). The voltage difference between the corona needle and the head electrode established the electric field to sustain the corona discharge. Synthetic dry air was continuously fed to the corona discharge region at a low flow Q_C as shown in Fig. 3.1 (at 13.3 ml/min, corresponding to plug-flow gas speed at the exit orifice of 71 mm/s). However, this flow did not significantly affect the current of ions available to the spray.

The electrospray capillary, the ring electrode, and the corona needle were each connected to a channel of a Ultravolt high voltage power supply (HVPS) (HVRACK-4-250-0032) each through a high voltage-rated 250 MΩ resistor, used for user safety. For the first two, we used voltage regulation, whereas for the corona needle we used current regulation. The electric potential at each electrode was continuously monitored by respective HV probes (Testec, TT-HVP-40, 1 GΩ), and the electrical currents flowing through these electrodes and through the corona head electrode were measured inline by battery powered nano-ammeters (home-made current-to-voltage amplifier-based designs). The signs of the reported currents are given in Fig. 3.1. The outputs from the ammeters, voltage, and current monitor from the HVPS, and from all the HV probes are fed to a National Instruments PCI-6221 DAQ card on a desktop computer.

C. Droplet collection systems

Discharged droplets from the spray were extracted into an antistatic tube (SCAT Conductive plastic tube, 4 mm ID, 6 mm OD, 6 cm length) inserted through the chamber Delrin® lateral wall. This extraction tube was connected to a Swinny filter holder made of either metal (stainless steel) or plastic (polypropylene). The holder housed a glass microfiber filter (a Whatman 25 mm diameter filter with 1.6 μm pore size). The extraction gas was provided by a vacuum pump (Laboport N86KT.18). The filter assembly (filter holder plus filter) was placed inside a purpose-made Faraday-cage, whose inner metal shell (for plastic filter holder) or the metal filter holder is connected to a Keithley 6485 picoammeter to monitor the residual electrical charge current carried by the electrospray droplets to the filter assembly.

D. Illumination and photography

Two cameras (Olympus PEN E-PL7 and Olympus PEN EP-1)) were used for photographing (i) the electrospray plume with a Nikkor macro lens (60 mm, 1:2.8) under darkfield illumination using a single white LED spot lamp, and (ii) the Taylor cone with an Edmund Optics VZM 450i zoom imaging lens under brightfield illumination to verify the cone-jet mode in all the experiments (Rosell-Llompart et al., 2018).

3.2.4 Electrospray discharging protocol

Stable combination of the electrospray with the ions and with the extraction gas flow relies on balancing the right electrode voltages and the right flow speeds. To achieve a stable balance, we used the following protocol with a closed chamber. Initially, with the extraction tube kept far from the spray axis, we set both the chamber airflow in (which vents to the fume hood) and the corona discharge airflow. With the corona head electrode covered, we established the electrospray in cone-jet mode and the corona discharge. For the first, we set the voltage difference between the ES capillary and the ring electrode at their approximate final values (known from previous practice runs), and then we feed the liquid solution through the capillary (with the coflow on when in use). The ES capillary and ring voltages were chosen

to be high enough to drive the droplets towards the head electrode (kept at Earth-ground), rather than back toward the ring (data shown later). The direct currents were monitored at the electrospray capillary (I_{ES}), at the ring (I_R), and at the corona head (I_H) (Fig. 3.1). Any positive ring current at this stage is interpreted as due to droplet deposition.

Next, after both the electrospray and the corona discharge were stable, the vacuum pump was turned on to start the extraction airflow. Within a few seconds, the head electrode was uncovered to allow the passage of ions through the head electrode orifice into the spray region. This disturbs the spray, which typically became a floating dense aerosol cloud. At the same time, typically, the Taylor cone shrunk a bit. If a change to multi-jet spraying mode happened (Rosell-Llompart et al., 2018), we regained stability in the cone-jet mode by lowering the ES capillary voltage. (Therefore, to prevent that the cone-jet will become unstable when the ions are introduced into the system, we start with a slightly elongated cone shape.) Often, we recorded a finite current at the ring electrode ($I_R < 0$), which is due to ion collection, and an increase in the ES capillary current (I^*_{ES}) (Fig. 3.1).

Immediately after, the extraction tube was approached to the aerosol cloud at the desired location. Often this distorted the discharging process, so, meanwhile the tube was positioned, the voltages were readjusted to maintain a steady and stable process (spray outline, cone, currents). We assumed that the droplet extraction was maximized when we saw the whole aerosol entering the tube. The 'dead' time between the moment when the corona orifice was uncovered (to admit ions into the spray region) and the moment when we started the timer (needed for establishing the particle collection time) was very small (typically one or a few seconds), and negligible compared to the total particle collection time.

3.3 Results and discussion

We have used a non-volatile solvent, ethylene glycol, to investigate the role of the various parameters on the generation of ions and of droplets separately (3.3.1), and the effects of the ions on the spray plume shape for a low-volatility solvent without the presence of solutes (3.3.2). This absence of solutes simplifies the system under study. Otherwise, accumulation of solutes on electrode surfaces could change the electrical field over time.

3.3.1 Electrostatic control of ion and droplet trajectories

The corona head acts as the counter electrode to the corona needle, thus collecting most of the ions emitted from the corona, and allowing only a small fraction of the corona current to pass through its orifice and become available to interact with the electrospray droplets. This current fraction must be small because corona currents (a few μA) far exceed electrospray currents (tens of nA). The capture of ions by the droplets (Fig. 3.1) depends critically on the droplets' and ions' trajectories, thus on the electrical field, which depends on the electrodes' voltages and geometries. First, in the absence of spray, we studied how sensitive the ionic current passing through the head electrode orifice into the spray region (I_{Ext}) is to both the corona current (I_C) and the ring voltage (V_R). In these experiments, the electrospray capillary was removed. Also, to ensure the trapping of any central ions, the ring was covered with a metal disc (12.7 mm diameter). These geometry changes allowed us to determine I_{Ext} without elimination of the essential elements. Fig. 3.4 shows that I_{Ext} is (i) weakly dependent of the corona current, and (ii) can be regulated by means of the electrical field E_{Ext} in the region outside of the corona device through V_R, where $E_{Ext} \sim V_R/H$ (same data presented in Chapter 2, subsection 2.5.4, pg. 46, is duplicated and reduced by selecting the ring voltage (V_R) range which has been used in next experiments).

It is shown that the electrical field outside of the corona device (head electrode) strongly influences the ion current available to discharge droplets. Note that in the absence of a ring electrode, it would be challenging to control the Taylor cone stabil-

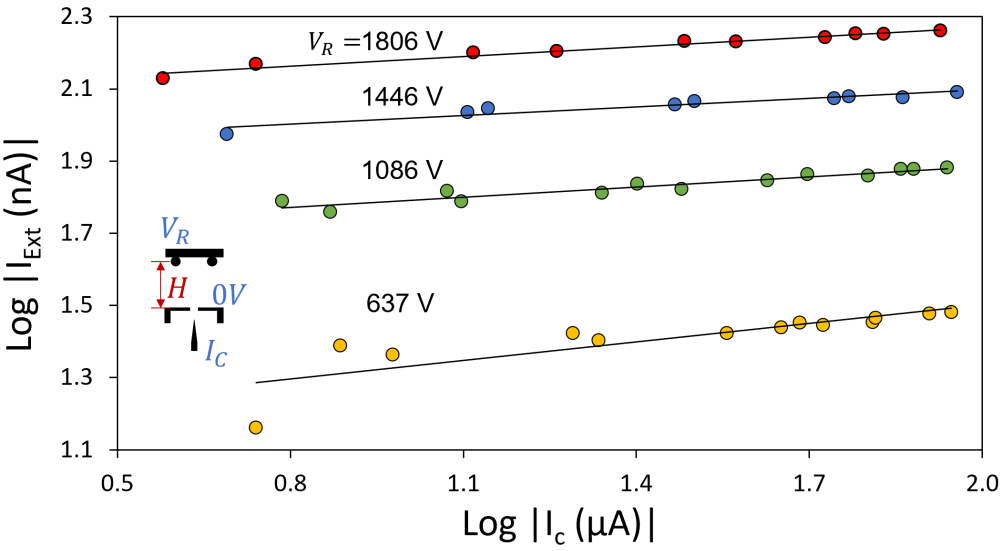

Figure 3.4. Log-Log plot of extracted ion current I_{Ext} (< 0) measured at the counter electrode (ring plus disk, as shown in the inset) versus the corona current I_C, at varying ring voltage, V_R (values displayed). (H = 17.0 mm. Q_C = 20 ml/min.). Electrode diagram is included, showing the absence of electrospray capillary and the covering of the ring with a disc. Lines are power-law fits.

ity. A single voltage difference (between the capillary and the head electrode) would be simultaneously controlling: (1) the droplet generation near the Taylor cone at the capillary exit, and (2) the ionic current available for droplets' discharging. Such configuration has, in fact, been proposed in the prior literature (see Introduction). The (better) configuration used here includes a ring electrode, and this allows independent control of (1) and (2). Its voltage difference with the head electrode (here, V_R) governs the trajectories of ions and droplets in the space between, while its difference with the electrospray capillary ($\Delta V = V_{ES} - V_R$) governs the formation of the Taylor cone.

Such independent control is demonstrated by Fig. 3.5. In Fig. 3.5a, the electrospray was monitored in the absence of corona, while varying both V_R and V_{ES} at constant difference (ΔV). We found near constancy for the electrical current at the capillary I_{ES} as shown in Fig. 3.5b. This demonstrates that the droplet generation process was affected minimally, if at all. Meanwhile, the electrospray droplet trajectories experienced big changes, as is evident from the spray appearance (Fig. 3.5c). Through the voltage scan, also the head electrode and ring currents varied widely, for low enough values of V_R (Fig. 3.5b). The former decreased and the latter increased as

part of the spray was diverted toward the ring, while both currents consistently add up to the electrospray capillary current, as expected.

Fig. 3.6 plots the ring current I_R versus ring voltage V_R from Figs. 3.5a-b. This current is associated with droplet deposition on the ring due to droplet flying-back toward it, causing liquid accumulation over time on the ring electrode (visible in Fig. 3.5c). The accumulated liquid probably attracted electrical field lines, thus reinforcing the flying-back. We believe this to be the reason for the increase in ring current over time as observed in Fig. 3.6, along with a shift in the V_R at which the flying-back starts (from ∼1.3 to 1.5 kV).

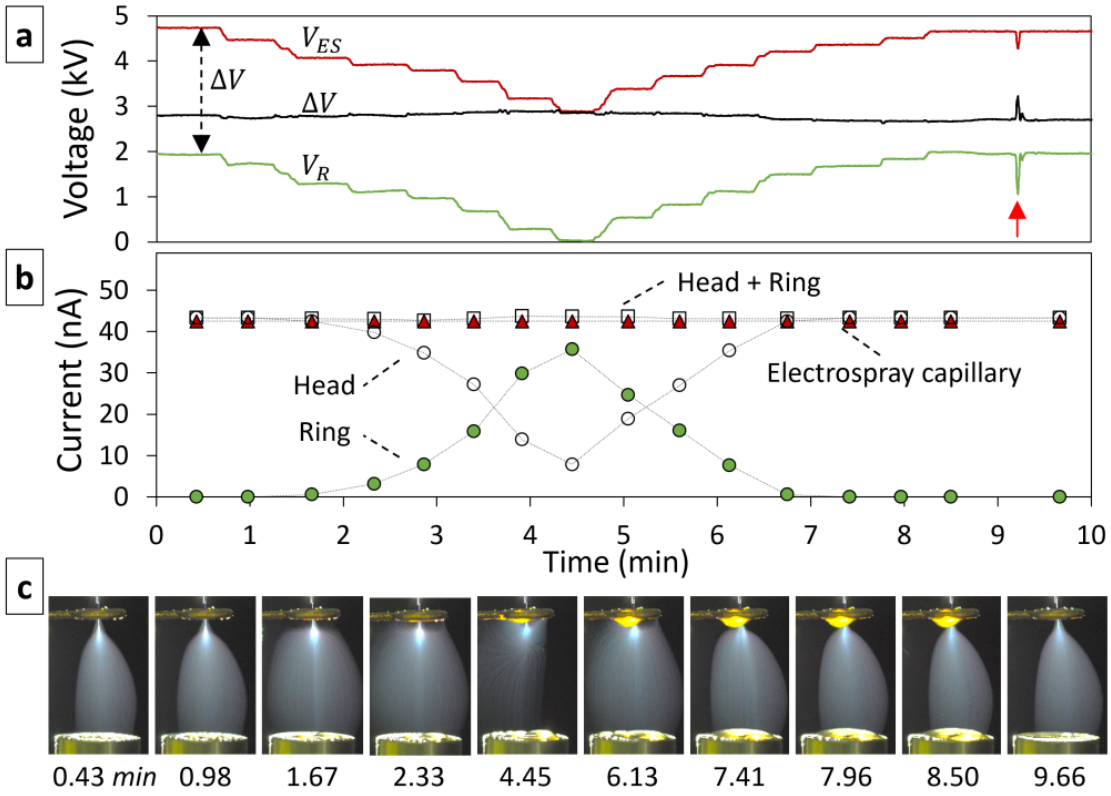

Figure 3.5. Experiment showing the effect of the electric field between ring and counter electrode (without ions) on the electrospray plume (for solution 0007EG). (a) V_R and V_{ES} versus experiment time, varied with ΔV ∼2.8 kV (also shown). (b) Electrode currents I_{ES}, I_R and I_H, and the sum of these two, versus experiment time. (c) Snapshots corresponding to some of the current measurements. The last photo was made after (at time shown with an arrow in (a)) the liquid accumulated on the ring and corona head was wiped with a cloth, without interrupting the spraying. (H = 17.0 mm, h = 1.3 mm, Q = 5 μl/min.).

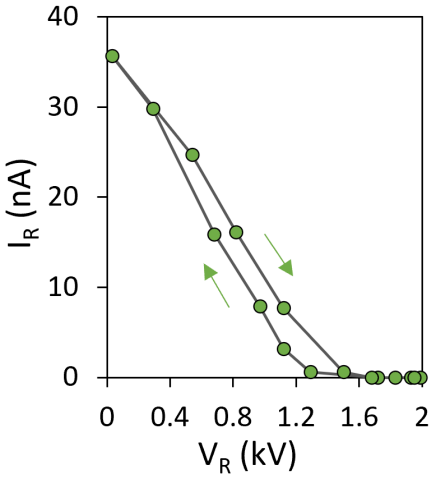

Figure 3.6. I_R as a function of V_R throughout the experiment.

3.3.2 Discharging of ethylene glycol electrosprays

The droplet neutralization process requires a suitable combination of three elements: 1) the electrospray plume, 2) the ion plume, and 3) the gas flow field responsible for removing discharged droplets (into the extraction tube). We have qualitatively investigated how the ions influence the spray plume shape using non-volatile (ethylene glycol) solutions in the presence or absence of extraction flow. Fig. 3.7 illustrates different situations in which the electrospray is electrically discharged, or not, by an ion stream having similar electric current to the electrospray. In Fig. 3.7a ions and extraction flow are absent, and the spray adopted a typical plume shape, in which the droplets follow predictable trajectories which are close to the electrical field lines (Arumugham-Achari et al., 2013; Higuera, 2012). In Fig. 3.7b, the addition of corona ions leads to chaotic wavy motions of the spray plume when the extraction tube is still far away from the spray. The droplet trajectories did not follow the electrical field lines, as they are convected by spurious gas currents. This proves that most of the droplets lost most of their initial charge. A similar situation was found when a ring electrode is not present. However, the use of a ring made it easier to control the system, as already mentioned for the ions and droplet separately.

In Fig. 3.7c, the extraction flow (set by the extraction tube) was brought near the spray region, cancelling the chaotic motion as the droplets were suctioned into the tube. In this case, the droplets followed nearly steady trajectories, which depart strongly from the electric field lines (which are nearly the same as the droplet

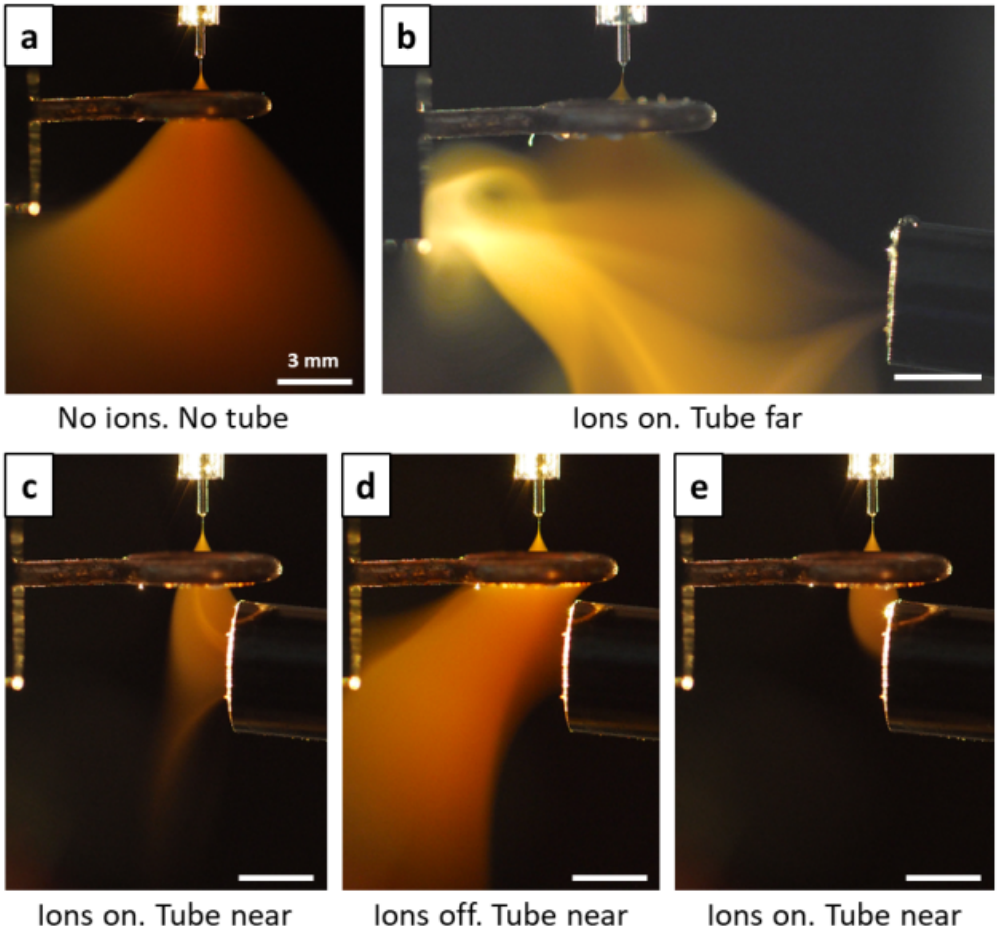

Figure 3.7. Ethylene glycol electrospray (solution 007EG) (a) in absence of extraction flow and ions, and (b-e) in presence of extraction flow under different situations: (b) Exposed to corona ions, but tube located far (for which the discharged aerosol does not follow the electric field lines). (c) Exposed to corona ions, but tube located near (controlled spray discharging and extraction). (d) Ions turned off, while tube is near the spray (presence affecting the droplet trajectories). (e) Ions are on, and tube closer. (Better extraction.) V_{ES} = 4.6 kV, V_R = 1.0 kV, I_{ES} = 46 nA, I_C = -12.0 μA, I_{Ext} = -60 nA, H = 17.0 mm, h = 2.2 mm, Q = 0.5 μl/min (without gas coflow). Q_C = 20 ml/min. v_{tube} = 5.5 m/s. The glass urn was removed in these experiments to attain best image quality. Scale bars: 3 mm.

trajectories in Fig. 3.7a). If, while the flow was on, the ions were turned off, the extraction flow became uncapable of suctioning the spray into the tube, as demonstrated in Fig. 3.7d. (They moved slightly away from the extraction tube, indicating electrostatic repulsion due to an initial accumulation of charged droplets.)

From these tests, we conclude that the droplets' trajectories are very different when the ions are present than when they are not. Therefore, the capture of ions by

the droplets is very efficient, enough to greatly reduce their initial net electrical charge. The droplets follow mostly the electrical field lines when the ions are not present, whereas they follow closely the gas streamlines when they are discharged (or significantly discharged). Interestingly, this observation allows us to roughly estimate the electrical mobility of the droplets before neutralization. As the air speed at the inlet of the tube v_{tube} is 5.5 m/s and the electrical field strength in this region is of the order of V_R/OD_{Ring} = 1.0 kV/7 mm = 1.4×10^5 V/m, the droplets' initial electrical mobility μ (speed/field strength) must be of the order of $v_{tube}/\left(V_R/OD_{Ring}\right)$, namely (5.5 m/s)/($1.4\times10^5$ V/m) = 4×10^{-5} m^2/(V·s).

In Figure 3.7e, the ions had been turned on again and the electrospray aerosol was extracted into the extraction tube as before (Fig. 3.7c), demonstrating that the process is reversible. Note that here the tube was very close to the spray axis, and the extraction was still robust.

In sum, the spray suffered dramatic changes when ions were introduced (with similar electrical current), and the proximity of the gas flow at the inlet of the extraction tube was critical to attain steady droplet discharging and extraction.

3.4 Conclusions

We demonstrate a continuous process for the effective reduction of the electrospray droplets' charge in situ using opposite-polarity unipolar ions from a corona source. In our design a fraction of the current produced in a negative corona discharge is introduced axially into the electrospray, approximately matching the electrospray current. The discharged aerosol is then extracted orthogonally by an antistatic extraction tube, and the droplets are then easily transported and collected on a filter. Electrospraying in capillary-ring configuration allows us to stabilize the spraying process independently from the presence of ions. Meanwhile, the spray-ions interactions are controlled mainly by the voltage difference between the ring electrode and the ion source. Droplet flyback towards the ring can be prevented robustly over a wide range of ring voltages.

Stable electrospray discharging allowed the continuous extraction of the discharged droplets into an antistatic tube with high efficiency. The removal of droplets by a proximal antistatic tube is critical to the stability of the process, as it prevents the charge reversal of the droplets with consequent migration toward the Taylor cone and/or collision events with other droplets.

We have found that the geometrical and electrostatic parameters are key to maximize droplet discharging and minimize droplet loss.

We found that the distance between the ring electrode and ion source controlled the location where the ions interacted with the droplets.

— Life is movement. Movement is change. Every time tiny particles swing through time and space, something is changing.

Neale Donald Walsch

4

Monodisperse Particles by Efficient Neutralization of Electrosprays

4.1 Introduction

Nanoparticles (< 100 nm), submicroparticles (< 1 μm), and small microparticles (1-10 μm) are receiving increasing interest in diverse technological, scientific, nutritional, and medical areas (Cun et al., 2021; Dima et al., 2020; Wicki et al., 2015; Cejková et al., 2013; Webster et al., 2013). Several technologies, such as Spray Drying, are widely used where the production of particles covers ranges from tens to hundreds of microns, and tolerates a wide dispersion of droplet size. This is the case of industrial production of dried foods, pharmaceuticals, and fertilizers (Vehring et al., 2020; Wang and Langrish, 2009; Masters, 1991). Yet, it has been difficult to extend such approaches to the droplet size range below about one micrometer (Jafari et al., 2021; Malamatari et al., 2020; Salama, 2020; Sosnik and Seremeta, 2015; Nandiyanto and Okuyama, 2011).

Fittingly, electrospraying is an atomization technique capable of generating droplets in the micron- and submicron size ranges with size homogeneity and high energy efficiency (Rosell-Llompart et al., 2018; Gañán-Calvo et al., 2018). Therefore, interest in the electrospray route for producing small particles has been rekindled in the areas of ceramics (Tang et al., 2016; Suhendi et al., 2013), pharmaceutics/therapeutics (Ali et al., 2021; Sverdlov Arzi and Sosnik, 2018; Boda et al., 2018; Nguyen et al., 2016; Bock et al., 2012; Yurteri et al., 2010), nutraceuticals (Rostamabadi et al., 2021), food encapsulation (Echegoyen et al., 2017), and cosmetics (Mehta et al., 2017).

Unfortunately, the net electrical charge carried by the electrospray droplets may lead to several issues. First, the fast speeds attained by the charged droplets in the

high electrical field (of order m/s) may lead them to reach the collection electrode as incompletely dried particles, thus forming a continuous film instead of a particulate film. Second, when multiplexing electrosprays, the electrostatic repulsion between different sprays limits the scalability of the process (Sochorakis et al., 2019; Almería et al., 2011; Deng et al., 2006; Bocanegra et al., 2005). Thirdly, Coulombic instabilities (CIs) during droplet evaporation (Duft et al., 2003; Saville, 1997; Gomez and Tang, 1994) are particularly unfavorable as they lead to non-spheroidal (elongated or filamentous) particle shapes or mixed fragment sizes (Bodnár et al., 2018; Almería et al., 2010; Li et al., 2007).

Although several works, focused on making small particles by electrospray, have attempted the reduction of the droplets' charge by gas-phase ions, by either of several approaches (Lenggoro et al., 2000; Yurkstas and Meisenzehl, 1964; Meesters et al., 1992; Cloupeau, 1994; Mustika et al., 2021). In none of the cited works combining electrosprays with corona ions to make particles could we find data on the droplet discharging efficiency, the particle morphology changes, or their dependence on the independent variables of the problem (electrode geometrical parameters, corona conditions, electrospray conditions, etc.). Nor have the ion losses and droplet losses to the electrodes been investigated typically, despite their importance. All these important questions must be answered to improve and optimize electrospray-corona systems. In addition, such data should be useful for informing numerical simulations on these systems (Higuera, 2016; Khalifehei and Higuera, 2020).

In this work, we have used three different polymer solutions in volatile solvents, which led to different particle sizes from small microparticles (diameter ~ 1 μm) to nanoparticles (diameter ~ 200 nm). In addition, we approximately match the ionic current to the electrospray current. We hypothesize that, in a stable process, these two currents must be alike (though not necessarily equal) to prevent that the ions discharge the Taylor cone. Therefore, an orifice plate ("corona extractor") placed in front of the corona needle limited the ionic current passing to the spray region. In the context of particle production by electrospray the use of an intermediate electrode was previously used only by Tang et al. (2017) and briefly by Cloupeau (1994). To prevent the ions from reaching the Taylor cone, a ring-shaped electrode was placed in front of the electrospray capillary. This configuration is commonly used in

electrospray practice to provide electrostatic shielding (Jaworek, 2007b; Cloupeau, 1994). Here, the ring has the important additional benefit of shaping the electrical field to guide the ions to interject the droplets' trajectories.

4.2 Methodology

The experiments for this Chapter were carried out in collaboration with Elena Barbero-Colmenar.

4.2.1 Materials

All the chemical reagents were used as purchased, without further purification. Polystyrene (PS) (CAS Number 9003-53-6, weight-average molecular weight (M_w) of 35 kDa), methyl ethyl ketone (MEK) also known as butanone (ACS grade, CAS Number 78-93-3, residue on evaporation 0.0020%), curcumin (CUR) (99% purity, CAS Number 458-37-7, 368.38 g/mol), and polyvinylpyrrolidone (PVP) (CAS Number 9003-39-8, M_w of 40 kDa) were purchased from Sigma Aldrich. Chitosan (CAS Number 9012-76-4, M_w of 150 kDa) was purchased from Acros organics. Acetic acid glacial extra pure was purchased from Scharlau. Ultrapure water (Millipore, USA) was used throughout. Sodium chloride (NaCl) (ACS grade, CAS Number 7647-14-5), ethanol absolute (ACS reagent grade, CAS Number 64-17-5), and acetone (ACS reagent grade, CAS Number 67-64-1) were purchased from Scharlau. Synthetic dry air 99,998% purity was purchased from Carburos Metálicos, Spain (20.9% ±1% O_2 with 3 ppm molar of H_2O, 0.2 ppm molar of THC and 1 ppm molar of CO and CO_2, the rest being N_2).

4.2.2 Solution preparation and characterization

We have used different liquid solutions based on polymer solutions in volatile solvents (PS in MEK, PVP in ethanol:acetone 1:1 by volume, and chitosan in ethanol:water:acetic acid 5:4:1 by volume). The necessary mass of solvent was added to a given mass of solute, followed by magnetic stirring overnight (3 hours in the case of the chitosan solution). However, PS solutions at 3% w/w were prepared by dilution of a 5% w/w PS in MEK prepared in this way. A 5 ml Gay-Lussac pycnometer was used to measure the density of some solutions. We measured the electrical conductivity with a portable conductivity meter (CRISON 35) using a glass-body probe (CRISON 50

61). The solutions concentrations and properties are given in Table 4.1.

Table 4.1. Properties of the polymer solutions.

Solution code	Solutes and concentrations	Solvent	Electrical conductivity, S/m	Solution density, g/cm^3
3PS-MEK	PS: 3% w/w	Butanone	6.9 $\times 10^{-5}$ (23.3°C)	0.807 (24.8°C)
1CUR-5PVP	PVP: 5% w/v CUR: 1% w/w	Ethanol/acetone (1:1 v/v)	1.43$\times 10^{-3}$ (24.0°C)	0.815 (20.5°C)
0.1CUR-5PVP	PVP: 5% w/v CUR: 0.1% w/w	Ethanol	1.21 $\times 10^{-3}$ (21.6°C)	0.790 (20.0°C)[a]
2C10A50E	Chitosan: 2% w/w	Eth:H_2O:AcOH (5:4:1 v/v)	0.105 (22.5°C)	0.883 (21.0°C)

[a]Not available. Value shown is for the pure solvent.

4.2.3 Electrospray-corona apparatus and particle extraction system

In addition to the electrospray-corona apparatus system presented in #3.2.3, the following elements were used for this study.

A. Particle collection systems

Discharged droplets/particles from the spray were extracted into an antistatic tube (SCAT Conductive plastic tube, 4 mm ID, 6 mm OD, 6 cm length) inserted through the chamber Delrin® lateral wall. This extraction tube was connected to a Swinny filter holder made of either metal (stainless steel) or plastic (polypropylene). The holder housed a glass microfiber filter (a Whatman 25 mm diameter filter with 1.6 μm pore size for PS aerosols, either a 25 mm $\times$ 1.0 μm or a 13 mm $\times$ 1.6 μm filter for PVP-CUR aerosols, and a 13 mm $\times$ 0.3 μm filter for chitosan aerosols). The extraction gas was provided by a vacuum pump (Laboport N86KT.18). The filter assembly (filter holder plus filter) was placed inside a purpose-made Faraday-cage, whose inner metal shell (for plastic filter holder) or the metal filter holder is connected to a Keithley 6485 picoammeter to monitor the residual electrical charge current carried by the electrospray droplets to the filter assembly. For comparison,

in the absence of corona ions, electrospray particles were also collected on silicon wafers (Si-Mat, Germany, <100>, 525 μm thickness, P/Boron, 1-30 ohm·cm). A silicon wafer fragment sitting on top of a thin steel ruler (165×13, mm) was placed underneath the spray, on top of the corona head electrode. The ruler was Earth-grounded and was inserted through a slit on the chamber Delrin® lateral wall, and the Si wafer remained on the ruler all the time during the collection.

B. Particles' collection and charge-reduction efficiencies

The particle masses collected on the filter assembly (FA) m_{FA} and on the extraction tube m_{tube} (which includes the connector to the FA) were obtained by the weight differences before and after particle collection determined with a 5-digit analytical balance (Mettler Toledo XS205 Dual Range). The *extracted particle mass* was computed as $m = m_{FA} + m_{tube}$ and the *extraction efficiency* as:

$$\eta = m/m_{ES} \tag{4.1}$$

where m_{ES} is the mass of polymer in the electrosprayed solution, which we computed from the polymer mass fraction in the solution C_p, the infusion flow rate Q, the solution density ρ, and the collection time t as $m_{ES} = C_p \cdot Q \cdot \rho \cdot t$. The extraction efficiency can be decomposed as the sum of the contributions from the filter assembly $\eta_{FA} = m_{FA}/m_{ES}$ and from the extraction tube $\eta_{tube} = m_{tube}/m_{ES}$:

$$\eta = \eta_{FA} + \eta_{tube} \tag{4.2}$$

The residual electrical charge current carried by the electrospray droplets to the filter assembly I_{FA}, time-averaged over the collection time, is used to determine the *discharge efficiency* ζ defined as the fractional reduction in the initial charge of the droplets which, after combining with the ions, lead to particles collected on the filter holder. Such efficiency is computed as:

$$\zeta = 1 - \frac{\langle I_{FA} \rangle}{I_{ES} \cdot \eta_{FA}} \tag{4.3}$$

where I_{ES} is the electrospray current, and $(I_{ES} \cdot \eta_{FA})$ is an estimate of the initial electrospray current associated with the droplets which correspond to the particles on the filter. "$\langle\ \rangle$" means time averaging (necessary when the I_{FA} signal changed with time). A value of 1 for ζ would mean that the aerosol collected on the filter holder is overall electrically neutral.

C. Particle morphology and size characterization

The particles were imaged by scanning electron microscopy (SEM) (FEI Quanta 600) to determine particle morphology and size. After they were collected, on filters or on Si wafers, they were stored in a dry ambient until imaged, done typically on the same or the following day. Before being imaged, particles collected on the filters were either transferred to the carbon tape of the SEM sample holder by gently dabbing the tape on the particle collection, or by sticking a cut piece of the filter membrane with particles onto the C tape. Prior to imaging any samples, they were coated with a ∼27 nm Au layer (30 mA, 180 s) in a sputter coater (either a Quorum Q150R ES or a Quorum Q150T S plus). The particle size distribution was determined by manually sizing particles in the SEM images using ImageJ software (version 1.53e).

D. Illumination and photography

Two cameras (Olympus PEN E-PL7 and Olympus PEN EP-1)) were used for photographing (i) the electrospray plume with a Nikkor macro lens (60 mm, 1:2.8) under darkfield illumination using a single white LED spot lamp, and (ii) the Taylor cone with an Edmund Optics VZM 450i zoom imaging lens under brightfield illumination to verify the cone-jet mode in all the experiments (Rosell-Llompart et al., 2018).

4.2.4 Electrospray discharging protocol

In this study, the protocol used to discharge the polymer solution electrosprays was the same as in the case of ethylene glycol electrosprays presented in subsection 3.2.4, pg. 71.

4.3 Results and discussion

We apply the developed system to the production of two different types of particles in example systems based on polystyrene (PS) solutions (#4.3.4), polyvinylpyrrolidone-curcumin (PVP-CUR) solutions (#4.3.5), and chitosan solutions (#4.3.6).

4.3.1 Polystyrene particles from discharged PS/MEK electrosprays

To demonstrate the use of our charge reduction method to produce particles we have chosen a solution of 3% w/w of 35 kDa PS in MEK. This polymer solution leads to Coulombic explosions of the droplets, as revealed by the formation of progeny particles (Bodnár, 2016). Indeed, we made a morphology test to choose the appropriate liquid flow rate at which, for this solution, the particles were carrying filaments.

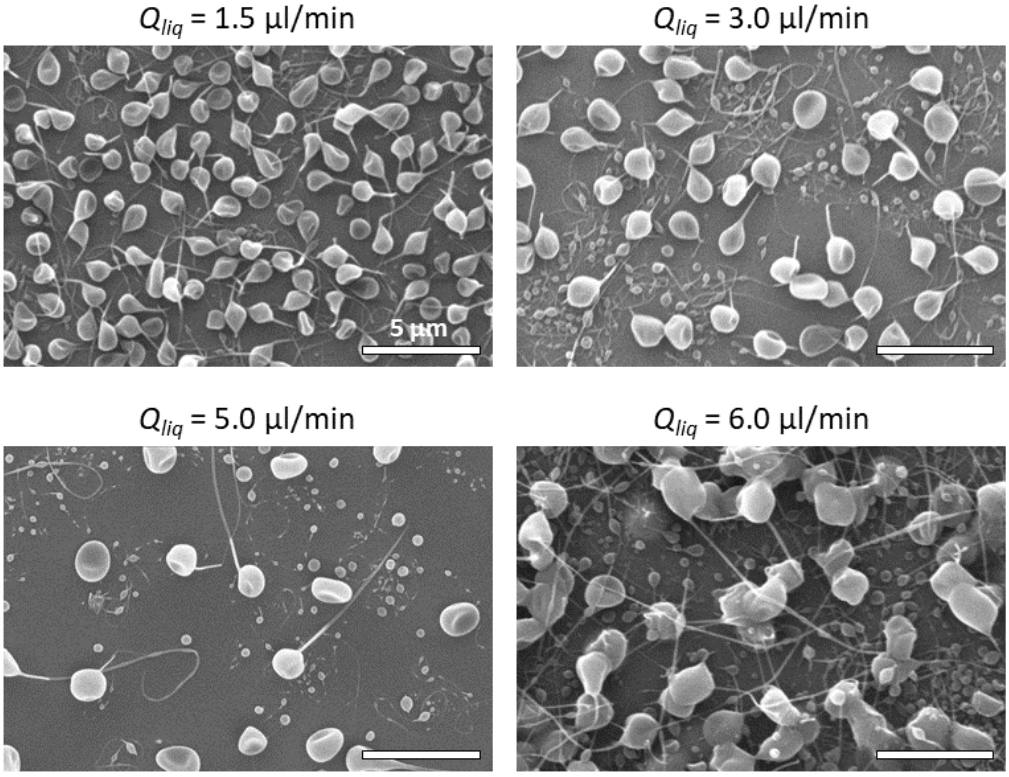

Figure 4.1. Filamentous PS particles made from 3PS-MEK solution which were collected on Si wafers, without corona ions. Conditions: low RH (<3%), 5 l/min dry air supplied to the chamber, images from the center of the deposition. Electrode configuration with $h = 1.7$ mm, and ring-to-wafer distance $H = 18.5$ mm. All scale bars: 5 μm.

Fig. 4.1 shows the resulting particles from electrosprayed particles, deposited on silicon wafers, at different liquid flow rate. The particles were most of them filamented, and we observed long filaments and also progenies. Particle size increases with the liquid flow (as it is expected). Based on these results we chose the 3PS-MEK solution at a liquid flow rate of 3.0 and 5.0 μl/min for the neutralization experiments. Therefore, this solution is suitable to test whether exposure to ions can reduce the droplets' initial charge sufficiently to prevent such explosions. We either sampled the electrospray by collecting it onto a Si wafer (to confirm the existence of progeny particles) or we extracted it by sucking it into an antistatic tube after discharging the spray by corona ions. The tube flow runs through a collection filter, where the collected particles were weighed and inspected by SEM. The filter was housed in either a metal or a plastic filter holder. When a metal holder was used, the Faraday cage electrical current was also monitored during collection (see Methodology, pg. 85). Collections for several tens of minutes were performed, at various test conditions and configurations, which are listed in Table 4.2.

Figure 4.2 shows images of electrospray discharging under different conditions. The sprays in all cases were substantially steady and their shape resembled comparable situations observed with the ethylene glycol sprays (subsection 3.3.2 and Fig. 3.7c,e). The Taylor cone was monitored throughout the experiments under bright-field illumination, as in the example of Fig. 4.2, to ensure that cone-jet mode was achieved (Rosell-Llompart et al., 2018). Between M.1 and M.2 (3 μl/min) the tube was placed at a height difference of 1 mm, with minimal impact on the shape of the spray plume, which appeared to completely enter the extraction tube. Raising the liquid flow rate from 3 to 5 μl/min (from M.2 to M.3) resulted in a widened spray plume and increase in light scattering. Both these changes are consistent with typical electrospray behavior. The spray plume widens due to electrostatic repulsion in the radial direction, as more charge is injected into the spray. Light scattering increases as the result of increased droplet size (obtained at the higher liquid flow rate).

Raising the corona current I_C threefold between M.3 and M.4 (from –5.4 to –14.8 μA) did not result in appreciable differences in plume shape or scattered light intensity. This is consistent with the fact established earlier in Fig. 3.4 that the ionic current

Table 4.2. Parameters and data for the particle collection experiments with polystyrene electrosprays.[a]

Sample[b]	Q (μl/min)	H (mm)	I_C (μA)	Tube radial position (mm)	I_{ES} (nA)[c]	I^*_{ES} (nA)[d]	I_R (nA)	I_{Ext} (nA)[e]	I'_{Ext} (nA)[f]	Collection time (min)	Extraction efficiency, η (%)	Filter assembly fraction, η_{FA} (%)	Discharge efficiency, ζ (%)
M.1	3.0	18.5	-5.5	2.0	25	25	-22	-40	-44	41.3	109	89	86
P.1										41.2	108	63	–
M.2	3.0	18.5	-5.4	2.7	25	27	-22	-40	-47	44.6	108	100	93
P.2										44.6	107	81	–
M.3	5.0	18.5	-5.4	2.5	29	43	-19	-40	-58	24.2	102	68	83
P.3										23.0	110	65	–
M.4	5.0	18.5	-14.8	3.3	29	36	-20	-50	-53	12.2	112	79	87
P.4										24.0	107	52	–
M.5	5.0	12.0	-12.4	2.0	30	40	–	-90	–	24.3	111	103	95

[a] In all cases: V_{ES} = 2.3 kV, V_R = 0.9 kV, v_{coflow} = 70 mm/s, v_{tube} = 5.5 m/s, Q_C = 20 ml/s, $RH < 2$ %.
[b] Metallic (M.x) and plastic (P.x) filter holder.
[c] Measured just before introducing the ions.
[d] Measured during spraying with corona ions present.
[e] Ionic current injected into the spray region estimated from Fig. 3.4 as a function of V_R and I_C.
[f] Ionic current injected into the spray region estimated according to a charge balance (see text).

I_{Ext} reaching the ring region is insensitive to the corona needle current. However, from M.4 to M.5, where H went from 18.5 to 12.0 mm (at constant voltages) to intensify the electric field, the ionic current I_{Ext} (shown in Table 4.2) had a big effect on the spray shapes (Fig. 4.2). In addition to the ionic current increase, H must change the ions' trajectories as they were injected closer to the ring. Therefore, the current flux (current per unit cross-sectional area) must be much greater in M.5 than in M.4 (or M.3). This explains why H is reduced from M.4 to M.5 the electrospray plume appears to be neutralized closer to the Taylor cone, where the droplet density is higher, the plume is narrower, and therefore the current flux for the droplets is also higher (than would be found further downstream in the absence of ions). In other words, one would expect that in order to discharge the electrospray efficiently, not only the ionic and spray currents, but their associated fluxes should be matched, as well. Note also that for the M.5 run, the plume electrostatic expansion appears to cease (with the spray attaining constant width).

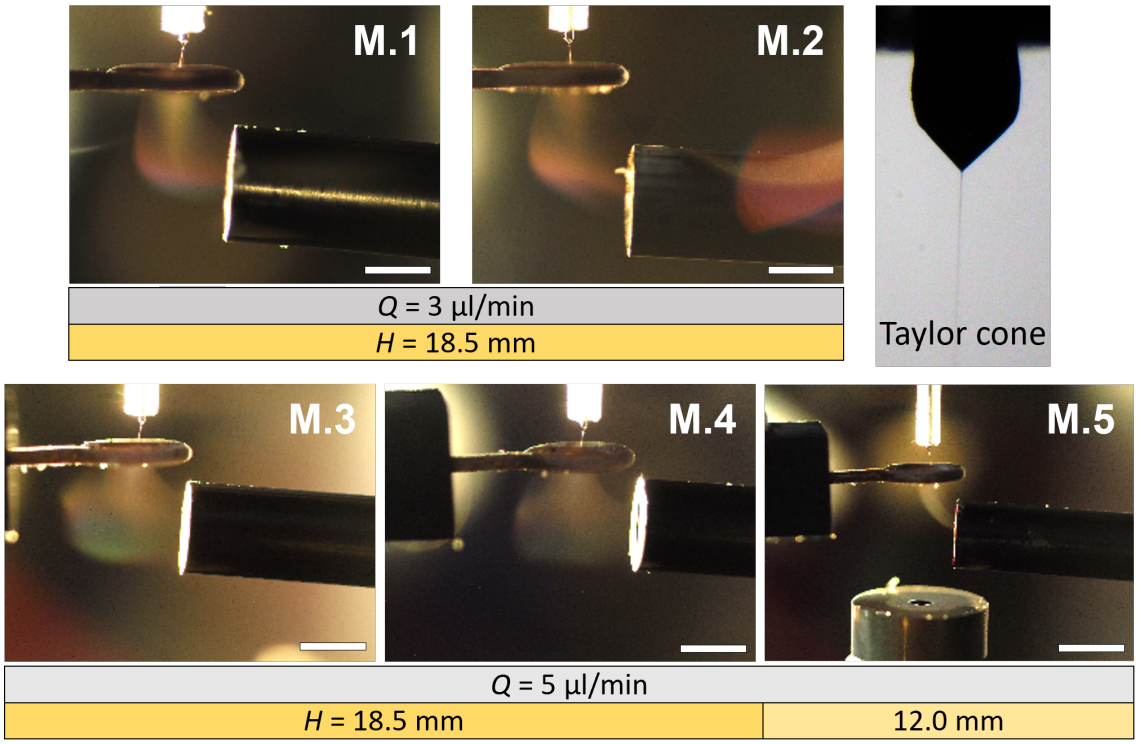

Figure 4.2. Polystyrene-MEK solution electrospray neutralization (3PS-MEK). Representative snapshots taken during the discharge (scale bar: 3 mm). Right: Taylor cone and jet. Common parameters: V_{ES} = 2.3 kV, V_R = 0.9 kV, h = 1.7 mm, v_{tube} = 5.5 m/s, v_{coflow} = 70 mm/s. See Table 4.2 for additional information.

Unlike in the ethylene glycol experiments (previous chapter), we did not observe liquid accumulation on the electrodes. However, we found small amounts of particles deposited at the entrance of the extraction tube (both on outer and inner walls), as is visible in Fig. 4.2 and Fig. 4.3. Maybe, the particles which had deposited early repelled other particles electrostatically, thus preventing continued deposition.

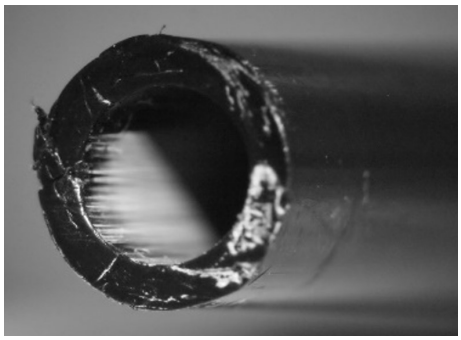

Figure 4.3. Particle deposition on the antistatic extraction tube walls.

Finally, it is interesting to compare the ionic current obtained from a charge balance, with the ionic current estimated from the direct measurements shown in Fig. 3.4.

The two values are shown in Table 4.2, as I'_{Ext} and I_{Ext} respectively. The former is the sum of the current contributions due to the ions only, namely: (i) the ring current (I_R), which is due to the ions (as its value is 0 before the ions are introduced), (ii) the electrospray capillary current (I^*_{Ext}) when the ions are present, which includes the part of the ions which reach the Taylor cone and the ions that combine with the droplets, (iii) decreased by the filter assembly current (I_{FA}), which is the residual droplets' charge which the ions were not able to cancel out: $I'_{Ext} = I_R - (I^*_{Ext} - I_{FA})$. The two values in the Table for I_{Ext} are quite similar, which leads to two conclusions: (i) That the droplets are indeed significantly discharged by the capture of ionic charge; and (ii) that the ionic plume spreads significantly, enough to reach the ring.

4.3.2 PS/MEK discharging efficiencies

Fig. 4.4 shows the time traces of the filter assembly current, I_{FA}, for the same conditions from Fig. 4.2 when a metal filter holder was used. These currents were always positive and slowly decreasing with time, with a similar decay rate. Such decay may be due to the slow buildup of charge on the filter, eventually leading to rejection of incoming positively charged particles. When plastic filter holders we used (P.x conditions) the FA currents were erratic, fluctuating around 0 nA (shown later in Fig. 4.6); so, these were not used to determine discharging efficiencies. In all cases, the current was always much smaller than I_{ES}, consistent with extensive discharging of the spray by the ions (Table 4.2). Note that a small but finite residual charge could be desirable to prevent coalescence while the droplets are drying up.

The I_{FA} traces were integrated and used to compute discharging efficiencies ζ by Eq. 4.3. These are shown in Fig. 4.5 by blue bars and ranged between 83 and 95%. Incomplete droplet discharging is not surprising because the extent of discharging of the individual droplets must depend on each droplet's exposure to a certain ion flux as it travels through its trajectory, which probably varies for different droplet trajectories. In addition, theoretically, under a constant influx of ions the droplets should eventually reverse sign and achieve a limiting stationary negative charge level. In fact, we cannot rule out the presence of negatively charged particles as I_{FA} is a *net* current.

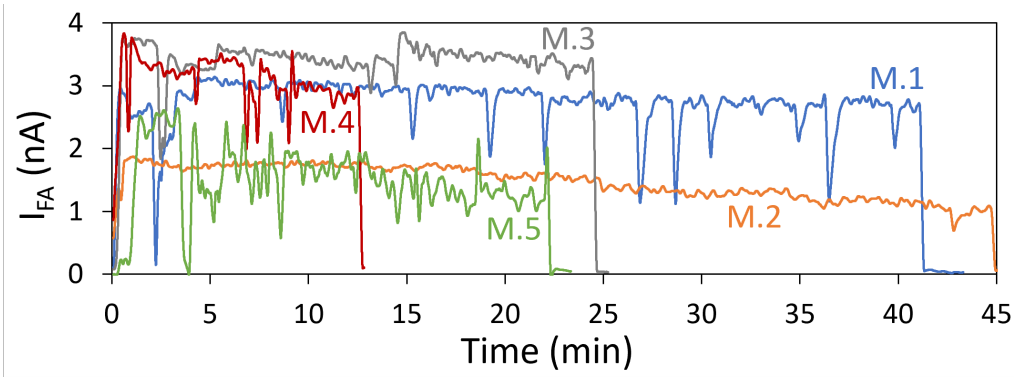

Figure 4.4. Faraday-cage electrometer signal I_{FA} corresponding to the residual current carried by the particles. Common parameters: V_{ES} = 2.3 kV, V_R = 0.9 kV, h = 1.7 mm, v_{tube} = 5.5 m/s, v_{coflow} = 70 mm/s. See Table 4.2 for additional information.

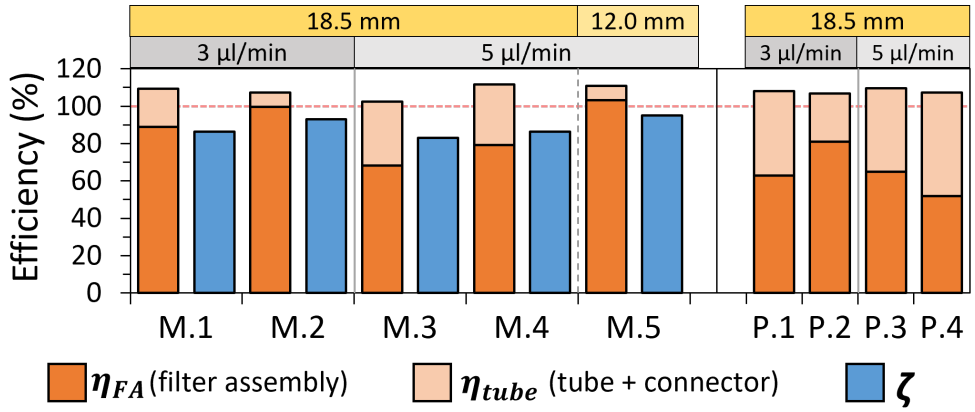

Figure 4.5. Efficiencies associated to the masses collected on the filter assembly η_{FA} (dark orange) and on the tube and connector η_{tube} (light orange), discharge efficiency ζ (blue bars). Common parameters: V_{ES} = 2.3 kV, V_R = 0.9 kV, h = 1.7 mm, v_{tube} = 5.5 m/s, v_{coflow} = 70 mm/s. See Table 4.2 for additional information.

4.3.3 PS/MEK mass efficiencies (extraction versus filter collection)

Fig. 4.5 also shows mass collection efficiencies (orange bars) associated with the mass fractions collected on the extraction tube η_{tube} (tube and connector) and on the filter assembly η_{FA} (filter and holder), whose sum equals the extraction efficiency η (Eq. (4.2)). The filter assembly fraction was systematically larger when a metal filter holder was used, compared to plastic (for otherwise the same conditions). For the metal holder set, the highest two filter collection fractions were observed for conditions M.2 and M.5, which also had the highest discharge efficiencies ζ. At

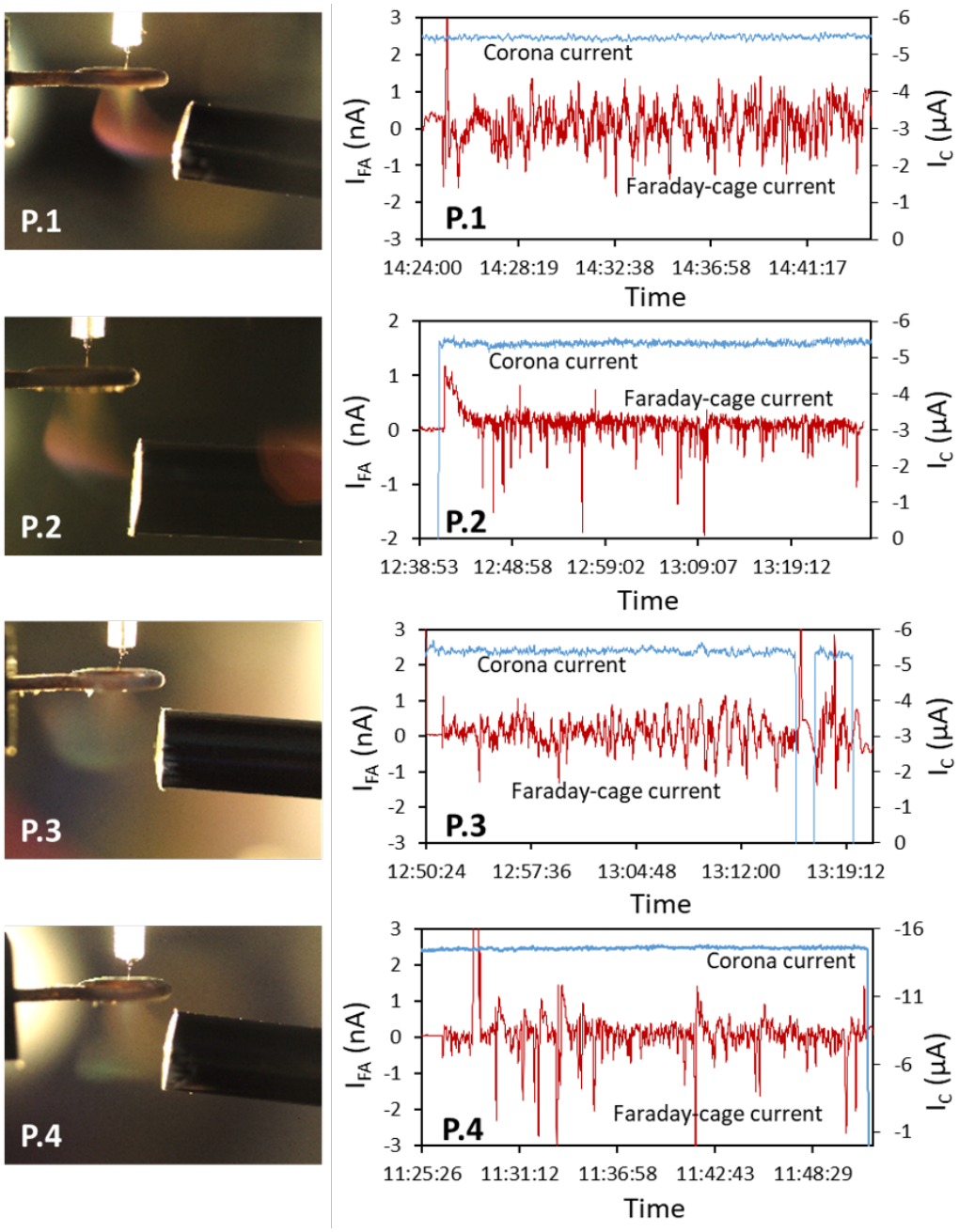

Figure 4.6. Electrospray neutralization when plastic filter holders were used. Left: Snapshots of the discharged ES plumes extractions. Right: Faraday-cage current of each run (P.x conditions).

the lowest flow rate, the filter collection efficiency depended on the extraction tube position. On increasing the flow rate from 3 to 5 μl/min, we observed a drop in the filter collection efficiency η_{FA}. This might be attributed to the difficulty of handling an increased spray current and wider spray plume. The filter efficiency increased dramatically when at 5 μl/min we reduced H (condition M.5), for which we think that the ionic and spray current fluxes are matched nearer to the droplet generation

zone (see earlier discussion).

The extraction efficiencies η were numerically higher than 100% (102 to 112%) for all the tested conditions. Ancillary tests indicate as most probable cause the absorption of solvent traces in the polymer matrix of the collected particles. Regardless, the important overall conclusion from these data is that the extraction efficiencies η were near 100% in all cases, consistently with the entering of the whole aerosol into the extraction tube observed (Fig. 4.2), and with the high discharging ζ (subsection 4.3.2).

4.3.4 Morphologies of the particles collected on filters from PS/MEK sprays

The characteristics of the particle residues observed by SEM reflects whether the droplets suffered the first Coulombic instability (CI) before it is prevented by the strength of the polymer shell forming by solvent drying (Bodnár et al., 2018). First, we imaged the particle residues by SEM to show that in the absence of ions the droplets underwent CI. These are shown in Fig. 4.7, in panels Si.1 and Si.2, corresponding to collections on Si wafers at flow rates of 3 and 5 μl/min. In both cases, filamented main particles and progeny particles were the predominant, structures, revealing CIs (Almería et al., 2010; Bodnár et al., 2018). This finding agrees with our previous work with this solution composition (made with even the same polymer batch) albeit for slightly lower Q of 2 μl/min (Bodnár, 2016).

When the electrospray at 3 μl/min was exposed to the corona ions, particles with globular morphology were instead collected on the filter, as shown in panel M.1 in Fig. 4.7. On the other hand, similar ion conditions were not as effective on the 5 μl/min spray as shown by the significant fraction of filamentous particles in panel M.3. Although this means that the droplets for this case suffered Coulombic instability, the low residual current, the high discharging efficiency, and the large collection efficiency shown in Fig. 4.5 (M.3) prove that the electrospray droplets still picked up a significant ionic current. On raising the corona current to -14 μA (M.4) (from -5.5 μA at condition M.3) the particles' morphologies did not vary appreciably

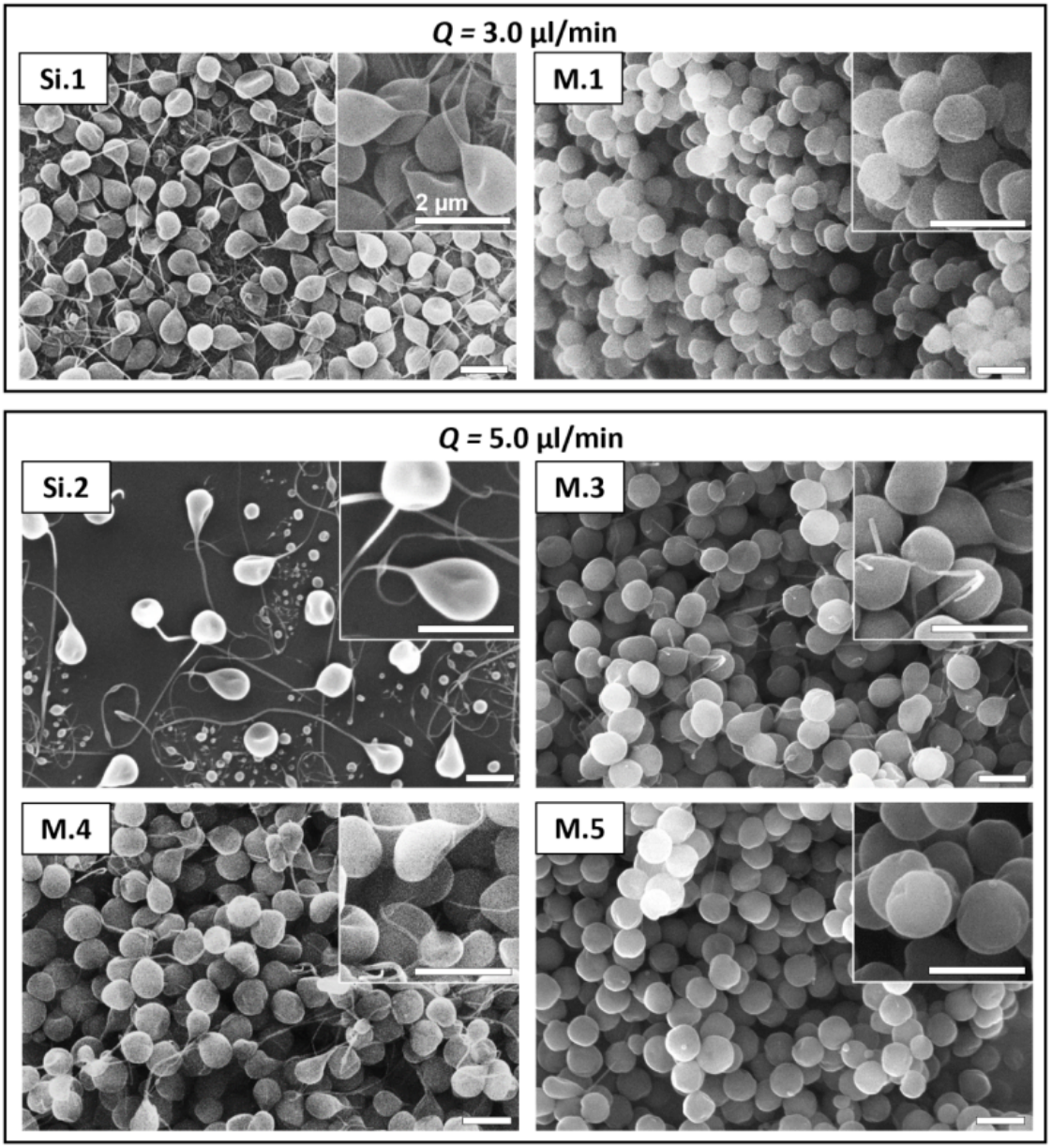

Figure 4.7. Comparison of morphology and sizes of PS particles made from 3PS-MEK solution which were collected either on Si wafer, without corona ions, (conditions Si.1 and Si.2) or on a filter, with corona ions present (conditions M.x, Table 4.2). Electrode configuration with $h = 1.7$ mm, $H = 18.5$ mm except for M.5 ($H = 12.0$ mm). The filters were housed in the metal holder. All scale bars: 2 μm.

from condition M.3. This is clearly consistent with the fact, shown earlier in Fig 3.4, that the current injected into the spray does not change much with corona current. Therefore, the neutralizing capacity of the ions was not significantly improved when the corona current was increased.

On the other hand, when the distance H between the ion source and the ring elec-

trode was decreased to 12.0 mm in condition M.5 (from 18.5 mm in M.4), spheroidal particles without filaments were collected (Fig. 4.7). This reveals that the droplets were electrically discharged early enough to prevent the first Coulombic instability. This finding is consistent with the images of the spray in Fig. 4.2, which show that the reduction in H between conditions M.4 and M.5 resulted in a significant narrowing of the spray plume and, probably, an upstream shifting of the discharging zone (as argued earlier).

Importantly, the addition of corona ions to the spray did not apparently change the sizes of the particles (comparing Si.x and M.x conditions in Fig. 4.7). This proves that the ions did not interfere with the jet formation process. At least, the jet diameter at the jet breakup position did not change appreciably, because the particle size remains approximately the same. However, the electrical current at the ES capillary increased when the ions were introduced (from I_{ES} to I_{ES}^{*} as shown in Table 4.2). This has been seen for many conditions. The current increase could be due to (i) ions reaching the Taylor cone, or (ii) ions reducing the space charge of the spray cloud (the net charge due to the ion and the spray clouds), thus increasing the electrical field at the Taylor cone and the current (partially offset by the down-adjustment of voltage explained in our protocol in pg. 71). Regardless, the fluid dynamics of the jet formation was not perturbed by the ions enough to change the jet width at breakup. If it had, a change would probably have been seen in the particle size between the Si-wafer and filter particle collections of Fig. 4.7.

The previous argument assumes the known fact that the length of jet transforming into a single droplet (the jet breakup wavelength) is fairly insensitive to how much electrical charge it carries (which would decrease if ions hit the jet) (Gamero-Castaño and Hruby, 2002). Nonetheless, the arrival of ions to the jet cannot be ruled out just from the insensitivity of particle size to them. This is due to two opposing tendencies. On the one hand, a significant deposition of ions on the jet near its breakup region would lower the net electrical surface charge, thus reducing the normal electrical stresses that oppose the surface tension stresses. As a consequence, the jet breakup process would be accelerated, happening "earlier", i.e., further upstream (as demonstrated with electrospinning jets by Fong et al. (1999); see also Saville (1971)). This would cause the breakup of the jet in a region where it is thicker, thus resulting

in slightly bigger particles. On the other hand, ions reaching the jet (and the spray) would also reduce the net charge on the jet (and the spray). Therefore, the electrical potential would be lowered at the site of ion arrival, thus intensifying the axial component of the electrical field, which is responsible for accelerating the charged jet. Therefore, its thinning rate would be increased, resulting in a thinner jet. Understanding the relative importance of these two tendencies is beyond the scope of this work. Nonetheless, we can conclude that if ions landed on the jet in our experiments, they did not appreciably affect the size of the jet at its breakup point.

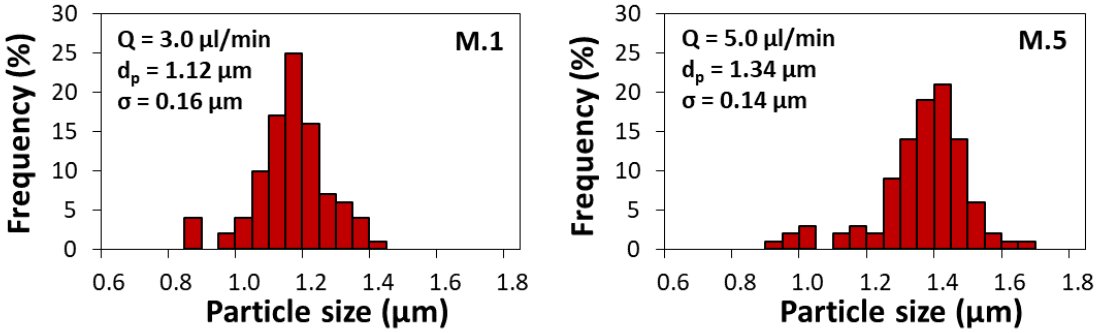

Figure 4.8. Particle diameter histograms from 100 particles (each) for the two conditions leading to filament-free particles (M.1 and M.5), where d_p = mean diameter, and σ = standard deviation.

Fig. 4.8 shows the particle size histograms of the particles collected on filters for the cases leading to globular (filament-free) particles: M.1 and M.5. The particles were uniformly sized and shaped at these conditions. Particle diameter count means increased slightly with flow rate from 1.12 μm at 3 μl/min (M.1) to 1.34 μm at 5 μl/min (M.5), while the standard deviations were similar. This increase in particle size with flow rate reflects the "scaling-law" dependence of droplet size with flow rate for which particle volume varies approximately linearly with solution flow rate (Rosell-Llompart et al., 2018).

Although most of the particles were collected on the filters (Fig. 4.9a), some of them landed on the inside of the filter holder cap (Fig. 4.9b), and for selected conditions (M.1, M.3, M.5) we inspected them by SEM, finding that a significant fraction of the particles had filaments. This may indicate that such particles either initially carried more charge or were not as efficiently discharged as those landing on the filter. SEM images of the particles deposited on the filter holder are shown in Fig.

4.10.

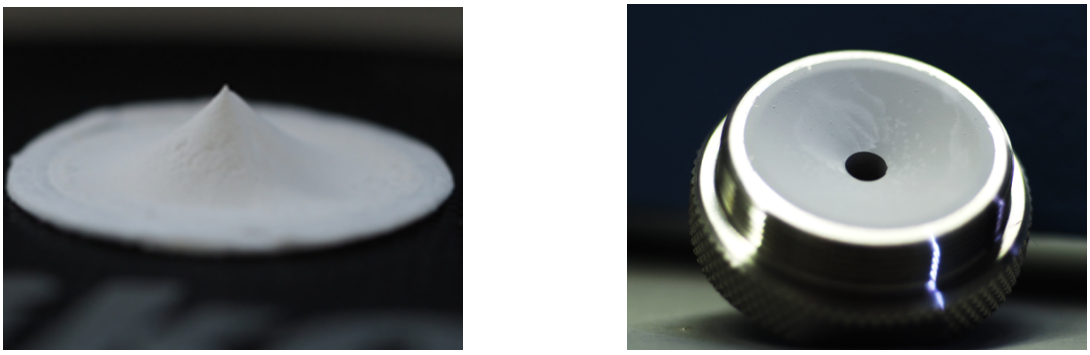

(a) Particle deposit **(b)** Metallic filter holder

Figure 4.9. Examples of particle collections on a 13 mm filter (a) and on metallic filter holder (25 mm) (b).

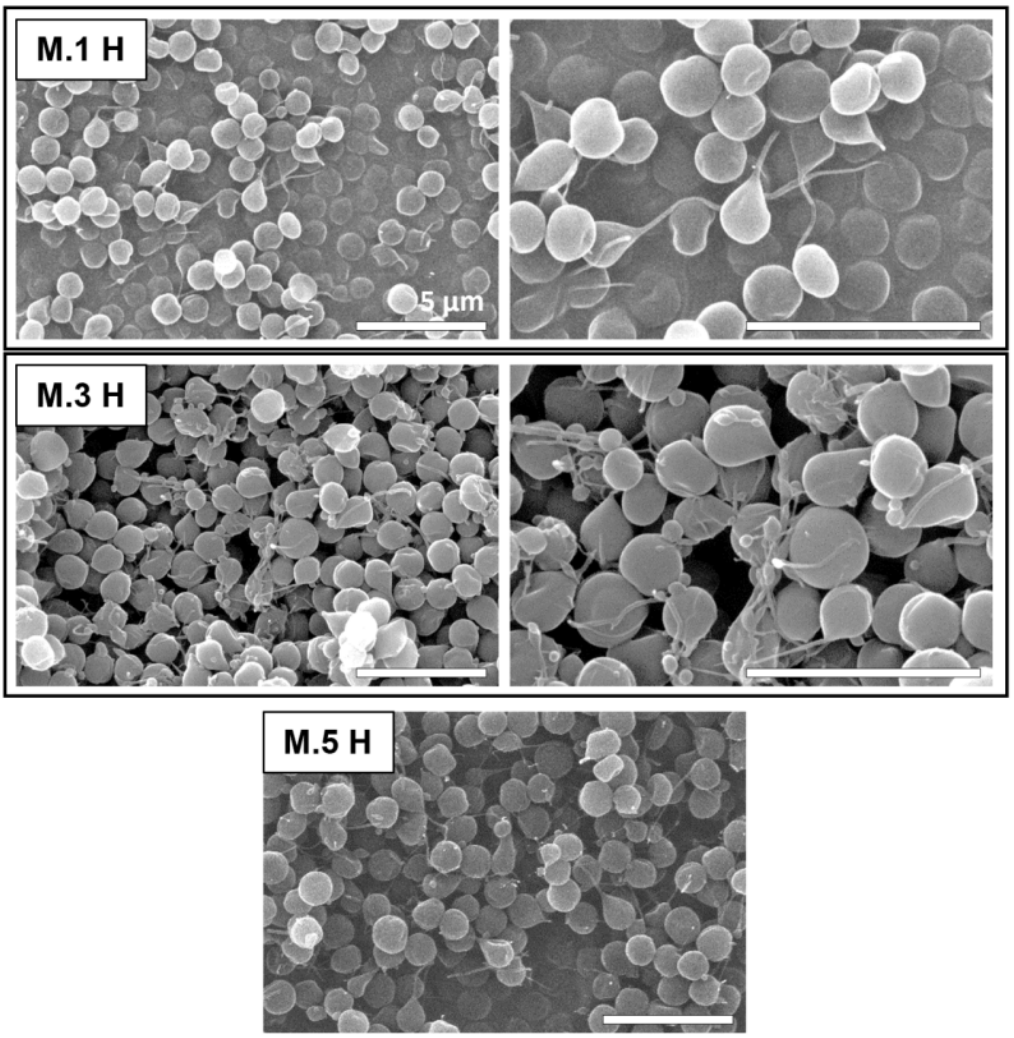

Figure 4.10. Representative SEM images of particles deposited on the metal holder inlet for conditions M.1, M.3 & M.5, where some of them were carrying filaments from Coulomb explosions.

4.3.5 Curcumin-loaded PVP particles from discharged electrosprays

We have also applied this methodology to produce polymer-model drug particles made of polyvinylpyrrolidone (PVP) and curcumin (CUR), as a carrier-drug model. We chose a composition of 5% w/w PVP and 1% w/w CUR in ethanol/acetone (1:1 v/v) as this is a relatively dilute solution capable of producing small particles. Using $h = 1.2$ mm and $H = 17.0$ mm, we established the cone-jet mode (Fig. 4.11a) at a liquid flow rate of 1.0 μl/min with an electrospray current of 32 nA. The particles collected on Si wafer without ionic discharging were filamentous, as shown in Fig. 4.11c, whereas the particles on the filter after discharging were mostly globular, with a minor presence of filaments, as shown in Fig. 4.11d. The size distribution on the filter particles is monomodal and homogeneous, with count mean (Martin) diameter and standard deviation of 655 ± 143 nm (Fig. 4.11e). The collection efficiencies η in two independent experiments were 100% and 97%, where the filter assembly fractions η_{FA} were 90% and 76% for collection times of 64 and 44 min, respectively. The averaged value for the residual current was +3.0 nA in both cases, corresponding to discharging efficiencies ζ of 90% and 88%.

We performed an ancillary experiment at elevated ambient humidity of 43-53% RH (after lifting the chamber glass urn), using a solution of 5% w/w PVP and 0.1% w/w CUR in ethanol, at liquid flow rate $Q = 0.75$ μl/min, and with $h = 1.0$ mm and $H = 27.0$ mm. Without ions, on a Si wafer we collected submicrometric particles having mixed geometries: globular, spherical, or elongated (Fig. 4.12a). With ions, a 20 min filter collection resulted in similarly sized nearly spherical and monomodal nanoparticles (Fig. 4.12b), with a narrow particle size distribution with count mean and standard deviation of 430 ± 64 nm, shown in Fig. 4.12c. Just as seen before in the PS experiments (#4.3.4), here the ions did not change the size of the particles, so we conclude that the ions did not affect the jet breakup pattern. The electrospray current did not change when the ions were added during the low relative humidity experiments ($I^*_{ES} = I_{ES} = 32$ nA), while I_R went from 0 to –3 nA.

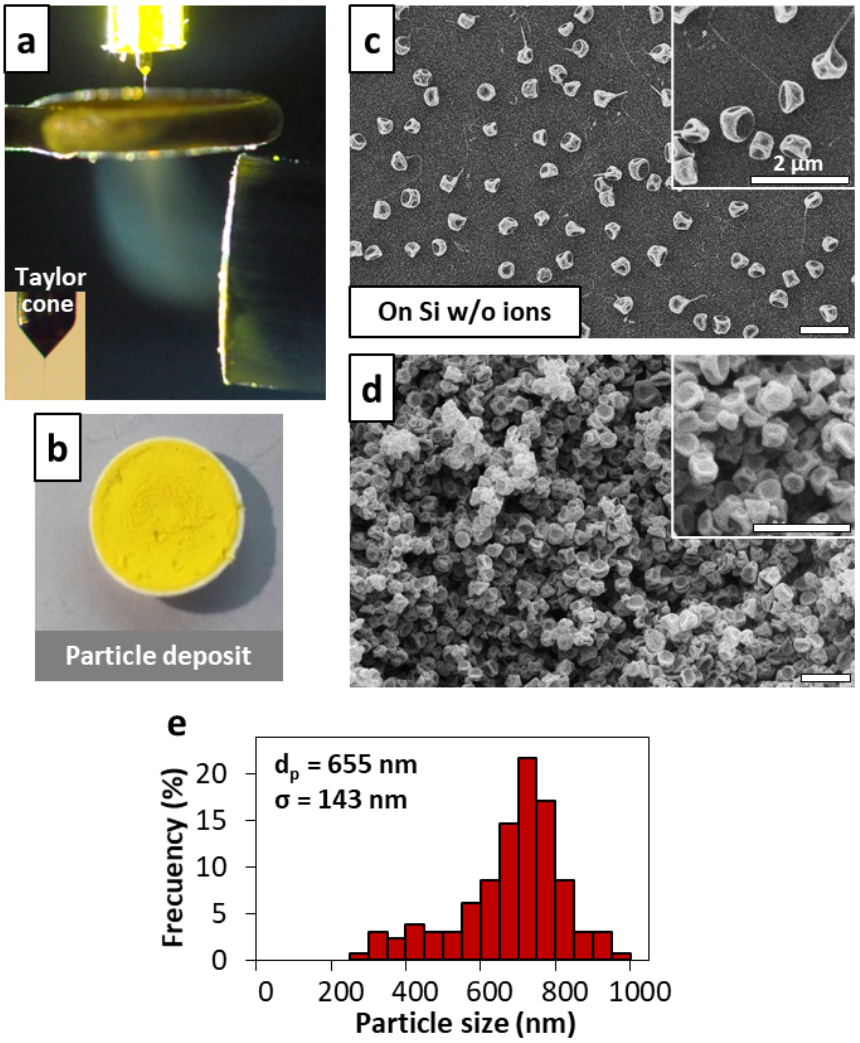

Figure 4.11. Morphology and sizes of particles made from PVP-curcumin solution 1CUR-5PVP. (a) Snapshot of a steady electrospray during discharging and extraction, inset showing the Taylor cone. (b) Example of particle deposit on filter (25 mm dia.). (c,d) SEM images of particles sprayed at Q = 1.0 μl/min, $RH < 2\%$, h = 1.2 mm, H = 17.0 mm, as collected on a Si wafer without ions (c) and on a filter (d). (e) Particle size histogram for (d) from 129 particles. d_p = particle mean diameter, σ = standard deviation. All scale bars: 2 μm.

4.3.6 Chitosan particles particles from discharged electrosprays

To check the robustness of this system, we have also tried to discharge the droplets of a more conductive electrosprayed solution, where the amount of ions must be increased to be capable of reduce the droplet charge and extract the resulting aerosol. Therefore, we have applied this methodology to produce polymer particles made of

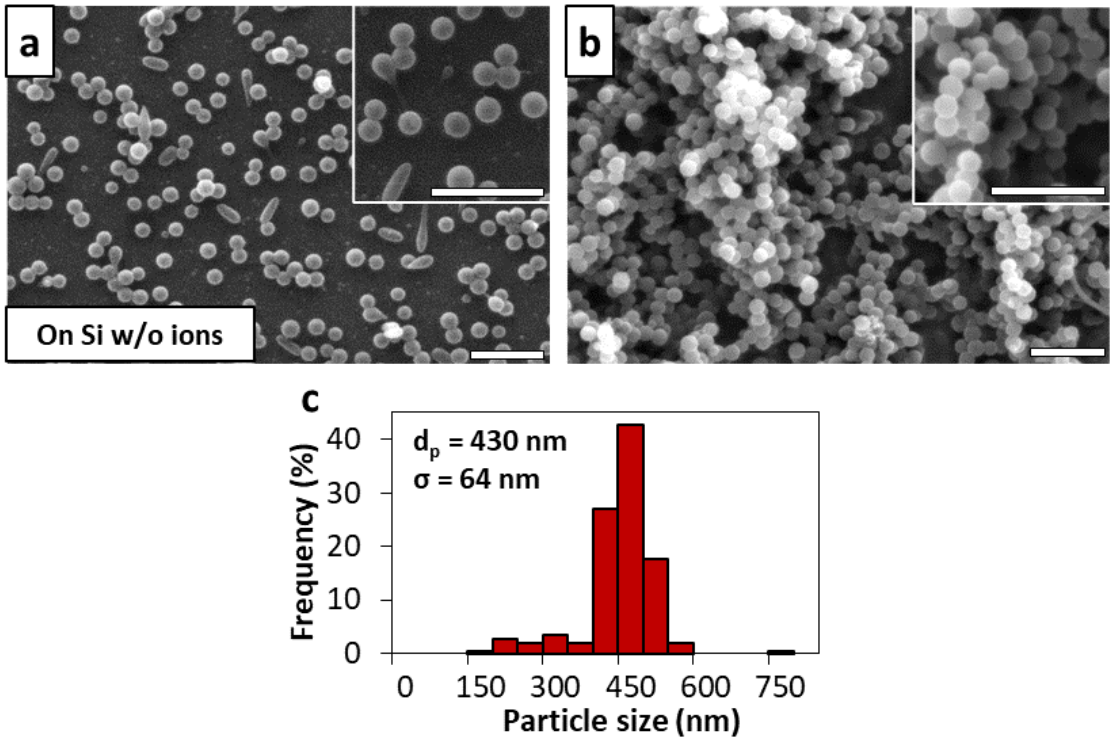

Figure 4.12. Morphology and sizes of particles made from PVP-curcumin solution 0.1CUR-5PVP. (a,b) SEM images of particles from solution 0.1CUR-5PVP sprayed at $Q = 0.75$ μl/min, $h = 1.0$ mm, $H = 27.0$ mm, $RH = 43\%$, as collected on Si wafer without ions (a) and on filter (b). (c) Particle size histogram for (b) from 300 particles. d_p = particle mean diameter, σ = standard deviation. All scale bars: 2 μm.

chitosan, a biodegradable and biocompatible polymer which has been used as a carrier in polymeric nanoparticles for drug delivery (Mohammed et al., 2017). We chose a composition of 2% w/w chitosan in ethanol:water:acetic acid (5:4:1 v/v) ethanol/acetone (1:1 v/v) as this solution is capable of producing smaller particles than previously due to a higher electrical conductivity. Using $h = 1.44$ mm and $H = 12.3$ mm, we established the cone-jet mode (Fig. 4.13) at a liquid flow rate of 0.8 μl/min, at $RH = 60$ %, which produced an electrospray current of 520 nA.

In this case, the particles collected on Si wafer without ionic discharging were globular (did not carry filaments), as shown in Fig. 4.14a, although the size distribution was not as narrow as in previous sections. The particles on the filter after discharging were globular as well, as shown in Fig. 4.14b, with a size of the main particles of 200-250 nm, where, as can be observed, the ion exposure did not change the particle size or morphology. The process was stable, with a collection time of 35 min where

we decided to stop the experiment. The averaged value for the residual current was +0.8 nA, corresponding to a discharging efficiency ζ close to 99%.

As a conclusion, we are able to reduce the charge of droplets from a chitosan solution electrospray with a high electrospray current ($I_{ES} = 520$ nA) and extract the aerosol with high efficiency and without distorting the particle morphology, expanding the possibilities of this methodology.

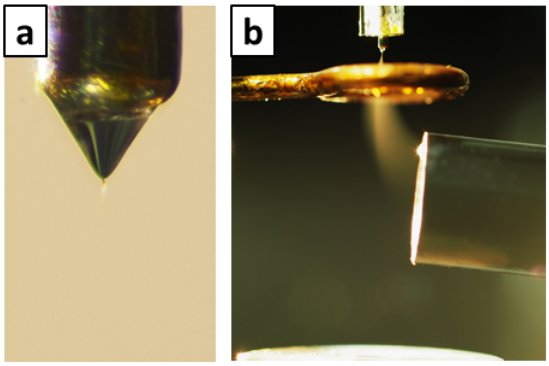

Figure 4.13. Neutralization and extraction of electrosprayed chitosan solution (2C10A50E). (a) Stable Taylor cone. (b) Snapshot of a steady electrospray during discharging and extraction. $Q = 0.8$ μl/min, $h = 1.0$ mm, $H = 27.0$ mm, $RH = 43\%$, $I_{ES} = 520$ nA.

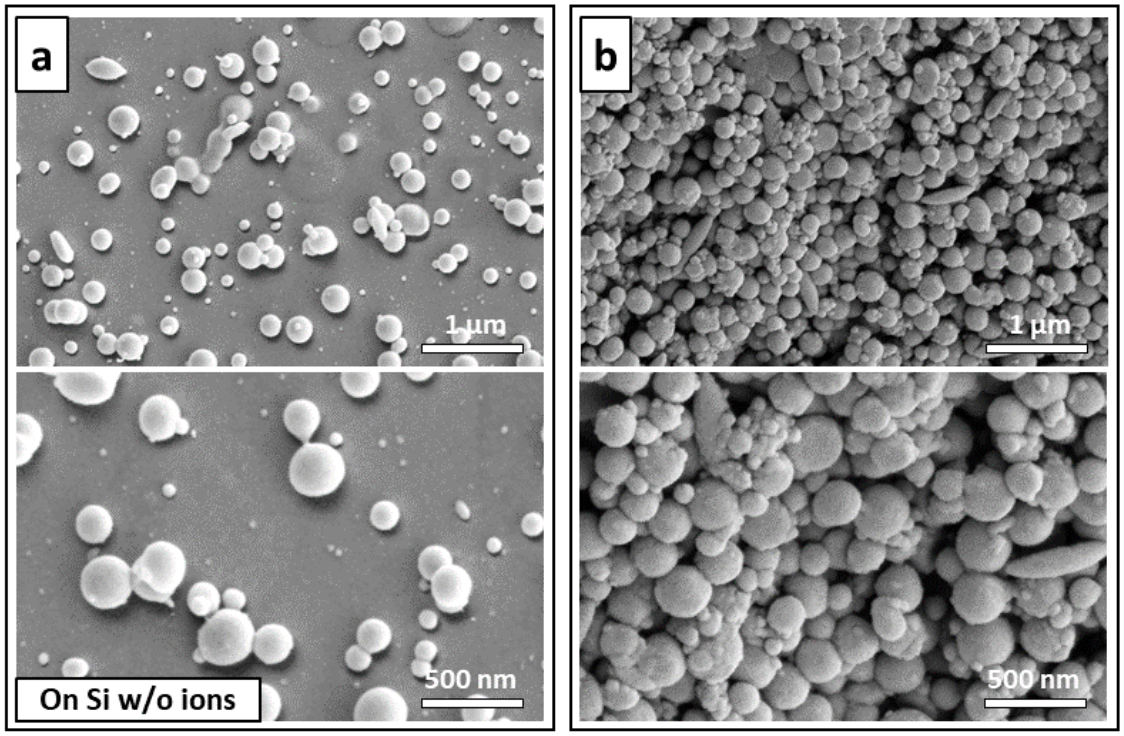

Figure 4.14. SEM images of particles made from solution 0.1CUR-5PVP sprayed at $Q = 0.8$ μl/min, $h = 1.0$ mm, $H = 27.0$ mm, $RH = 43\%$, $I_{ES} =$ 520 nA, as collected on Si wafer without ions (a) and on filter (b).

4.4 Conclusions

We demonstrate, for different cases of polymer solution electrosprays, a continuous process for the effective prevention of Coulombic instabilities in electrospray droplets' by reducing their charge in situ using opposite-polarity unipolar ions from a corona source. The discharged aerosol is then extracted orthogonally by an antistatic extraction tube, and dry particles are then collected on a filter where their residual electrical charge is continuously measured.

Stable electrospray discharging allowed the continuous extraction of the discharged droplets/particles into an antistatic tube with near 100% efficiency. The removal of particles by a proximal antistatic tube is critical to the stability of the process, as it prevents the charge reversal of the droplets with consequent migration toward the Taylor cone and/or agglomeration events with other particles.

We have found that the geometrical and electrostatic parameters are key to maximize droplet discharging and minimize droplet loss.

We found that the distance between the ring electrode and ion source controlled the location where the ions interacted with the droplets. Reducing this distance intensified the electric field, it increased ionic current flux near the axis (current/area), causing the upstream shift of the droplet discharging by the ions, and resulting in higher extraction efficiency, filter collection fraction, and more globular particles. Therefore, an ion stream with higher current flux seems capable of matching the spray current nearer to the Taylor cone, where it has a higher current flux as well. This finding is significant because it suggests that ultra-compact systems based on this principle could be developed.

For the fraction reaching the (metal) filter assembly, the electrical discharging is greater than 80%. The presence of residual electric charge on the extracted droplets/particles may explain why the mass on the filter is lower when a plastic filter holder is used than when a metal one is used (when electrical fields are weaker). The extracted aerosols had a significant residual charge (less than 20% the electrospray current). This suggests that dissimilar degrees of discharging are attained by droplets following different trajectories in the spray. Nonetheless, in future applications of this method, a small residual electrostatic charge on the extracted particles could be beneficial to prevent agglomeration in the aerosol phase.

Regarding particle size and shape, the discharging process did not affect the overall size of the electrospray particles (droplet residues), while greatly reducing the fraction of elongated/filamentous particles (which is a typical signature of Coulombic instabilities). Particle globularity was positively correlated with collection and discharging efficiencies. For the PS and PVP particles, the size distributions for the particles collected on the filters were monomodal and homogeneous, with small relative standard deviations (as small as 10.6%).

For the case of the chitosan particles, although there was no improvement in particle morphology, we still managed to successfully discharge and extract with high efficiency a polymer solution with an electrical conductivity three orders of magnitude higher than the previous ones, expanding the possibilities and making the system more robust.

In sum, the use of corona ions significantly expands the range of polymer concentra-

tions over which globular particles with monomodal size distribution can be made by electrospray. We hope that, in addition, the ability to transport the particles away from the electrospray region, will also inspire studies where the particles are subject to secondary in-line thermal or chemical post-processing of the particles in aerosol form.

— *Equipped with his five senses, man explores the universe around him and calls the adventure Science.*

Edwin Hubble

5

General Conclusions

In the second chapter, we have presented a purpose-made unipolar ion source device which has been characterized, obtainin different conclusions:

Regarding the corona discharge characteristics in a point-to-plane configuration, we have observed that by comparing two different gas compositions for the DC corona discharge, synthetic air and nitrogen, we have found that with air the system works much more stably than in the case of nitrogen. Although when using nitrogen the extracted ion current was significantly higher in our system, due to the need of operating in stable conditions for long periods of time, the best option was to use air. We have compared positive and negative corona discharge polarities, and only in the case of negative polarity we could produce a stable ion current for long periods of time, being the appropriate polarity for next experiments. The corona needle tip radius was also studied. Smaller radius generates more corona current at lower voltage, shifting the onset voltage to lower values.

Regarding the study of the extracted ion current through the ion source orifice we can conclude that:

It is possible to generate a stable ion flux which is adjustable with current similar to that of the typical electrospray current, by means of the presented unipolar ion source. The extracted ion current was adjusted by tuning the corona discharge current, although the sensitivity is not high. Higher extraction efficiencies were obtained at low corona current values, probably due to a weaker space charge. Moreover, the extracted ion current was adjusted over a wide current range by tuning the external electric field. In this case, higher extraction efficiencies were obtained at a higher external electric field. This conclusion was also reached with a configuration in which a covered ring as the counter electrode was used, being this

configuration more similar to an electrospray setup.

The orifice dimensions strongly affects the ion current extraction. The extracted ion current was higher, as the orifice diameter was increased, and as the orifice thickness was decreased. The extracted ion current is not affected by the flow rate of the corona discharge feeding gas (synthetic air) at low values (<60 ml/min). On the other hand, the corona discharge was unstable above ∼60 ml/min and below the corona onset voltage. Extracted ion current profiles revealed that the ion distribution is typically symmetrical with the maximum at the axis, as expected. An increase of the external electric field increased the ion density near the axis, whereas the profile tails were less affected. On the other hand, the gas velocity at the orifice did not affect the ion profile shape. Therefore, a low gas flow rate can be used to renew the gas environment near the corona needle tip.

Needle tip evolution: there exist a balance between the extracted current, and the stability of the needle tip shape, which, for the same material, strongly depends on the needle tip radius, suggesting to preferentially use larger tip radius values which, even though provide less extracted current, would preserve the stability of the process. For the case of the 15-μm radius tungsten needle, the shape of the tip did not change considerably over time, demonstrating the high durability of this tungsten needle.

In the second chapter, we have demonstrated a continuous process for the effective reduction of the electrospray droplets' charge in situ using opposite-polarity unipolar ions from a corona source. In our design a fraction of the current produced in a negative corona discharge is introduced axially into the electrospray, approximately matching the electrospray current. The discharged aerosol is then extracted orthogonally by an antistatic extraction tube, and the droplets are then collected on a filter. Electrospraying in capillary-ring configuration allows us to stabilize the spraying process independently from the presence of ions. Meanwhile, the spray-ions interactions are controlled mainly by the voltage difference between the ring electrode and the ion source. Droplet flyback towards the ring can be prevented robustly over a wide range of ring voltages.

Stable electrospray discharging allowed the continuous extraction of the discharged

droplets into an antistatic tube with high efficiency. The removal of droplets by a proximal antistatic tube is critical to the stability of the process, as it prevents the charge reversal of the droplets with consequent migration toward the Taylor cone and/or collision events with other droplets.

We have found that the geometrical and electrostatic parameters are key to maximize droplet discharging and minimize droplet loss.

We found that the distance between the ring electrode and ion source controlled the location where the ions interacted with the droplets.

In the third chapter, we have demonstrated a continuous process for the effective prevention of Coulombic instabilities in electrospray droplets' by reducing their charge in situ using opposite-polarity unipolar ions from a corona source. The discharged aerosol is then extracted orthogonally by an antistatic extraction tube, and dry particles are then collected on a filter where their residual electrical charge is continuously measured. Stable electrospray discharging allowed the continuous extraction of the discharged droplets/particles into an antistatic tube with near 100% efficiency. The removal of particles by a proximal antistatic tube is critical to the stability of the process, as it prevents the charge reversal of the droplets with consequent migration toward the Taylor cone and/or agglomeration events with other particles. Reducing this distance intensified the electric field, it increased ionic current flux near the axis (current/area), causing the upstream shift of the droplet discharging by the ions, and resulting in higher extraction efficiency, filter collection fraction, and more globular particles. Therefore, an ion stream with higher current flux seems capable of matching the spray current nearer to the Taylor cone, where it has a higher current flux as well. This finding is significant because it suggests that ultra-compact systems based on this principle could be developed.

For the fraction reaching the (metal) filter assembly, the electrical discharging is greater than 80%. The presence of residual electric charge on the extracted droplets and/or particles may explain why the mass on the filter is lower when a plastic filter holder is used than when a metal one is used (when electrical fields are weaker). The extracted aerosols had a significant residual charge (less than 20% the electrospray current). This suggests that dissimilar degrees of discharging are attained by

droplets following different trajectories in the spray. Nonetheless, in future applications of this method, a small residual electrostatic charge on the extracted particles could be beneficial to prevent agglomeration in the aerosol phase.

Regarding particle size and shape, the discharging process did not affect the overall size of the electrospray particles (droplet residues), while greatly reducing the fraction of elongated/filamentous particles (which is a typical signature of Coulombic instabilities). Particle globularity was positively correlated with collection and discharging efficiencies. The size distributions for the particles collected on the filters were monomodal and homogeneous, with small relative standard deviations (as small as 10.6%).

In sum, the use of corona ions significantly expands the range of polymer concentrations over which globular particles with monomodal size distribution can be made by electrospray. We hope that, in addition, the ability to transport the particles away from the electrospray region, will also inspire studies where the particles are subject to secondary in-line thermal or chemical post-processing of the particles in aerosol form.

Bibliography

Achtzehn, T., Müller, R., Duft, D., and Leisner, T. (2005). The Coulomb instability of charged microdroplets: dynamics and scaling. *The European Physical Journal D - Atomic, Molecular, Optical and Plasma Physics*, 34(1):311–313.

Adachi, M., Okuyama, K., and Kousaka, Y. (1983). Electrical neutralization of charged aerosol particles by bipolar ions. *Journal of Chemical Engineering of Japan*, 16(3):229–235.

Adachi, M., Pui, D. Y., and Liu, B. Y. (1993). Aerosol charge neutralization by a corona ionizer. *Aerosol science and technology*, 18(1):48–58.

Adali, M. B., Barresi, A. A., Boccardo, G., and Pisano, R. (2020). Spray Freeze-Drying as a Solution to Continuous Manufacturing of Pharmaceutical Products in Bulk. *Processes*, 8(6).

Adamiak, K. and Atten, P. (2004). Simulation of corona discharge in point-plane configuration. *Journal of Electrostatics*, 61(2):85–98.

Alexander, M. S., Stark, J., Smith, K. L., Stevens, B., and Kent, B. (2006). Electrospray Performance of Microfabricated Colloid Thruster Arrays. *Journal of Propulsion and Power*, 22(3):620–627.

Ali, A., Zaman, A., Sayed, E., Evans, D., Morgan, S., Samwell, C., Hall, J., Sohail Arshad, M., Simgh, N., Qutachi, O., Chang, M.-W., and Ahmad, Z. (2021). Electrohydrodynamic Atomisation Driven Design and Engineering of Opportunistic

Particulate Systems For Applications in Drug Delivery, Therapeutics and Pharmaceutics. *Advanced Drug Delivery Reviews*.

Almería, B., Deng, W., Fahmy, T. M., and Gomez, A. (2010). Controlling the morphology of electrospray-generated PLGA microparticles for drug delivery. *Journal of Colloid and Interface Science*, 343(1):125–133.

Almería, B., Fahmy, T. M., and Gomez, A. (2011). A multiplexed electrospray process for single-step synthesis of stabilized polymer particles for drug delivery. *Journal of Controlled Release*, 154(2):203–210.

Almería, B. and Gomez, A. (2014). Electrospray synthesis of monodisperse polymer particles in a broad (60nm-2μm) diameter range: Guiding principles and formulation recipes. *Journal of Colloid and Interface Science*, 417:121–130.

Altmann, K., Schulze, R. D., and Friedrich, J. (2014). Polymer deposition morphology by electrospray deposition - Modifications through distance variation. *Thin Solid Films*, 564:269–276.

Anderson, D. S., Sydor, M., Fletcher, P., and Holian, A. (2016). Nanotechnology: The risks and benefits for medical diagnosis and treatment. *J. Nanomed. Nanotechnol*, 7(4):e143.

Artiga, Á., Ramos-Sánchez, F., Serrano-Sevilla, I., De Matteis, L., Mitchell, S. G., Sánchez-Somolinos, C., and de la Fuente, J. M. (2020). Inkjet-Based Technology for Microencapsulation of Gold Nanoparticles within Biocompatible Hydrogels. *Particle and Particle Systems Characterization*, 37(4).

Arumugham-Achari, A. K., Grifoll, J., and Rosell-Llompart, J. (2013). Two-way coupled numerical simulation of electrospray with induced gas flow. *Journal of Aerosol Science*, 65:121–133.

Bae, S. B., Nam, H. C., and Park, W. H. (2019). Electrospraying of environmentally sustainable alginate microbeads for cosmetic additives. *International Journal of Biological Macromolecules*, 133:278–283.

Barrero, A. and Loscertales, I. G. (2007). Micro- and nanoparticles via capillary flows. *Annual Review of Fluid Mechanics*, 39(1):89–106.

Basak, S., Chen, D. R., and Biswas, P. (2007). Electrospray of ionic precursor solutions to synthesize iron oxide nanoparticles: Modified scaling law. *Chemical Engineering Science*, 62(4):1263–1268.

Bayda, S., Adeel, M., Tuccinardi, T., Cordani, M., and Rizzolio, F. (2020). The History of Nanoscience and Nanotechnology: From Chemical-Physical Applications to Nanomedicine. *Molecules*, 25(1):112.

Berkland, C., Kim, K. K., and Pack, D. W. (2001). Fabrication of PLG microspheres with precisely controlled and monodisperse size distributions. *Journal of Controlled Release*, 73(1):59–74.

Bilal, M. and Iqbal, H. M. N. (2020). New Insights on Unique Features and Role of Nanostructured Materials in Cosmetics. *Cosmetics*, 7(2):24.

Bisht, S., Mizuma, M., Feldmann, G., Ottenhof, N. A., Hong, S.-M., Pramanik, D., Chenna, V., Karikari, C., Sharma, R., Goggins, M. G., Rudek, M. A., Ravi, R., Maitra, A., and Maitra, A. (2010). Systemic Administration of Polymeric Nanoparticle-Encapsulated Curcumin (NanoCurc) Blocks Tumor Growth and Metastases in Preclinical Models of Pancreatic Cancer. *Molecular Cancer Therapeutics*, 9(8):2255 LP – 2264.

Bober, D. B. and Chen, C.-H. (2011). Pulsating electrohydrodynamic cone-jets: from choked jet to oscillating cone. *Journal of Fluid Mechanics*, 689:552–563.

Bocanegra, R., Galán, D., Márquez, M., Loscertales, I. G., and Barrero, A. (2005). Multiple electrosprays emitted from an array of holes. *Journal of Aerosol Science*, 36(12):1387–1399.

Bock, N., Dargaville, T. R., and Woodruff, M. A. (2012). Electrospraying of polymers with therapeutic molecules: State of the art. *Progress in Polymer Science*, 37(11):1510–1551.

Boda, S. K., Li, X., and Xie, J. (2018). Electrospraying an enabling technology for pharmaceutical and biomedical applications: A review. *Journal of Aerosol Science*, 125:164–181.

Bodnár, E. (2016). *Electrospraying of polymer solutions for the generation of microparticles, nanostructures, and granular films.* PhD thesis, Universitat Rovira i Virgili.

Bodnár, E., Grifoll, J., and Rosell-Llompart, J. (2018). Polymer solution electrospraying: A tool for engineering particles and films with controlled morphology. *Journal of Aerosol Science*, 125:93–118.

Bodnár, E. and Rosell-Llompart, J. (2013). Growth dynamics of granular films produced by electrospray. *Journal of Colloid and Interface Science*, 407:536–545.

Boel, E., Koekoekx, R., Dedroog, S., Babkin, I., Vetrano, M. R., Clasen, C., and Van Den Mooter, G. (2020). Unraveling Particle Formation: From Single Droplet Drying to Spray Drying and Electrospraying. *Pharmaceutics*, 12(7):625.

Bornschein, R. E. and Ruotolo, B. T. (2015). Ion mobility-mass spectrometry of charge-reduced protein complexes reveals general trends in the collisional ejection of compact subunits. *Analyst*, 140(20):7020–7029.

Borra, J. P., Camelot, D., Chou, K. L., Kooyman, P. J., Marijnissen, J. C. M., and Scarlett, B. (1999). Bipolar coagulation for powder production: Micro-mixing inside droplets. *Journal of Aerosol Science*, 30(7):945–958.

Brito de Souza, V., Thomazini, M., Chaves, I. E., Ferro-Furtado, R., and Favaro-Trindade, C. S. (2020). Microencapsulation by complex coacervation as a tool to protect bioactive compounds and to reduce astringency and strong flavor of vegetable extracts. *Food Hydrocolloids*, 98:105244.

Brodie, I. (1975). Bombardment of field-emission cathodes by positive ions formed in the interelectrode region. *International Journal of Electronics*, 38(4):541–550.

Burtscher, H. (1992). Measurement and characteristics of combustion aerosols with special consideration of photoelectric charging and charging by flame ions. *Journal of Aerosol Science*, 23(6):549–595.

Burtscher, H., Scherrer, L., Siegmann, H. C., Schmidt-Ott, A., and Federer, B. (1982). Probing aerosols by photoelectric charging. *Journal of Applied Physics*, 53(5):3787–3791.

Calzoni, E., Cesaretti, A., Polchi, A., Di Michele, A., Tancini, B., and Emiliani, C. (2019). Biocompatible Polymer Nanoparticles for Drug Delivery Applications in Cancer and Neurodegenerative Disorder Therapies.

Camelot, D., Marijnissen, J. C. M., and Scarlett, B. (1999). Bipolar coagulation process for the production of powders. *Industrial & Engineering Chemistry Research*, 38(3):631–638.

Campuzano, I. D. G. and Schnier, P. D. (2013). Coupling electrospray corona discharge, charge reduction and ion mobility mass spectrometry: From peptides to large macromolecular protein complexes. *International Journal for Ion Mobility Spectrometry*, 16(1):51–60.

Carrasco-Munoz, A., Barbero-Colmenar, E., Bodnár, E., Grifoll, J., and Rosell-Llompart, J. (2021). Monodisperse droplets and particles by efficient neutralization of electrosprays. *Journal of Aerosol Science*, page 105909.

Castillo, J. L., Martin, S., Rodriguez-Perez, D., Higuera, F. J., and Garcia-Ybarra, P. L. (2018). Nanostructured porous coatings via electrospray atomization and deposition of nanoparticle suspensions. *Journal of Aerosol Science*, 125:148–163.

Cejková, J., Stepánek, F., Cejkova, J., and Stepanek, F. (2013). Compartmentalized and internally structured particles for drug delivery - a review. *Current Pharmaceutical Design*, 19(35):6298–6314.

Chang, J.-S., Lawless, P. A., and Yamamoto, T. (1992). Corona discharge processes. *IEEE Transactions on Plasma Science*, 19(6):1152–1166.

Chen, D.-R. and Pui, D. Y. H. (1997). Experimental investigation of scaling laws for electrospraying: dielectric constant effect. *Aerosol Science and Technology*, 27(3):367–380.

Chen, D.-R. and Pui, D. Y. H. (2010). *Electrospray and its medical applications*. Springer Netherlands, Dordrecht.

Chen, D. R., Pui, D. Y. H., and Kaufman, S. L. (1995). Electrospraying of conducting liquids for monodisperse aerosol generation in the 4 nm to 1.8 μm diameter range. *Journal of Aerosol Science*, 26(6):963–977.

Cheng, Y. S., Yeh, H. C., and Kanapilly, G. M. (1981). Collection efficiencies of a point-to-plane electrostatic precipitator. *American Industrial Hygiene Association Journal*, 42(8):605–610.

Ciach, T. (2006). Microencapsulation of drugs by electro-hydro-dynamic atomization. *International Journal of Pharmaceutics*, 324(1):51–55.

Ciach, T. (2007). Application of electro-hydro-dynamic atomization in drug delivery. *Journal of Drug Delivery Science and Technology*, 17(6):367–375.

Cloupeau, M. (1994). Recipes for use of EHD spraying in cone-jet mode and notes on corona discharge effects. *Journal of Aerosol Science*, 25(6):1143–1157.

Cloupeau, M. and Prunet-Foch, B. (1989). Electrostatic spraying of liquids in cone-jet mode. *Journal of Electrostatics*, 22(2):135–159.

Cloupeau, M. and Prunet-Foch, B. (1990). Electrostatic spraying of liquids: Main functioning modes. *Journal of Electrostatics*, 25(2):165–184.

Conangla, G. P., Rica, R. A., and Quidant, R. (2020). Extending Vacuum Trapping to Absorbing Objects with Hybrid Paul-Optical Traps. *Nano Letters*, 20(8):6018–6023.

Cooper, D. W. and Reist, P. C. (1973). Neutralizing charged aerosols with radioactive sources. *Journal of Colloid and Interface Science*, 45(1):17–26.

Cun, D., Zhang, C., Bera, H., and Yang, M. (2021). Particle engineering principles and technologies for pharmaceutical biologics. *Advanced Drug Delivery Reviews*, 174:140–167.

Dai, Q., Bertleff-Zieschang, N., Braunger, J. A., Bjornmalm, M., Cortez-Jugo, C., and Caruso, F. (2018). Particle Targeting in Complex Biological Media. *Advanced Healthcare Materials*, 7(1).

Dandavino, S., Ataman, C., Ryan, C. N., Chakraborty, S., Courtney, D., Stark, J. P. W., and Shea, H. (2014). Microfabricated electrospray emitter arrays with integrated extractor and accelerator electrodes for the propulsion of small spacecraft. *Journal of Micromechanics and Microengineering*, 24(7):75011.

Dau, V. T., Nguyen, T. K., and Dao, D. V. (2020). Charge reduced nanoparticles by sub-kHz ac electrohydrodynamic atomization toward drug delivery applications. *Applied Physics Letters*, 116(2):023703.

Davies, L. A., Hannavy, K., Davies, N., Pirrie, A., Coffee, R. A., Hyde, S. C., and Gill, D. R. (2005). Electrohydrodynamic Comminution: A Novel Technique for the Aerosolisation of Plasmid DNA. *Pharmaceutical Research*, 22(8):1294–1304.

Davis, E. J. (1997). A History of Single Aerosol Particle Levitation. *Aerosol Science and Technology*, 26(3):212–254.

Davis, E. J. and Bridges, M. A. (1994). The Rayleigh limit of charge revisited: light scattering from exploding droplets. *Journal of Aerosol Science*, 25(6):1179–1199.

Deng, W. and Gomez, A. (2007). Influence of space charge on the scale-up of multiplexed electrosprays. *Journal of Aerosol Science*, 38(10):1062–1078.

Deng, W., Klemic, J. F., Li, X., Reed, M. A., and Gomez, A. (2006). Increase of electrospray throughput using multiplexed microfabricated sources for the scalable generation of monodisperse droplets. *Journal of Aerosol Science*, 37(6):696–714.

Dhaniyala, S., Fierz, M., Keskinen, J., and Marjamäki, M. (2011). Instruments Based on Electrical Detection of Aerosols. In *Aerosol Measurement*, chapter 18, pages 393–416. John Wiley & Sons, Ltd.

Dhiman, S., Yadav, A., Debnath, N., and Das, S. (2021). Application of Core/Shell Nanoparticles in Smart Farming: A Paradigm Shift for Making the Agriculture Sector More Sustainable. *Journal of Agricultural and Food Chemistry*, 69(11):3267–3283.

Dima, C., Assadpour, E., Dima, S., and Jafari, S. M. (2020). Bioavailability of nutraceuticals: Role of the food matrix, processing conditions, the gastrointestinal tract, and nanodelivery systems. *Comprehensive Reviews in Food Science and Food Safety*, 19(3):954–994.

Duft, D., Achtzehn, T., Müller, R., Huber, B. a., and Leisner, T. (2003). Coulomb fission: Rayleigh jets from levitated microdroplets. *Nature*, 421(6919):128.

Ebeling, D. D., Westphall, M. S., Scalf, M., and Smith, L. M. (2000). Corona Discharge in Charge Reduction Electrospray Mass Spectrometry. *Analytical Chemistry*, 72(21):5158–5161.

Ebeling, D. D., Westphall, M. S., Scalf, M., and Smith, L. M. (2001). A cylindrical capacitor ionization source: droplet generation and controlled charge reduction for mass spectrometry. *Rapid Communications in Mass Spectrometry*, 15(6):401–405.

Echegoyen, Y., Fabra, M. J., Castro-Mayorga, J. L., Cherpinski, A., and Lagaron, J. M. (2017). High throughput electro-hydrodynamic processing in food encapsulation and food packaging applications : Viewpoint. *Trends in Food Science & Technology*, 60:71–79.

Eggers, J. and Villermaux, E. (2008). Physics of liquid jets. *Reports on Progress in Physics*, 71(3):036601 (79pp).

Elsabahy, M. and Wooley, K. L. (2012). Design of polymeric nanoparticles for biomedical delivery applications. *Chemical Society Reviews*, 41(7):2545–2561.

Emami, F., Vatanara, A., Park, E. J., and Na, D. H. (2018). Drying Technologies for the Stability and Bioavailability of Biopharmaceuticals. *Pharmaceutics*, 10(3).

Fan, S., Kim, P. C., Lee, E. R., Lee, I. T., Perl, M. L., and Rogers, H. (2003). A device for precision neutralization of electric charge of small drops using ionized air. *Review of Scientific Instruments*, 74:4305–4309.

Fantini, D., Zanetti, M., and Costa, L. (2006). Polystyrene microspheres and nanospheres produced by electrospray. *Macromolecular Rapid Communications*, 27(23):2038–2042.

Faramarzi, A. R., Barzin, J., and Mobedi, H. (2016). Effect of solution and apparatus parameters on the morphology and size of electrosprayed PLGA microparticles. *Fibers and Polymers*, 17(11):1806–1819.

Fenn, J., Rosell, J., Nohmi, T., Shen, S., and Banks Jr., F. (1996). Electrospray ion formation: desorption versus desertion. In *ACS Symposium Series - Biochemical and Biotechnological Applications of Electrospray Ionization Mass Spectrometry*, volume 619, chapter 3, pages 60–80. American Chemical Society, first edition.

Fenn, J. B. (2003). Electrospray wings for molecular elephants (Nobel lecture). *Angewandte Chemie International Edition*, 42(33):3871–3894.

Fenn, J. B., Mann, M., Meng, C. K., Wong, S. F., and Whitehouse, C. M. (1989). Electrospray ionization for mass spectrometry of large biomolecules. *Science*, 246(4926):64–71.

Fernández de la Mora, J. (2007). The fluid dynamics of Taylor cones. *Annual Review of Fluid Mechanics*, 39(1):217–243.

Fernandez de la Mora, J. (2018). Mobility Analysis of Proteins by Charge Reduction in a Bipolar Electrospray Source. *Analytical Chemistry*, 90(20):12187–12190.

Fernandez de la Mora, J. and Barrios-Collado, C. (2017). A bipolar electrospray source of singly charged salt clusters of precisely controlled composition. *Aerosol Science and Technology*, 51(6):778–786.

Fernández de la Mora, J. and Loscertales, I. G. (1994). The current emitted by highly conducting Taylor cones. *Journal of Fluid Mechanics*, 260:155–184.

Feynman, R. P. (1960). There's Plenty of Room at the Bottom. *Engineering and Science*, 23(5):22–36.

Flagan, R. C. (2011). Electrical Mobility Methods for Submicrometer Particle Characterization. In *Aerosol Measurement*, chapter 15, pages 339–364. John Wiley & Sons, Ltd.

Flagan, R. C. and Seinfeld, J. H. (1988). *Fundamentals of Air Pollution Engineering*. Prentice-Hall, Inc., Englewood Cliffs, NJ.

Fong, H., Chun, I., and Reneker, D. H. (1999). Beaded nanofibers formed during electrospinning. *Polymer*, 40(16):4585–4592.

Forsyth, B., Liu, B. Y. H., and Romay, F. J. (1998). Particle Charge Distribution Measurement for Commonly Generated Laboratory Aerosols. *Aerosol Science and Technology*, 28(6):489–501.

Frey, B. L., Lin, Y., Westphall, M. S., and Smith, L. M. (2005). Controlling gas-phase reactions for efficient charge reduction electrospray mass spectrometry of intact

proteins. *Journal of the American Society for Mass Spectrometry*, 16(11):1876–1887.

Fu, H., Liu, Q., and Chen, D.-R. (2012). Performance study of a twin-head electrospray system. *Journal of Aerosol Science*, 52:33–44.

Fytianos, G., Rahdar, A., and Kyzas, G. Z. (2020). Nanomaterials in Cosmetics: Recent Updates. *Nanomaterials*, 10(5):979.

Gamero-Castaño, M. and Hruby, V. (2001). Electrospray as a source of nanoparticles for efficient colloid thrusters. *Journal of Propulsion and Power*, 17(5):977–987.

Gamero-Castaño, M. and Hruby, V. (2002). Electric measurements of charged sprays emitted by cone-jets. *Journal of Fluid Mechanics*, 459:245–276.

Gañán-Calvo, A. M. (1999). The surface charge in electrospraying: Its nature and its universal scaling laws. *Journal of Aerosol Science*, 30(7):863–872.

Gañán-Calvo, A. M. (2004). On the general scaling theory for electrospraying. *Journal of Fluid Mechanics*, 507:203–212.

Gañán-Calvo, A. M., Dávila, J., and Barrero, A. (1997). Current and droplet size in the electrospraying of liquids. Scaling laws. *Journal of Aerosol Science*, 28(2):249–275.

Gañán-Calvo, A. M., López-Herrera, J. M., Herrada, M. A., Ramos, A., and Montanero, J. M. (2018). Review on the physics of electrospray: From electrokinetics to the operating conditions of single and coaxial Taylor cone-jets, and AC electrospray. *Journal of Aerosol Science*, 125:32–56.

Gañán-Calvo, A. M. and Montanero, J. M. (2009). Revision of capillary cone-jet physics: Electrospray and flow focusing. *Physical Review E - Statistical, Nonlinear, and Soft Matter Physics*, 79(6):1–18.

Gañán-Calvo, A. M., Rebollo-Muñoz, N., and Montanero, J. M. (2013). The minimum or natural rate of flow and droplet size ejected by Taylor cone-jets: physical symmetries and scaling laws. *New Journal of Physics*, 15(3):033035.

Gassend, B., Velasquez-Garcia, L. F., Akinwande, A. I., and Martinez-Sanchez, M. (2009). A microfabricated planar electrospray array ionic liquid ion source with integrated extractor. *Journal of Microelectromechanical Systems*, 18(3):679–694.

Giorgiutti-Dauphiné, F. and Pauchard, L. (2018). Drying drops: Drying drops containing solutes: From hydrodynamical to mechanical instabilities. *European Physical Journal E*, 41(3).

Giubbilini, P. (1988). The current-voltage characteristics of point-to-ring corona. *Journal of Applied Physics*, 64(7):3730–3732.

Goldman, M., Goldman, A., and Sigmond, R. S. (1985). The corona discharge, its properties and specific uses. *Pure and Applied Chemistry*, 57(9):1353–1362.

Gomez, A. and Tang, K. (1994). Charge and fission of droplets in electrostatic sprays. *Physics of Fluids*, 6(1):404–414.

Gomez-Estaca, J., Balaguer, M. P., Gavara, R., and Hernandez-Munoz, P. (2012). Formation of zein nanoparticles by electrohydrodynamic atomization: Effect of the main processing variables and suitability for encapsulating the food coloring and active ingredient curcumin. *Food Hydrocolloids*, 28(1):82–91.

Gómez-Mascaraque, L. G., Tordera, F., Fabra, M. J., Martínez-Sanz, M., and Lopez-Rubio, A. (2019). Coaxial electrospraying of biopolymers as a strategy to improve protection of bioactive food ingredients. *Innovative Food Science and Emerging Technologies*, 51:2–11.

Grace, J. M. and Marijnissen, J. C. M. (1994). A review of liquid atomization by electrical means. *Journal of Aerosol Science*, 25(6):1005–1019.

Gulfam, M., Kim, J.-e., Lee, J. M., Ku, B., Chung, B. H., and Chung, B. G. (2012). Anticancer drug-loaded gliadin nanoparticles induce apoptosis in breast cancer cells. *Langmuir*, 28(21):8216–8223.

Hartman, R., Brunner, D., Camelot, D., Marijnissen, J., and Scarlett, B. (1999). Electrohydrodynamic atomization in the cone–jet mode physical modeling of the liquid cone and jet. *Journal of Aerosol Science*, 30(7):823–849.

Hartman, R., Brunner, D., Camelot, D., Marijnissen, J., and Scarlett, B. (2000). Jet break-up in electrohydrodynamic atomization in the cone-jet mode. *Journal of Aerosol Science*, 31(1):65–95.

Hartman, R., Spijkers, S., Marijnissen, J., and Scarlett, B. (1995). The electrohydrodynamic atomization of liquids in the delft aerosol generator. *Journal of Aerosol Science*, 26:S181–S182. Abstracts of the 1995 European Aerosol Conference.

Higuera, F. J. (2012). Eulerian model of a dilute spray of charged droplets. *Journal of Aerosol Science*, 48:34–45.

Higuera, F. J. (2016). Neutralization of a spray of electrically charged droplets by a corona discharge. *Journal of Fluid Mechanics*, 801:130–149.

Higuera, J. F. (2009). Charge separation in the conical meniscus of an electrospray of a very polar liquid: Its effect on the minimum flow rate. *Physics of Fluids*, 21(3):032104 (11pp).

Hijano, A. J., Loscertales, I. G., Ibáñez, S. E., and Higuera, F. J. (2015). Periodic emission of droplets from an oscillating electrified meniscus of a low-viscosity, highly conductive liquid. *Physical Review E - Statistical, Nonlinear, and Soft Matter Physics*, 91(1):013011 (12pp).

Hill, E. K. and Li, J. (2017). Current and future prospects for nanotechnology in animal production. *Journal of Animal Science and Biotechnology*, 8:26.

Hinds, W. C. (1999). *Aerosol technology: properties, behavior, and measurement of airborne particles*. Wiley-Interscience. Wiley.

Ho Lee, K., Ireland, M., Miller, B. L., Wyslouzil, B. E., and Winter, J. O. (2021). Synthesis of polymer nanoparticles via electrohydrodynamic emulsification-mediated self-assembly. *Journal of Colloid and Interface Science*, 586:445–456.

Hogan, C. J. and Biswas, P. (2008). Porous film deposition by electrohydrodynamic atomization of nanoparticle sols. *Aerosol Science and Technology*, 42(1):75–85.

Hogan, C. J., Yun, K. M., Chen, D. R., Lenggoro, I. W., Biswas, P., and Okuyama, K. (2007). Controlled size polymer particle production via electrohydrodynamic

atomization. *Colloids and Surfaces A: Physicochemical and Engineering Aspects*, 311(1-3):67–76.

Hogrefe, O., Drewnick, F., Lala, G. G., Schwab, J. J., and Demerjian, K. L. (2004). Development, operation and applications of an aerosol generation, calibration and research facility. *Aerosol Science and Technology*, 38(S1):196–214.

Hoyer, B., Sørensen, G., Jensen, N., Nielsen, D. B., and Larsen, B. (1996). Electrostatic spraying: a novel technique for preparation of polymer coatings on electrodes. *Analytical chemistry*, 68(21):3840–3844.

Huebner, A. L. and Chu, H. N. (1971). Instability and breakup of charged liquid jets. *Journal of Fluid Mechanics*, 49(2):361–372.

Ibrahim, R. K., Hayyan, M., AlSaadi, M. A., Hayyan, A., and Ibrahim, S. (2016). Environmental application of nanotechnology: air, soil, and water. *Environmental Science and Pollution Research*, 23(14):13754–13788.

Ijsebaert, J. C., Geerse, K. B., Marijnissen, J. C. M., Lammers, J. W., and Zanen, P. (2001). Electro-hydrodynamic atomization of drug solutions for inhalation purposes. *Journal of Applied Physiology*, 91(6):2735–2741.

Jafari, S. M., Arpagaus, C., Cerqueira, M. A., and Samborska, K. (2021). Nano spray drying of food ingredients; materials, processing and applications. *Trends in Food Science & Technology*, 109:632–646.

Jaworek, A. (2007a). Electrospray droplet sources for thin film deposition. *Journal of Materials Science*, 42(1):266–297.

Jaworek, A. (2007b). Micro- and nanoparticle production by electrospraying. *Powder Technology*, 176(1):18–35.

Jaworek, A. (2008). Electrostatic micro- and nanoencapsulation and electroemulsification: A brief review. *Journal of Microencapsulation*, 25(7):443–468.

Jaworek, A., Balachandran, W., Lackowski, M., Kulon, J., and Krupa, A. (2006). Multi-nozzle electrospray system for gas cleaning processes. *Journal of Electrostatics*, 64(3-4):194–202.

Jaworek, A., Gañán-Calvo, A. M., and Machala, Z. (2019). Low temperature plasmas and electrosprays. *Journal of Physics D: Applied Physics*, 52(23):233001.

Jaworek, A. and Krupa, A. (1999). Classification of the modes of EHD spraying. *Journal of Aerosol Science*, 30(7):873–893.

Jaworek, A., Krupa, A., and Czech, T. (2007). Modern electrostatic devices and methods for exhaust gas cleaning: A brief review. *Journal of Electrostatics*, 65(3):133–155.

Jaworek, A. and Sobczyk, A. T. (2008). Electrospraying route to nanotechnology: An overview. *Journal of Electrostatics*, 66(3-4):197–219.

Jaworek, A., Sobczyk, A. T., and Krupa, A. (2018). Electrospray application to powder production and surface coating. *Journal of Aerosol Science*, 125:57–92.

Ji, J. H., Bae, G. N., and Hwang, J. (2004). Characteristics of aerosol charge neutralizers for highly charged particles. *Journal of Aerosol Science*, 35(11):1347–1358.

Juraschek, R. and Röllgen, F. W. (1998). Pulsation phenomena during electrospray ionization. *International Journal of Mass Spectrometry*, 177(1):1–15.

Katz, L. M., Dewan, K., and Bronaugh, R. L. (2015). Nanotechnology in cosmetics. *Food and Chemical Toxicology*, 85:127–137. Nanotoxicology and Nanomedicine.

Kaufman, S. L., Skogen, J. W., Dorman, F. D., Zarrin, F., and Lewis, K. C. (1996). Macromolecule Analysis Based on Electrophoretic Mobility in Air: Globular Proteins. *Analytical Chemistry*, 68(11):1895–1904.

Kavadiya, S. and Biswas, P. (2018). Electrospray deposition of biomolecules: Applications, challenges, and recommendations. *Journal of Aerosol Science*, 125:182–207.

Kelder, E. M., Marijnissen, J. C. M., and Karuga, S. W. (2018). EHDA for energy production, storage and conversion devices. *Journal of Aerosol Science*, 125:119–147.

Keskinen, J., Pietarinen, K., and Lehtimäki, M. (1992). Electrical low pressure impactor. *Journal of Aerosol Science*, 23(4):353–360.

Khalifehei, M. and Higuera, F. (2020). Neutralization of an electrospray by a corona discharge. *Journal of Aerosol Science*, 145:105547.

Khan, M. K. I., Schutyser, M. A. I., Schroën, K., and Boom, R. (2012). The potential of electrospraying for hydrophobic film coating on foods. *Journal of Food Engineering*, 108(3):410–416.

Kipp, J. E. (2004). The role of solid nanoparticle technology in the parenteral delivery of poorly water-soluble drugs. *International Journal of Pharmaceutics*, 284(1):109–122.

Koekoekx, R., Zawacka, N. C., Van den Mooter, G., Hens, Z., and Clasen, C. (2020). Electrospraying the Triblock Copolymer SEBS: The Effect of Solvent System and the Embedding of Quantum Dots. *Macromolecular Materials and Engineering*, 305(2):1900658.

Ku, B. K. and Kim, S. S. (2002). Electrospray characteristics of highly viscous liquids. *Journal of Aerosol Science*, 33(10):1361–1378.

Lama, W. L. and Gallo, C. (1974). Systematic study of the electrical characteristics of the "trichel" current pulses from negative needle-to-plane coronas. *Journal of Applied Physics*, 45(1):103–113.

Larsen, G., Spretz, R., and Velarde-Ortiz, R. (2004). Use of coaxial gas jackets to stabilize Taylor cones of volatile solutions and to induce particle-to-fiber transitions. *Advanced Materials*, 16(2):166–169.

Lemmer, K. (2017). Propulsion for CubeSats. *Acta Astronautica*, 134:231–243.

Lenggoro, I. W., Okuyama, K., Fernández de la Mora, J., and Tohge, N. (2000). Preparation of ZnS nanoparticles by electrospray pyrolysis. *Journal of Aerosol Science*, 31(1):121–136.

Lenggoro, I. W., Xia, B., Okuyama, K., and Fernandez de la Mora, J. (2002). Sizing of colloidal nanoparticles by electrospray and differential mobility analyzer methods. *Langmuir*, 18(12):4584–4591.

Lewis, K. C., Dohmeier, D. M., Jorgenson, J. W., Kaufman, S. L., Zarrin, F., and Dorman, F. D. (1994). Electrospray-condensation particle counter: a molecule-counting LC detector for macromolecules. *Analytical Chemistry*, 66(14):2285–2292.

Li, D., Marquez, M., and Xia, Y. (2007). Capturing electrified nanodroplets under Rayleigh instability by coupling electrospray with a sol-gel reaction. *Chemical Physics Letters*, 445(4-6):271–275.

Librán, C. M., Castro, S., Lagaron, J. M., Libran, C. M., Castro, S., and Lagaron, J. M. (2017). Encapsulation by electrospray coating atomization of probiotic strains. *Innovative Food Science and Emerging Technologies*, 39:216–222.

Liu, B. Y. H., Pui, D. Y. H., Rubow, K. L., and Szymanski, W. W. (1985). Electrostatic effects in aerosol sampling and filtration. *Annals of Occupational Hygiene*, 29(2):251–269.

Liu, Q. and Chen, D. R. (2014). An electrospray aerosol generator with X-ray photoionizer for particle charge reduction. *Journal of Aerosol Science*, 76:148–162.

Loeb, L. B. (1948). Recent developments in analysis of the mechanisms of positive and negative coronas in air. *Journal of Applied Physics*, 19(10):882–897.

Lojewski, B., Yang, W., Duan, H., Xu, C., and Deng, W. (2013). Design, fabrication, and characterization of linear multiplexed electrospray atomizers micro-machined from metal and polymers. *Aerosol Science and Technology*, 47(2):146–152.

Loscertales, I. G., Barrero, A., and Márquez, M. (2004). Production of complex nano-structures by electro-hydro-dynamics. *MRS Proceedings*, 860:LL5.9(1–6).

Loscertales, I. G. and Gañán-Calvo, A. M. (2002). Micro / nano encapsulation via electrified coaxial liquid jets. *Science*, 295(5560):1695–1698.

Lu, Q. and Koropchak, J. A. (2004). Corona discharge neutralizer for electrospray aerosols used with condensation nucleation light-scattering detection. *Analytical Chemistry*, 76(18):5539–5546.

López-Herrera, J. M., Riesco-Chueca, P., and Gañán-Calvo, A. M. (2005). Linear stability analysis of axisymmetric perturbations in imperfectly conducting liquid jets. *Physics of Fluids*, 17(3):034106.

Mai, Z., Chen, J., He, T., Hu, Y., Dong, X., Zhang, H., Huang, W., Ko, F., and Zhou, W. (2017). Electrospray biodegradable microcapsules loaded with curcumin for drug delivery systems with high bioactivity. *RSC Advances*, 7(3):1724–1734.

Maißer, A., Attoui, M. B., Gañán-Calvo, A. M., and Szymanski, W. W. (2013). Electro-hydrodynamic generation of monodisperse nanoparticles in the sub-10 nm size range from strongly electrolytic salt solutions: Governing parameters of scaling laws. *Journal of Nanoparticle Research*, 15(1):1318 (13pp).

Malamatari, M., Charisi, A., Malamataris, S., Kachrimanis, K., and Nikolakakis, I. (2020). Spray Drying for the Preparation of Nanoparticle-Based Drug Formulations as Dry Powders for Inhalation.

Marginean, I., Parvin, L., Heffernan, L., and Vertes, A. (2004). Flexing the electrified meniscus: The birth of a jet in electrosprays. *Analytical Chemistry*, 76(14):4202–4207.

Masters, K. (1991). *Spray drying handbook*. Longman Scientific & Technical, London, 5th edition.

Mathon, R., Jidenko, N., and Borra, J.-P. (2017). Ozone-free post-DBD aerosol bipolar diffusion charger: Evaluation as neutralizer for SMPS size distribution measurements. *Aerosol Science and Technology*, 51(3):282–291.

Matter, D., Mohr, M., Fendel, W., Schmidtott, A., and Burtscher, H. (1995). Multiple wavelength aerosol photoemission by excimer lamps. *Journal of Aerosol Science*, 26(7):1101–1115.

Meesters, G. M. H., Vercoulen, P. H. W., Marijnissen, J. C. M., and Scarlett, B. (1992). Generation of micron-sized droplets from the Taylor cone. *Journal of Aerosol Science*, 23(1):37–49.

Mehta, P., Haj-Ahmad, R., Rasekh, M., Arshad, M. S., Smith, A., van der Merwe, S. M., Li, X., Chang, M. W., and Ahmad, Z. (2017). Pharmaceutical and biomaterial engineering via electrohydrodynamic atomization technologies. *Drug Discovery Today*, 22(1):157–165.

Meng, F., Jiang, Y., Sun, Z., Yin, Y., and Li, Y. (2009). Electrohydrodynamic liquid atomization of biodegradable polymer microparticles: Effect of electrohydrodynamic liquid atomization variables on microparticles. *Journal of Applied Polymer Science*, 113(1):526–534.

Mizuno, A. (2000). Electrostatic precipitation. *IEEE Transactions on Dielectrics and Electrical Insulation*, 7(5):615–624.

Modesto-Lopez, L. B., Kettleson, E. M., and Biswas, P. (2011). Soft X-ray charger (SXC) system for use with electrospray for mobility measurement of bioaerosols. *Journal of Electrostatics*, 69(4):357–364.

Mohammed, M. A., Syeda, J. T. M., Wasan, K. M., and Wasan, E. K. (2017). An overview of chitosan nanoparticles and its application in non-parenteral drug delivery. *Pharmaceutics*, 9(4).

Montané, X., Bajek, A., Roszkowski, K., Montornés, J. M., Giamberini, M., Roszkowski, S., Kowalczyk, O., Garcia-Valls, R., and Tylkowski, B. (2020). Encapsulation for Cancer Therapy. *Molecules*, 25(7):1605.

Morad, M. R., Rajabi, A., Razavi, M., and Sereshkeh, S. R. P. (2016). A very stable high throughput Taylor cone-jet in electrohydrodynamics. *Scientific Reports*, 6(1):38509 (10pp).

Morozov, V. N. (2010). *Electrospray Deposition of Biomolecules*, pages 115–162. Springer Berlin Heidelberg, Berlin, Heidelberg.

Morozov, V. N. (2011). Generation of biologically active nano-aerosol by an electrospray-neutralization method. *Journal of Aerosol Science*, 42(5):341–354.

Mou, F., Chen, C., Guan, J., Chen, D.-R., and Jing, H. (2013). Oppositely charged twin-head electrospray: a general strategy for building Janus particles with controlled structures. *Nanoscale*, 5(5):2055–64.

Mustika, W. S., Hapidin, D. A., Saputra, C., and Munir, M. M. (2021). Dual needle corona discharge to generate stable bipolar ion for neutralizing electrosprayed nanoparticles. *Advanced Powder Technology*, 32(1):166–174.

Nagato, K., Matsui, Y., Miyata, T., and Yamauchi, T. (2006). An analysis of the evolution of negative ions produced by a corona ionizer in air. *International Journal of Mass Spectrometry*, 248(3):142–147.

Nandiyanto, A. B. D. and Okuyama, K. (2011). Progress in developing spray-drying methods for the production of controlled morphology particles: From the nanometer to submicrometer size ranges. *Advanced Powder Technology*, 22(1):1–19.

Nashimoto, K. (1988). Silicon Oxide Projections Grown by Negative Corona Discharge. 27(Part 1, No. 6):892–898.

Nature (2019). Nanomaterials definition matters. *Nature Nanotechnology*, 14(3):193.

Nguyen, D. N., Clasen, C., and Van den Mooter, G. (2016). Pharmaceutical applications of electrospraying. *Journal of Pharmaceutical Sciences*, 105(9):2601–2620.

Nikolaou, M. and Krasia-Christoforou, T. (2018). Electrohydrodynamic methods for the development of pulmonary drug delivery systems. *European Journal of Pharmaceutical Sciences*, 113(August 2017):29–40.

Niu, B., Shao, P., Luo, Y., and Sun, P. (2020). Recent advances of electrosprayed particles as encapsulation systems of bioactives for food application. *Food Hydrocolloids*, 99:105376.

Noakes, T. J., Pavey, I. D., Bray, D., and Rowe, R. C. (1989). Apparatus for Producing a Spray of Droplets of a Liquid.

Okuyama, K. and Lenggoro, W. W. (2003). Preparation of nanoparticles via spray route. *Chemical Engineering Science*, 58(3-6):537–547.

Olvera-Trejo, D. and Velásquez-García, L. F. (2016). Additively manufactured MEMS multiplexed coaxial electrospray sources for high-throughput, uniform generation of core–shell microparticles. *Lab Chip*, 16(21):4121–4132.

Pähtz, T., Herrmann, H. J., and Shinbrot, T. (2010). Why do particle clouds generate electric charges? *Nature Physics*, 6(5):364–368.

Paramo, L. A., Feregrino-Perez, A. A., Guevara, R., Mendoza, S., and Esquivel, K. (2020). Nanoparticles in Agroindustry: Applications, Toxicity, Challenges, and Trends. *Nanomaterials*, 10(9):1654.

Pardeshi, S., More, M., Patil, P., Pardeshi, C., Deshmukh, P., Mujumdar, A., and Naik, J. (2021). A meticulous overview on drying-based (spray-, freeze-, and spray-freeze) particle engineering approaches for pharmaceutical technologies. *Drying Technology*, 0(0):1–45.

Parisi, C., Vigani, M., and Rodríguez-Cerezo, E. (2015). Agricultural Nanotechnologies: What are the current possibilities? *Nano Today*, 10(2):124–127.

Park, S.-J. and Kim, S.-H. (2004). Preparation and characterization of biodegradable poly(l-lactide)/poly(ethylene glycol) microcapsules containing erythromycin by emulsion solvent evaporation technique. *Journal of Colloid and Interface Science*, 271(2):336–341.

Pawar, A., Thakkar, S., and Misra, M. (2018). A bird's eye view of nanoparticles prepared by electrospraying: advancements in drug delivery field. *Journal of Controlled Release*, 286:179–200.

Peters, R. J., Bouwmeester, H., Gottardo, S., Amenta, V., Arena, M., Brandhoff, P., Marvin, H. J., Mech, A., Moniz, F. B., Pesudo, L. Q., Rauscher, H., Schoonjans, R., Undas, A. K., Vettori, M. V., Weigel, S., and Aschberger, K. (2016). Nanomaterials for products and application in agriculture, feed and food. *Trends in Food Science & Technology*, 54:155–164.

Qu, X., Alvarez, P. J. J., and Li, Q. (2013). Applications of nanotechnology in water and wastewater treatment. *Water Research*, 47(12):3931–3946.

Rayleigh, L. (1878). On The Instability Of Jets. *Proceedings of the London Mathematical Society*, s1-10(1):4–13.

Rayleigh, L. (1882). On the equilibrium of liquid conducting masses charged with electricity. *Philosophical Magazine and Journal of Science*, 14(87):184–186.

Rietveld, I. B., Kobayashi, K., Yamada, H., and Matsushige, K. (2006). Electrospray deposition, model, and experiment: Toward general control of film morphology. *Journal of Physical Chemistry B*, 110(46):23351–23364.

Romay, F. J., Liu, B. Y. H., and Pui, D. Y. H. (1994). A sonic jet corona ionizer for electrostatic discharge and aerosol neutralization. *Aerosol Science and Technology*, 20(1):31–41.

Rosell-Llompart, J. and Fernández de la Mora, J. (1994). Generation of monodisperse droplets 0.3 to 4 μm in diameter from electrified cone-jets of highly conducting and viscous liquids. *Journal of Aerosol Science*, 25(6):1093–1119.

Rosell-Llompart, J. and Gañán-Calvo, A. M. (2008). Turbulence in pneumatic flow focusing and flow blurring regimes. *Physical Review E*, 77(3):36321.

Rosell-Llompart, J., Grifoll, J., and Loscertales, I. G. (2018). Electrosprays in the cone-jet mode: From Taylor cone formation to spray development. *Journal of Aerosol Science*, 125:2–31.

Rostamabadi, H., Falsafi, S. R., Rostamabadi, M. M., Assadpour, E., and Jafari, S. M. (2021). Electrospraying as a novel process for the synthesis of particles/nanoparticles loaded with poorly water-soluble bioactive molecules. *Advances in Colloid and Interface Science*, 290:102384.

Rulison, A. J. and Flagan, R. C. (1994). Synthesis of Yttria Powders by Electrospray Pyrolysis. *Journal of the American Ceramic Society*, 77(12):3244–3250.

Russell, L. M., Flagan, R. C., and Seinfeld, J. H. (1995). Asymmetric Instrument Response Resulting from Mixing Effects in Accelerated DMA-CPC Measurements. *Aerosol Science and Technology*, 23(4):491–509.

Rutz, J. K., Borges, C. D., Zambiazi, R. C., Crizel-Cardozo, M. M., Kuck, L. S., and Noreña, C. P. Z. (2017). Microencapsulation of palm oil by complex coacervation for application in food systems. *Food Chemistry*, 220:59–66.

Salama, A. H. (2020). Spray drying as an advantageous strategy for enhancing pharmaceuticals bioavailability. *Drug Delivery and Translational Research*, 10(1):1–12.

Sample, S. B. and Bollini, R. (1972). Production of liquid aerosols by harmonic electrical spraying. *Journal of Colloid and Interface Science*, 41(2):185–193.

Saville, D. A. (1971). Stability of electrically charged viscous cylinders. *Physics of Fluids*, 14(6):1095–1099.

Saville, D. A. (1997). Electrohydrodynamics: The Taylor-Melcher leaky dielectric model. *Annual Review of Fluid Mechanics*, 29(1):27–64.

Scheideler, W. J. and Chen, C.-H. (2014). The minimum flow rate scaling of Taylor cone-jets issued from a nozzle. *Applied Physics Letters*, 104(2):24103.

Schiffter, H., Condliffe, J., and Vonhoff, S. (2010). Spray-freeze-drying of nanosuspensions: the manufacture of insulin particles for needle-free ballistic powder delivery. *Journal of The Royal Society Interface*, 7(suppl_4):S483–S500.

Sebastiao, I. B., Bhatnagar, B., Tchessalov, S., Ohtake, S., Plitzko, M., Luy, B., and Alexeenko, A. (2019). Bulk Dynamic Spray Freeze-Drying Part 2: Model-Based Parametric Study for Spray-Freezing Process Characterization. *Journal of Pharmaceutical Sciences*, 108(6):2075–2085.

Sharma, S., Rana, V. S., Pawar, R., Lakra, J., and Racchapannavar, V. (2021). Nanofertilizers for sustainable fruit production: a review. *Environmental Chemistry Letters*, 19(2):1693–1714.

Sheorey, D. S., Sai, M. S., and Dorle, A. K. (1991). A new technique for the encapsulation of water insoluble drugs using ethyl cellulose. *Journal of Microencapsulation*, 8(3):359–368.

Smeets, A., Clasen, C., and den Mooter, G. V. (2017). Electrospraying of polymer solutions: Study of formulation and process parameters. *European Journal of Pharmaceutics and Biopharmaceutics*, 119(Supplement C):114–124.

Smeets, A., Koekoekx, R., Clasen, C., and den Mooter, G. (2018). Amorphous solid dispersions of darunavir: Comparison between spray drying and electrospraying. *European Journal of Pharmaceutics and Biopharmaceutics*, 130:96–107.

Smeets, A., Koekoekx, R., Ruelens, W., Smet, M., Clasen, C., and den Mooter, G. V. (2019). Gastro-resistant encapsulation of amorphous solid dispersions containing darunavir by coaxial electrospraying. *International Journal of Pharmaceutics*, page 118885.

Smith, D. P. H. (1986). The electrohydrodynamic atomization of liquids. *IEEE Transactions on Industry Applications*, IA-22(3):527–535.

Smith, K. L., Alexander, M. S., and Stark, J. P. W. (2006). The role of molar conductivity in electrospray cone-jet mode current scaling. *Journal of Applied Physics*, 100(1):014905 (6pp).

Sochorakis, N. (2018). *Electrospray scale-up for the production of particles of pharmaceutical interest.* PhD thesis, Universitat Rovira i Virgili.

Sochorakis, N., Grifoll, J., and Rosell-Llompart, J. (2019). Scaling up of extractor-free electrosprays in linear arrays. *Chemical Engineering Science*, 195:281–298.

Sosnik, A. and Seremeta, K. P. (2015). Advantages and challenges of the spray-drying technology for the production of pure drug particles and drug-loaded polymeric carriers. *Advances in Colloid and Interface Science*, 223:40–54.

Sridhar, A., Ponnuchamy, M., Kumar, P. S., and Kapoor, A. (2021). Food preservation techniques and nanotechnology for increased shelf life of fruits, vegetables, beverages and spices: a review. *Environmental Chemistry Letters*, 19(2):1715–1735.

Stark, J., Stevens, B., Alexander, M., and Kent, B. (2005). Fabrication and Operation of Microfabricated Emitters as Components for a Colloid Thruster. *Journal of Spacecraft and Rockets*, 42(4):628–639.

Steiner, G., Franchin, A., Kangasluoma, J., Kerminen, V. M., Kulmala, M., and Petäjä, T. (2017). Production of neutral molecular clusters by controlled neutralization of mobility standards. *Aerosol Science and Technology*, 51(8):946–955.

Steipel, R. T., Gallovic, M. D., Batty, C. J., Bachelder, E. M., and Ainslie, K. M. (2019). Electrospray for generation of drug delivery and vaccine particles applied in vitro and in vivo. *Materials Science and Engineering: C*, 105(August):110070.

Stommel, Y. G. and Riebel, U. (2004). A new corona discharge-based aerosol charger for submicron particles with low initial charge. *Journal of Aerosol Science*, 35(9):1051–1069.

Suhendi, A., Nandiyanto, A. B. D., Munir, M. M., Ogi, T., Gradon, L., and Okuyama, K. (2013). Self-assembly of colloidal nanoparticles inside charged droplets during spray-drying in the fabrication of nanostructured particles. *Langmuir*, 29(43):13152–13161.

Sverdlov Arzi, R. and Sosnik, A. (2018). Electrohydrodynamic atomization and spray-drying for the production of pure drug nanocrystals and co-crystals. *Advanced Drug Delivery Reviews*, 131:79–100.

Tan, H. W., An, J., Chua, C. K., and Tran, T. (2019). Metallic Nanoparticle Inks for 3D Printing of Electronics. *Advanced Electronic Materials*, 5(5):1800831.

Tang, J. and Gomez, A. (2017). Controlled mesoporous film formation from the deposition of electrosprayed nanoparticles. *Aerosol Science and Technology*, 51(6):755–765.

Tang, J., Liu, W., Wang, H., and Gomez, A. (2016). High Performance Metal Oxide–Graphene Hybrid Nanomaterials Synthesized via Opposite-Polarity Electrosprays. *Advanced Materials*, 28(46):10298–10303.

Tang, J., Wang, H., and Gomez, A. (2017). Controlled nanoparticle synthesis via opposite-polarity electrospray pyrolysis. *Journal of Aerosol Science*, 113:201–211.

Tang, K. and Gomez, A. (1994). Generation by electrospray of monodisperse water droplets for targeted drug delivery by inhalation. *Journal of Aerosol Science*, 25(6):1237–1249.

Taylor, G. (1964). Disintegration of water drops in an electric field. *Proceedings of the Royal Society A: Mathematical, Physical and Engineering Sciences*, 280(1382):383–397.

Torres-Giner, S., Prieto, C., and Lagaron, J. M. (2020). Nanomaterials to Enhance Food Quality, Safety, and Health Impact. *Nanomaterials*, 10(5):941.

Townsend, J. S. (1915). *Electricity in gases*. Oxford University Press, New York.

Tsai, S. and Ting, Y. (2019). Synthesize of alginate/chitosan bilayer nanocarrier by CCD-RSM guided co-axial electrospray: A novel and versatile approach. *Food Research International*, 116:1163–1172.

Uecker, J. C., Tepper, G. C., and Rosell-Llompart, J. (2010). Ion-assisted collection of Nylon-4,6 electrospun nanofibers. *Polymer*, 51(22):5221–5228.

Vehring, R., Snyder, H., and Lechuga-Ballesteros, D. (2020). Spray Drying.

Verdoold, S., Agostinho, L. L. F., Yurteri, C. U., and Marijnissen, J. C. M. (2014). A generic electrospray classification. *Journal of Aerosol Science*, 67:87–103.

Viikov, A. N., Laiko, V. V., and Doroshenko, V. M. (2009). Peptide fragmentation induced by radicals at atmospheric pressure. *Journal of Mass Spectrometry*, 44(4):477–484.

Wan, F., Maltesen, M. J., Bjerregaard, S., Foged, C., Rantanen, J., and Yang, M. (2013). Particle engineering technologies for improving the delivery of peptide and protein drugs. *Journal of Drug Delivery Science and Technology*, 23(4):355–363.

Wang, J., Jansen, J. A., and Yang, F. (2019). Electrospraying: Possibilities and Challenges of Engineering Carriers for Biomedical Applications—A Mini Review. *Frontiers in Chemistry*, 7:258.

Wang, S. and Langrish, T. (2009). A review of process simulations and the use of additives in spray drying. *Food Research International*, 42(1):13–25.

Wang, Y., Zhang, R., Qin, W., Dai, J., Zhang, Q., Lee, K., and Liu, Y. (2020). Physicochemical properties of gelatin films containing tea polyphenol-loaded chitosan nanoparticles generated by electrospray. *Materials & Design*, 185:108277.

Wang, Y., Zhang, Y., Wang, B., Cao, Y., Yu, Q., and Yin, T. (2013). Fabrication of core-shell micro/nanoparticles for programmable dual drug release by emulsion electrospraying. *Journal of Nanoparticle Research*, 15(6):1–12.

Webster, D. M., Sundaram, P., and Byrne, M. E. (2013). Injectable nanomaterials for drug delivery: Carriers, targeting moieties, and therapeutics. *European Journal of Pharmaceutics and Biopharmaceutics*, 84(1):1–20.

Wicki, A., Witzigmann, D., Balasubramanian, V., and Huwyler, J. (2015). Nanomedicine in cancer therapy: Challenges, opportunities, and clinical applications. *Journal of Controlled Release*, 200:138–157.

Wuerker, R. F., Shelton, H., and Langmuir, R. V. (1959). Electrodynamic Containment of Charged Particles. *Journal of Applied Physics*, 30(3):342–349.

Xia, H. H., Ismail, A., Yao, J., and Stark, J. P. W. (2019). Scaling Laws for Transition from Varicose to Whipping Instabilities in Electrohydrodynamic Jetting. *Physical Review Applied*, 12(1):1.

Xie, J., Lim, L. K., Phua, Y., Hua, J., and Wang, C. H. (2006a). Electrohydrodynamic atomization for biodegradable polymeric particle production. *Journal of Colloid and Interface Science*, 302(1):103–112.

Xie, J., Marijnissen, J. C. M., and Wang, C. H. (2006b). Microparticles developed by electrohydrodynamic atomization for the local delivery of anticancer drug to treat C6 glioma in vitro. *Biomaterials*, 27(17):3321–3332.

Xie, J. and Wang, C.-H. (2007). Encapsulation of proteins in biodegradable polymeric microparticles using electrospray in the Taylor cone-jet mode. *Biotechnology and Bioengineering*, 97(5):1278–1290.

Xu, Q., Hashimoto, M., Dang, T. T., Hoare, T., Kohane, D. S., Whitesides, G. M., Langer, R., and Anderson, D. G. (2009). Preparation of monodisperse biodegradable polymer microparticles using a microfluidic flow-focusing device for controlled drug delivery. *Small (Weinheim an der Bergstrasse, Germany)*, 5(13):1575–1581.

Yamashita, M. and Fenn, J. B. (1984). Electrospray ion source. Another variation on the free-jet theme. *The Journal of Physical Chemistry*, 88(20):4451–4459.

Yang, W., Lojewski, B., Wei, Y., and Deng, W. (2012). Interactions and deposition patterns of multiplexed electrosprays. *Journal of Aerosol Science*, 46:20–33.

Yilmaz, M. T., Yilmaz, A., Akman, P. K., Bozkurt, F., Dertli, E., Basahel, A., Al-Sasi, B., Taylan, O., and Sagdic, O. (2019). Electrospraying method for fabrication of essential oil loaded-chitosan nanoparticle delivery systems characterized by molecular, thermal, morphological and antifungal properties. *Innovative Food Science and Emerging Technologies*, 52:166–178.

You, R., Li, M., Guha, S., Mulholland, G. W., and Zachariah, M. R. (2014). Bionanoparticles as Candidate Reference Materials for Mobility Analysis of Nanoparticles. *Analytical Chemistry*, 86(14):6836–6842.

Yurkstas, E. P. and Meisenzehl, C. J. (1964). Solid Homogeneous Aerosol Production by Electrical Atomization. AEC Research and Development Report UR-652. Technical report, Rochester, New York.

Yurteri, C., Hartman, R., and Marijnissen, J. (2010). Producing pharmaceutical particles via electrospraying with an emphasis on nano and nano structured particles - A review. *KONA Powder and Particle Journal*, 28:91–115.

Zamorani, E. and Ottobrini, G. (1978). Aerosol particle neutralization to Boltzmann's equilibrium by a.c. corona discharge. *Journal of Aerosol Science*, 9(1):31–39.

Zeleny, J. (1917). Instability of electrified liquid surfaces. *Physical Review*, 10(1):1–6.

Zimlich, W., Ding, J., Busick, D., Pham, S., Palmer, D., and Placke, M. (2002). Development of multiple clinical and commercial applications using mystic inhalation delivery technologies. In Dalby, R., Byron, P., Peart, J., and Farr, S., editors, *Respiratory Drug Delivery VIII*, pages 363–366, Tucson, Arizona. RDD Online.

Zong, H., Xia, X., Liang, Y., Dai, S., Alsaedi, A., Hayat, T., Kong, F., and Pan, J. H. (2018). Designing function-oriented artificial nanomaterials and membranes via electrospinning and electrospraying techniques. *Materials Science and Engineering: C*, 92:1075–1091.

UNIVERSITAT
ROVIRA i VIRGILI